



# Infrastructure Monitoring Data Management



## Final Report

July 7, 2015

### Prepared by:

Ihab Darwish, PhD, PE, SE  
Senior Project Manager  
Alfred Benesch & Company  
4660 S. Hagadorn Rd, Suite 315  
East Lansing, MI, 48823

Steven J. Cook, PE  
Engineer of Operations & Maintenance  
Operations Field Service Division  
Michigan Department of Transportation  
6333 Lansing Road  
Lansing, MI 48917

## Technical Report Documentation Page

<b>1. Report No.</b> RC-1625	<b>2. Government Accession No.</b> N/A	<b>3. MDOT Project Manager</b> Steven J. Cook, PE	
<b>4. Title and Subtitle</b> INFRASTRUCTURE MONITORING DATA MANAGEMENT		<b>5. Report Date</b> July 7, 2015	
		<b>6. Performing Organization Code</b> N/A	
<b>7. Author(s)</b> Ihab Darwish, PhD, PE, SE Matthew Garratt, PE Matthew Longfield Jr, PE Ziad Hanna, PE Melissa Donoso, EIT		<b>8. Performing Org. Report No.</b> N/A	
<b>9. Performing Organization Name and Address</b> Alfred Benesch & Company 4660 South Hagadorn Road, Suite 315 East Lansing, Michigan 48823		<b>10. Work Unit No. (TRAIS)</b> N/A	
		<b>11. Contract No.</b> 2009-0642	
		<b>11(a). Authorization No.</b> Z1	
<b>12. Sponsoring Agency Name and Address</b> Michigan Department of Transportation Research Administration 8885 Ricks Rd. P.O. Box 30049 Lansing MI 48909		<b>13. Type of Report &amp; Period Covered</b> Final Report 9/30/2009 to 6/1/2015	
		<b>14. Sponsoring Agency Code</b> N/A	
<b>15. Supplementary Notes</b>			
<b>16. Abstract</b> The primary objective of this project is to advance the development of a structural health monitoring system (SHMS) for the Cut River Bridge. The scope includes performing an analysis from the fiber optic strain gauge readings and making recommendations for any future application of a SHMS in Michigan. Additionally, the recorded data from the fiber optic strain gauges and weigh-in-motion (WIM) station were used to calibrate a 3D finite element model. The finite element model will enhance assessment of the remaining structural members that are not equipped with fiber optic strain gauges. Specifically for the Cut River Bridge, recommendations have been made for coordinating the SHMS with MDOT's Data Use Analysis Processing (DUAP) project. The analysis and recommendations will be focused on meeting MDOT's connected technologies initiatives and core goals of safety, mobility, planning, and asset management.			
<b>17. Key Words</b> Cut River Bridge, Structural Health Monitoring, Wireless Infrastructure		<b>18. Distribution Statement</b> No restrictions. This document is available to the public through the Michigan Department of Transportation.	
<b>19. Security Classification - report</b> Unclassified	<b>20. Security Classification - page</b> Unclassified	<b>21. No. of Pages</b> 95	<b>22. Price</b> N/A

## **ACKNOWLEDGMENTS**

This project was funded by the Michigan Department of Transportation. The authors would like to acknowledge the support and effort of Mr. Steven J. Cook, MDOT Engineer of Operations and Maintenance Field Services, for his continuous assistance and support during the project. The authors also wish to acknowledge the assistance of Mr. Collin Castle and Mr. Luke Biernbaum of MDOT for their general assistance and systems operations/equipment maintenance.

## **DISCLAIMER**

*This publication is disseminated in the interest of information exchange. The Michigan Department of Transportation (hereinafter referred to as MDOT) expressly disclaims any liability, of any kind, or for any reason, that might otherwise arise out of any use of this publication or the information or data provided in the publication. MDOT further disclaims any responsibility for typographical errors or accuracy of the information provided or contained within this information. MDOT makes no warranties or representations whatsoever regarding the quality, content, completeness, suitability, adequacy, sequence, accuracy or timeliness of the information and data provided, or that the contents represent standards, specifications, or regulations.*

# Infrastructure Monitoring Data Management

## Table of Contents

List of Figures .....	vii
List of Tables .....	ix
Executive Summary .....	x
1 Introduction .....	1
1.1 Background .....	1
1.2 Objectives and Scope .....	4
2 Literature Review .....	6
3 Devices and Equipment .....	6
3.1 System Overview .....	6
3.2 Weigh-in-Motion (WIM) Station .....	6
3.3 Strain Gauges & Temperature Sensors .....	9
3.4 Traffic Sensors .....	14
3.5 Environmental Sensor Station .....	19
3.6 Traffic Cameras .....	24
4 Data Collection and Processing .....	27
4.1 Data Collection Overview .....	27
4.2 Truck Data .....	27
4.2.1 Introduction .....	27
4.2.2 Methodology: Data Collection and Processing .....	27
4.2.3 Collected Data .....	28
4.2.4 Summary and Discussion .....	36
4.3 Strain Gauge Readings .....	36
4.3.1 Introduction .....	36
4.3.2 Methodology: Data Collection and Processing .....	38
4.3.3 Collected Data .....	38
4.4 Traffic Count .....	41
4.4.1 Introduction .....	41

4.4.2	Methodology: Data Collection and Processing.....	41
4.4.3	Collected Data.....	41
4.5	Pavement and Weather.....	43
5	Finite Element Analysis.....	45
5.1	FE Model Description .....	45
5.2	Validation and Verification of the Finite Element Model.....	46
6	Future Implementation and Improvements.....	54
6.1	Equipment and Communication Improvements.....	54
6.2	New Technologies.....	56
6.3	Future Implementation/DUAP .....	57
7	Recommendations and Conclusions.....	58
7.1	Recommendations .....	58
7.2	Conclusions .....	59
8	References .....	61
	Appendix A: FHWA Vehicle Classifications.....	63
	Appendix B: Strain Gauge Specifications .....	64
	Appendix C: Temperature Sensor Specifications .....	65
	Appendix D: Interrogator Specifications.....	66
	Appendix E: Traffic Sensor Specifications.....	67
	Appendix F: Traffic Sensor Access Point Specifications.....	68
	Appendix G: Temperature & Relative Humidity Probe Specifications.....	69
	Appendix H: Wind Monitor Specifications .....	70
	Appendix I: Rain Gauge Specifications.....	71
	Appendix J: Intelligent Road Sensor Specifications.....	72
	Appendix K: Environmental Sensor Station Data Logger Specifications .....	73
	Appendix L: NetCam SC Specifications .....	74
	Appendix M: Axis Specifications.....	75
	Appendix N: Control DeviceMaster Specifications .....	76
	Appendix O: Literature Review.....	77
O.1	Structural Health Monitoring on Bridges.....	77
O.2	Dynamic Impact Factor.....	87

## List of Figures

Figure 1: Location Map .....	2
Figure 2: Cut River Bridge Elevation .....	3
Figure 3: Cut River Bridge Cross-Section .....	3
Figure 4: Cut River Bridge SHMS Overview.....	8
Figure 5: WIM Station .....	9
Figure 6: Strain Gauge (Top) and Temperature Sensor (Bottom) .....	10
Figure 7: Strain Gauge Location Overview .....	11
Figure 8: Cross Section of Member U4_U5 (North or South Truss Looking West).....	11
Figure 9: Cross Section of Member L4_U5 (North or South Truss Looking West) .....	11
Figure 10: Strain Gauge Locations (Looking North).....	12
Figure 11: Installed Strain Gauge and Temperature Sensor .....	13
Figure 12: Optical Sensing Interrogator sm130.....	14
Figure 13: Traffic Sensor .....	16
Figure 14: Installed Traffic Sensor .....	16
Figure 15: Traffic Sensor Access Point .....	17
Figure 16: Environmental Sensor Station (ESS) Layout .....	18
Figure 17: Temperature and Relative Humidity Probe.....	20
Figure 18: Wind Monitor .....	20
Figure 19: Rain Gauge .....	21
Figure 20: Lufft Intelligent Road Sensor .....	21
Figure 21: ESS Data Logger .....	22
Figure 22: Towers at Bridge Site .....	23
Figure 23: Traffic Camera at Bridge Site .....	25
Figure 24: Bridge Camera Screenshot .....	25
Figure 25: Traffic Camera at WIM Station.....	26
Figure 26: WIM Station Camera Screenshot .....	26
Figure 27: WPC and Advanced Serial Data Logger Screenshot .....	30
Figure 28: Control DeviceMaster .....	30
Figure 29: Number of Trucks per Lane .....	31
Figure 30: Hourly Truck Traffic Volume .....	31
Figure 31: Truck Volume per Number of Truck Axles .....	32
Figure 32: Volume of Trucks per FHWA Vehicle Classification .....	32
Figure 33: Truck Volume per Truck Gross Weight.....	33
Figure 34: Gross Weight per Number of Axles .....	33
Figure 35: Gross Truck Weight per Overall Truck Length .....	34
Figure 36: Truck Volume per Overall Truck Length.....	34
Figure 37: Truck Volume per Speed.....	35
Figure 38: ENLIGHT Screenshot (Strain Values).....	37

Figure 39: ENLIGHT Screenshot (Plot of Strain Values) .....	37
Figure 40: Example Graph of Strain vs Time .....	39
Figure 41: Maximum Strains in Top Chord Members.....	40
Figure 42: Maximum Strains in Diagonal Members .....	40
Figure 43: TrafficDOT 2 Screenshot .....	42
Figure 44: Average Daily Traffic (ADT) per Month.....	42
Figure 45: LoggerNet Screenshot .....	44
Figure 46: MxVision WeatherSentry Online Website Screenshot .....	44
Figure 47: Three-Dimensional Finite Element Model of the Bridge.....	46
Figure 48: Measured Dynamic Strain and Equivalent Static Strain .....	49

## List of Tables

Table 5.1: Truck Configuration used for the Calibration of The Finite Element Model.....	47
Table 5.2: Maximum Truck Force in Instrumented Truss Members.....	48
Table 5.3: Measured Vs. Computed Member Forces for Truck 1 .....	51
Table 5.4: Measured Vs. Computed Member Forces for Truck 2 .....	51
Table 5.5: Measured Vs. Computed Member Forces for Truck 3 .....	52
Table 5.6: Measured Vs. Computed Member Forces for Truck 4 .....	52
Table 5.7: Measured Vs. Computed Member Forces for Truck 5 .....	53
Table 5.8: Measured Vs. Computed Member Forces for Truck 6 .....	53

## Executive Summary

A pilot structural health monitoring (SHM) project has been initiated at the Cut River Bridge along U.S. Route 2 in Michigan's Upper Peninsula. The project is focused on developing the Michigan Department of Transportation's (MDOT) connected vehicle/technologies (CV) initiatives and meeting MDOT's core goals of safety, mobility, asset management, and planning. The structure is a three span, cantilevered deck truss and is a fracture critical structure. After the collapse of the I-35W Bridge over the Mississippi River, fracture critical structures have received additional scrutiny in an effort to prevent a similar catastrophic event from occurring. Installing a structural health monitoring system (SHMS) at the Cut River Bridge presented MDOT with a method of closely monitoring the fracture critical structure and working towards its CV initiatives and core goals. Additionally, the pilot project would provide valuable lessons learned for employing the SHMS technology at future bridge locations throughout Michigan.

The SHMS consists of fiber optic strain gauges, a weigh-in-motion (WIM) station, traffic sensors, environmental deck sensors, cameras, and a weather station. Due to the remote location of the bridge, the system utilizes wireless technology to transmit the data to MDOT through a series of radio towers installed at the bridge, the Mackinac Bridge, and the Mackinac Bridge Authority office in St. Ignace. From there, the collected data is available through MDOT's computer network. The system was designed to provide MDOT with real-time information from the structure that can be accessed from any MDOT location. Once the SHMS system is fully operational and the research complete, the final stage in the pilot project is integration of the SHMS with MDOT's Data Use Analysis and Processing (DUAP) project. This final step will aid in automating and monitoring the real-time information from the structure. Through the DUAP project, the SHMS will be able to alert MDOT and emergency personnel of any detected structural safety issues as they occur. Other conditions such as weather and traffic can be monitored as well.

Throughout the course of the project, there have been many delays due to various issues with the equipment, including power supply and communication equipment. These have limited the amount of data collected during the course of the project. However, an analysis was able to be performed with the available collected data. Additionally, a three dimensional (3D) finite element model was developed using the LUSAS finite element software and calibrated to more closely match the actual results from the bridge to aid in understanding the behavior of the entire structure. Sufficient data was collected to calibrate the 3D model.

Recommendations and improvements are presented based on the analysis of the data and the issues experienced with the data collection. The recommendations are oriented towards improving the reliability of the current system, integrating with MDOT's Data Use Analysis Processing (DUAP) project, and lessons learned that can be applied to future SHMS projects. A common theme among the recommendations is incorporating redundancy into the system. Redundancy with

the monitoring and communication equipment will greatly enhance the reliability of the system and ensure the structure is continuously monitored with minimum disruptions.

# 1 Introduction

## 1.1 Background

The Michigan Department of Transportation (MDOT) has deployed a pilot project at the Cut River Bridge to investigate and develop a Structural Health Monitoring System (SHMS) that will aid in MDOT's Connected Vehicle (CV) Program. Connected vehicles aims to increase safety, mobility and reduce emissions by deploying vehicle to vehicle (V2V) communications and vehicle to infrastructure (V2I) technologies. The project utilizes a variety of sensors to monitor the structural behavior of the bridge and other conditions at the site. The SHMS will be able to report an overstressed critical member in the bridge, overweight trucks on the highway, weather, traffic conditions, and bridge deck environmental condition state. The goal of the project is to determine how the use of sensors installed on the bridge can be used to collect data to monitor structural behavior and to evaluate safety, mobility, asset management and planning applications with the remote sensors. The project also investigates and makes recommendations for a future SHMS deployment at other bridge locations in Michigan.

The Cut River Bridge is located on U.S. Route 2 approximately twenty five miles west of St. Ignace in Michigan's Upper Peninsula between the towns of Epoufette and Brevort, in Henricks Township, Mackinac County (Figure 1). The structure is a three span, cantilevered deck truss that spans the Cut River Valley where it meets Lake Michigan (Figure 2). It carries two lanes of U.S. Route 2 traffic over the Cut River (Figure 3). The structure was constructed in 1947 and considered historic. U.S. Route 2 is one of the primary highways in the Upper Peninsula and is a vital transportation link for the region. Residents, logging trucks, campers, and tourists traveling through the Upper Peninsula cross the bridge daily. The ADT at the bridge is 4,100 vehicles. Roadside parks are located on both sides of the bridge.

There are several types of sensors that have been installed at the bridge. The SHMS at the bridge is powered by batteries located in a concrete vault near the east abutment. Five solar panels situated on a tower adjacent to the bridge provide charge to the battery system. All the collected information is delivered from the tower wirelessly to MDOT. To perform the structural health monitoring (SHM), sixteen fiber optic strain gauges have been installed on several primary tension members in the deck truss. In addition, four temperature sensors were mounted adjacent to four of the fiber optic strain gauges. The temperature sensors aid in correcting for any "drift" of the strain gauges due to temperature effects. In order to understand the truck loads causing the observed strains, a weigh-in-motion (WIM) station was placed underneath the roadway approximately two miles east of the bridge. The WIM station provides axle weight and spacing for any truck traveling on the highway.



Figure 1: Location Map

Other types of equipment have been installed at the bridge as well. Two sets of traffic point detectors are located in the east approaches to the bridge to capture traffic speed, volume, and occupancy. There are two bridge deck environmental sensors that provide data on the bridge deck such as moisture content, deck temperature, chloride content, and icing conditions. There are closed-circuit television (CCTV) cameras at the bridge and at the WIM station to deliver visual verification and quality control of the data from the other sensors. MDOT installed an Environmental Sensor Station (ESS) to capture weather data and correlate the data obtained from the other sensors at the site.

Data collection from both the fiber optic strain gauges and the WIM station started in early 2013. Communication and software advancements such as calibrating the fiber optic strain gauges, were made which provided consistent collection of data starting in March of 2014. Connection with the instruments at the structure was obtained for several months, sufficient enough to obtain a data sample size for this report. Data has not been collected since September of 2014 due a lack of communication with the bridge.



## 1.2 Objectives and Scope

The Cut River Bridge is instrumented as a part of a research project to determine the feasibility of collecting data to monitor structural behavior, evaluate safety, mobility, asset management and planning applications using remote sensors. The bridge was selected for instrumentation due to its stand-alone remote location without power, extreme weather conditions at the bridge site, and long distance communication challenges between the bridge and the monitoring location. Developing a functional SHMS at the Cut River Bridge will create a blueprint for future SHMS that could be applied anywhere throughout the state of Michigan.

The research objectives to be accomplished include:

1. Analyze the ability of data retrieval in a remote environment using an off-grid power supply.
2. Analyze communication and data collection from several infrastructure sensors.
3. Analyze the ability to collect, store, archive, and use infrastructure data collection for comparisons, correlations, asset management, and control purposes.
4. Analyze the ability of vehicle probe data collection and dissemination.
5. Provide recommendations for integration with the DUAP project to automate the SHMS which includes threshold strain values to be used in an early warning system for the structure.

The scope of the project also includes the development and calibration of a 3D finite element model. The finite element model assists in the assessment of the remaining structural members that are not equipped with fiber optic strain gauges, and is also used in the load rating of the structure. The model is calibrated using the data collected from the strain gauges and from the WIM station.

The project is also a part of MDOT's CV initiatives to connect infrastructure with vehicles. CV relies on wireless technology for the vehicles and the infrastructure to communicate with each other to increase safety and mobility (Underwood, Cook, & Tansil, 2008). The instruments and sensors provide real-time information on the current conditions of the bridge; all of which are transmitted wirelessly. The information is currently being used by engineers to monitor the health of the structure. The weather and traffic information can be incorporated into MDOT's MiDrive system for the travelling public to use. The information can be readily available to diagnose and resolve any potential issues in a more timely fashion.

The Cut River Bridge SHM project also aids in advancing MDOT's core goals of safety, mobility, asset management, and planning. Safety is enhanced in multiple ways with the project. Critical structural members of the bridge can be monitored through the SHM. The bridge is considered a fracture critical structure. According to the National Bridge Inspection

Standards (NBIS), the definition of a fracture critical member is “a steel member in tension or with a tension element, whose failure would probably cause a portion of or the entire bridge to collapse” (Lwin, 2012). Typically, a fracture critical structure is inspected once every two years. However, the inspection will only observe and record defects of the structure that are identified visually or through non-destructive evaluation (NDE). The stress in the structural members of the bridge is not evaluated and can only be observed if a member is experiencing noticeable deformation. With the SHMS, the stress in the critical members can be monitored and comparisons between the demand and the capacity of the structural member can be made. The monitoring serves as an early warning system for any potential overstressing in any structural member. This is especially important with a fracture critical structure where little to no visual warning may be given before a failure. When a threshold strain value for safety is surpassed, the system can be designed to alert MDOT and emergency response staff of a potential concern at the bridge. Safety can be improved with the environmental and weather sensors as well. Unsafe weather conditions such as poor visibility and ice buildup on the deck can be observed and relayed to motorists in a timely fashion.

MDOT’s other core goals of mobility, asset management, and planning all tie in to the Cut River Bridge SHM project. Mobility can be increased with the real-time data stream that can immediately alert MDOT of traffic issues at the site. Maintaining the safety of the structure and avoid frequent closures also improve mobility. Asset management and planning are enhanced with the better estimation of the remaining service life of the structure using the collected data and also determine the elements that may require rehabilitation. The SHMS can aid in determining load distribution between structural members, which may be an indication of section loss and changes in stiffness of the structure. With the accurate measurements of forces in the structural members, the ability of the structure to continue safely carrying traffic is better estimated. This will help MDOT in planning any future repairs and assessing any risks associated with the bridge. The effectiveness of repairs can be monitored by comparing the strain values before and after a retrofit is made, which will also aid in estimating remaining service life.

The pilot project at the Cut River Bridge is also intended to serve as a model that can be used at other bridge locations throughout Michigan. Lessons learned from this project will help with future implementations of SHM at other bridge sites. Given the remote location of the bridge, lessons learned would be applicable to any future on or off-grid SHMS. The same benefits to MDOT’s CV initiatives and core goals can also be accomplished in future applications.

## **2 Literature Review**

The literature review for this project has been divided into two parts. The first is a general overview of SHM projects that have been performed previously. The second part is related to estimating the dynamic impact factor of trucks crossing bridges. Estimation of dynamic impact factors from collected data is important in order to calibrate the finite element model established for the bridge. See Appendix O for literature review.

## **3 Devices and Equipment**

### **3.1 System Overview**

Data for the Cut River Bridge SHM project was collected from two locations. One location is approximately 2 miles east of the bridge along U.S. Route 2. This site consists of a weigh-in-motion (WIM) sensor, a data logger, and a traffic camera. A traffic camera and an antenna at this site are mounted on a 120 feet tower. This antenna transmits data from the WIM station to the bridge site. Equipment at the bridge consists of strain gauges, traffic sensors, pavement sensors, a traffic camera, and an Environmental Sensor Station (ESS). A concrete vault is used to house the data logger in addition to batteries for powering the equipment. A 70 feet high tower at the bridge site is used to mount the traffic camera, solar panels for charging the batteries in the vault, and a 3 feet dish antenna. The antenna transmits the data from the WIM station and sensors at the bridge site to an antenna at the top of the south Mackinac Bridge tower. The data is then transmitted to the Mackinac Bridge Authority (MBA) office as well as the MDOT St. Ignace Maintenance Garage. From the maintenance garage, the data is made available to access via internet connection. This system is shown schematically in Figure 4. Details of each component are described in further sections.

### **3.2 Weigh-in-Motion (WIM) Station**

A WIM Station was installed approximately 2 miles east of the Cut River Bridge along U.S. Route 2. This is used to record the weights and spacing of axles of passing trucks as well as other information. The WIM station installed is a Mettler Toledo Virtual By-Pass WIM. Figure 5 shows the WIM station tower used to mount the antenna, the pole used to mount the traffic camera, and data logger.

This system captures truck information while it passes across at normal highway speeds. This type of system was calibrated by the manufacturer according to ASTM E1318-09 to produce the static weights of the trucks. It was installed under the pavement, undetectable to motorists. Data from the WIM station is made available to special authorities such as the Michigan State Police (MSP).

The WIM station is powered via the electrical grid. The data is transmitted through the series of antennas as previously described and finally made available from any computer with an internet connection. A separate secured communication backhaul system for the WIM is used by MSP.

# Cut River Bridge Monitoring System Overview

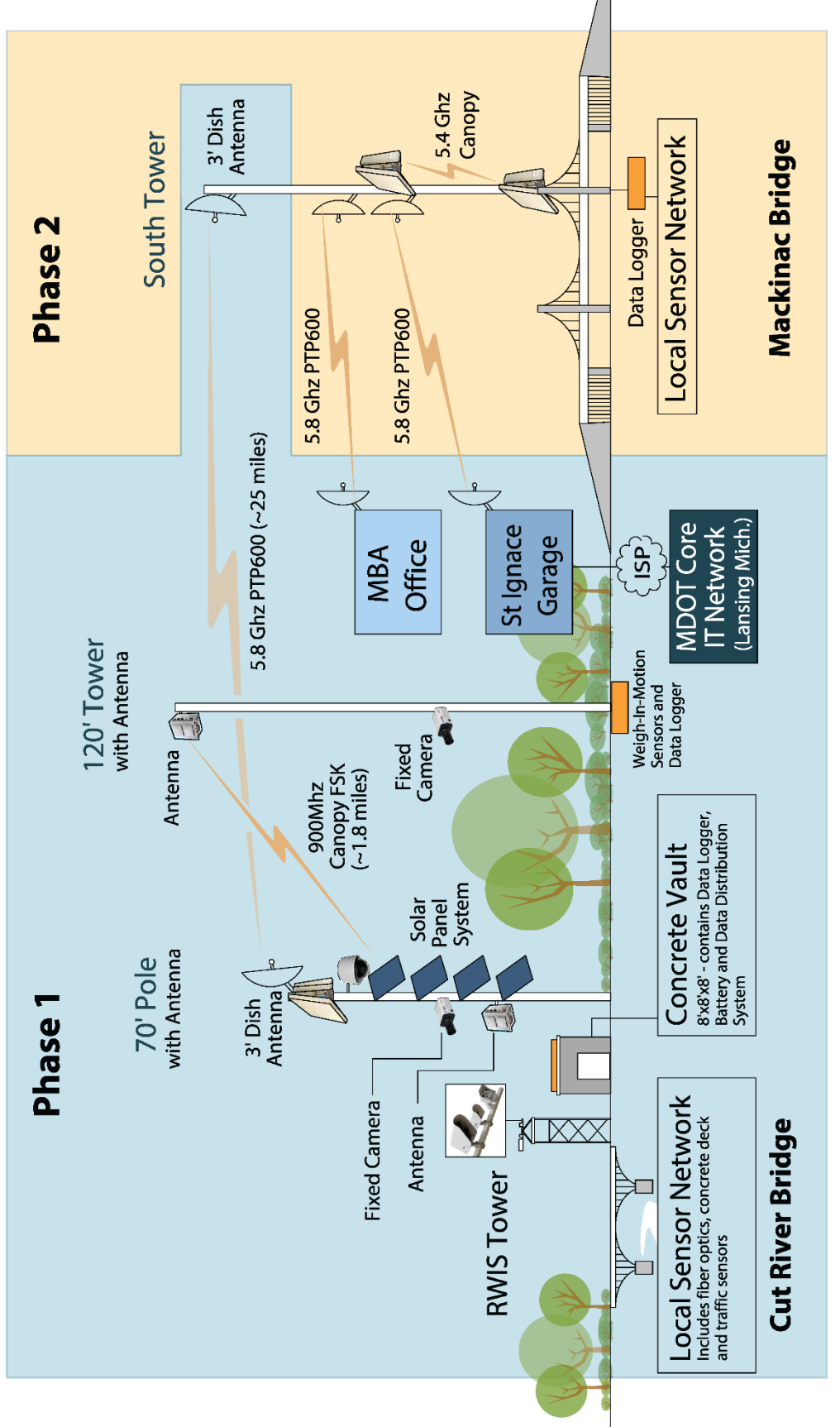


Figure 4: Cut River Bridge SHMS Overview



Figure 5: WIM Station

### 3.3 Strain Gauges & Temperature Sensors

Fiber optic strain gauges and temperature sensors are used for strain measurements. These sensors utilize fiber Bragg grating (FBG) technology. A fiber Bragg grating is an area within a fiber optic cable with a specific refractive index. As light passes through the fiber and the grating, the wavelengths are continuously measured. In an unstressed state, some light within a certain narrow band of wavelengths is reflected. When the bridge member, and thus the grating, is stressed, the refractive index changes and the band of reflected wavelengths is shifted. The strain in the bridge member is determined by measuring this shift in reflected wavelengths (Micron Optics, Inc., 2015).

Other types of strain gauges were available to use for this project such as electrical foil or vibrating wire gauges. Fiber optic strain gauges offered many advantages over these types such as:

- Greater strain range
- Longer fatigue life
- Not affected by surrounding electromagnetic waves
- Faster sampling rates

The strain gauges are manufactured by Micron Optics. The model numbers of the strain gauges and temperature compensation sensors are os3110 and os4100, respectively, shown in Figure 6. The strain gauge and the temperature sensors are designed to work together to provide accurate measurements of the strain in the bridge. The strain gauges measure strain experienced by the material. The strain readings are corrected for thermal effect through temperature sensors.



Figure 6: Strain Gauge (Top) and Temperature Sensor (Bottom)  
(Micron Optics, Inc., 2014)

The sensors were tested by the manufacturer for thermal cycling, high temperature and humidity soak, and fatigue testing with acceptable results. The operating temperature range is  $-40$  to  $120^{\circ}\text{C}$  ( $150^{\circ}\text{C}$  short-term). The strain limits are  $\pm 2,500 \mu\epsilon$ . The fatigue life is  $100 \times 10^6$  cycles,  $\pm 2,000 \mu\epsilon$ . See Appendix B and Appendix C for specifications of strain gauge and temperature sensors, respectively.

The strain gauges are located at the midspan of the two (2) diagonal and the two (2) top horizontal truss members in the panels adjacent to the east pier. The gauges were installed at both the inside and outside faces of each of these members at the north and south truss for a total of sixteen (16) locations. Temperature sensors were installed adjacent to the strain gauges only at one (1) diagonal and one (1) top horizontal truss member. They were installed on the outside face of each of these members at the north and south truss for a total of four (4) locations. Locations of the gauges and sensors are shown in Figure 7 through Figure 10.

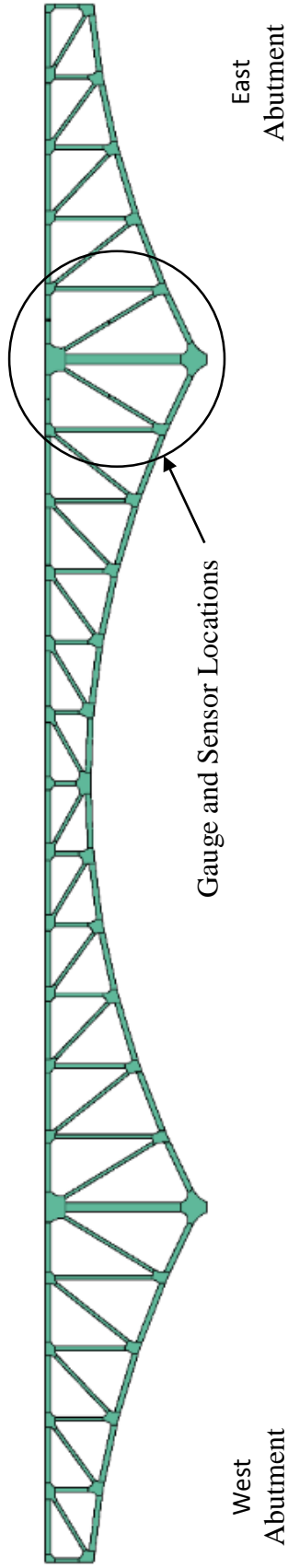


Figure 7: Strain Gauge Location Overview

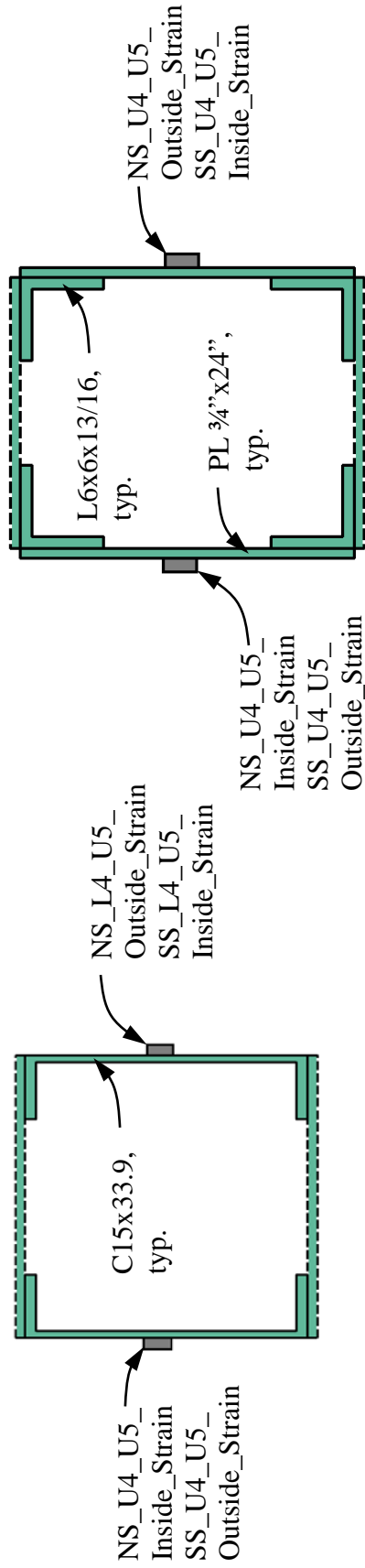


Figure 8: Cross Section of Member U4\_U5  
(North or South Truss Looking West)

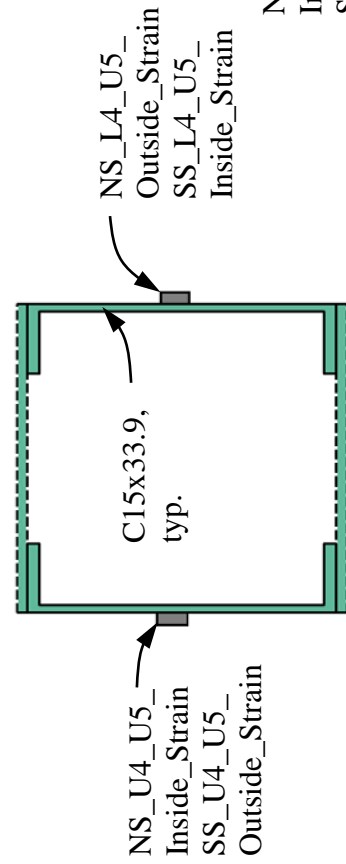


Figure 9: Cross Section of Member L4\_U5  
(North or South Truss Looking West)

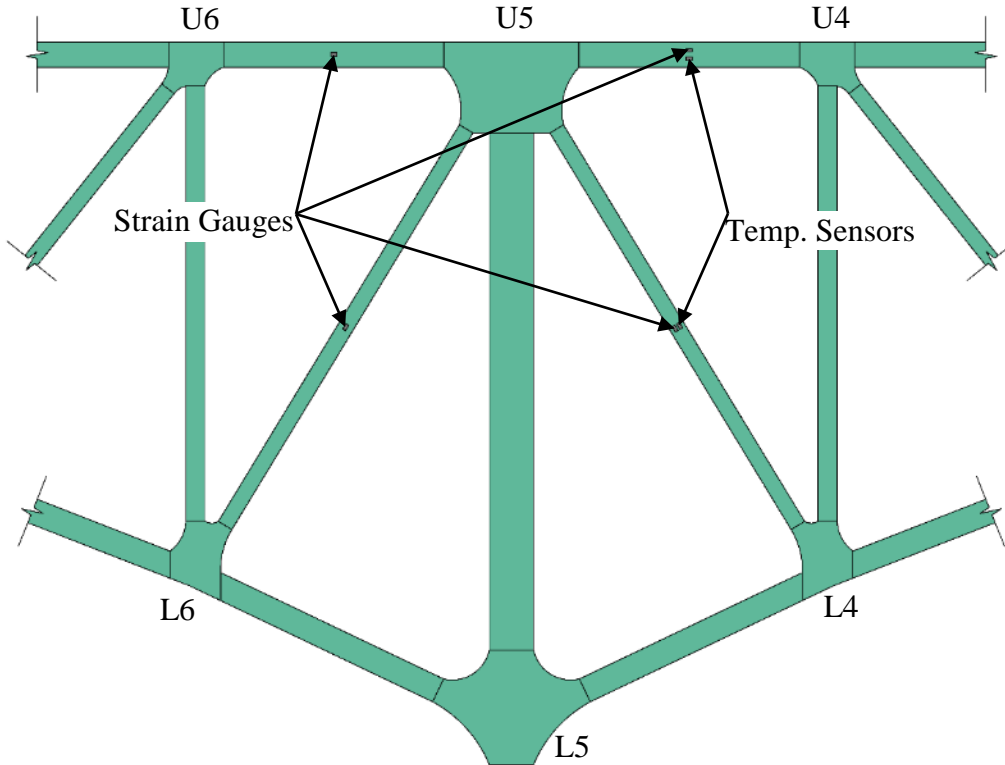


Figure 10: Strain Gauge Locations (Looking North)

A list of the sensors is as follows:

- |                           |                           |
|---------------------------|---------------------------|
| • SS_U4_U5_Outside_Strain | • NS_U4_U5_Outside_Strain |
| • SS_U4_U5_Inside_Strain  | • NS_U4_U5_Inside_Strain  |
| • SS_U4_U5_Outside_Temp   | • NS_U4_U5_Outside_Temp   |
| • SS_L4_U5_Outside_Strain | • NS_L4_U5_Outside_Strain |
| • SS_L4_U5_Inside_Strain  | • NS_L4_U5_Inside_Strain  |
| • SS_L4_U5_Outside_Temp   | • NS_L4_U5_Outside_Temp   |
| • SS_L6_U5_Outside_Strain | • NS_L6_U5_Outside_Strain |
| • SS_L6_U5_Inside_Strain  | • NS_L6_U5_Inside_Strain  |
| • SS_U5_U6_Outside_Strain | • NS_U5_U6_Outside_Strain |
| • SS_U5_U6_Inside_Strain  | • NS_U5_U6_Inside_Strain  |

“SS” strain gauges are located on the south truss, while “NS” strain gauges are located on the north truss. Since the sensors were mounted on steel surfaces, they were installed by spot welding. Per the manufacturer recommendations, the surface of the steel was prepared by

removing the paint and thoroughly cleaning the surface. The sensors were installed and then covered and protected from the outside elements (strain gauge covered with tape and brushed over with organic zinc rich primer). An installed strain gauge and temperature sensor are shown in Figure 11.

As previously mentioned, as light passes through the fiber optic cable and through the sensor its wavelength changes as the strain in the FBG sensor, and thus in the bridge member, changes. The Micron Optics sm130 Optical Sensing Interrogator is connected to the sensors and used to continuously measure these wavelengths. It is powered by a 12V DC solar power system located in the concrete vault. The data from the interrogator is transmitted through the series of antennas as previously described and finally made available from any computer with an internet connection. The interrogator is shown in Figure 12 with specifications given in Appendix D.

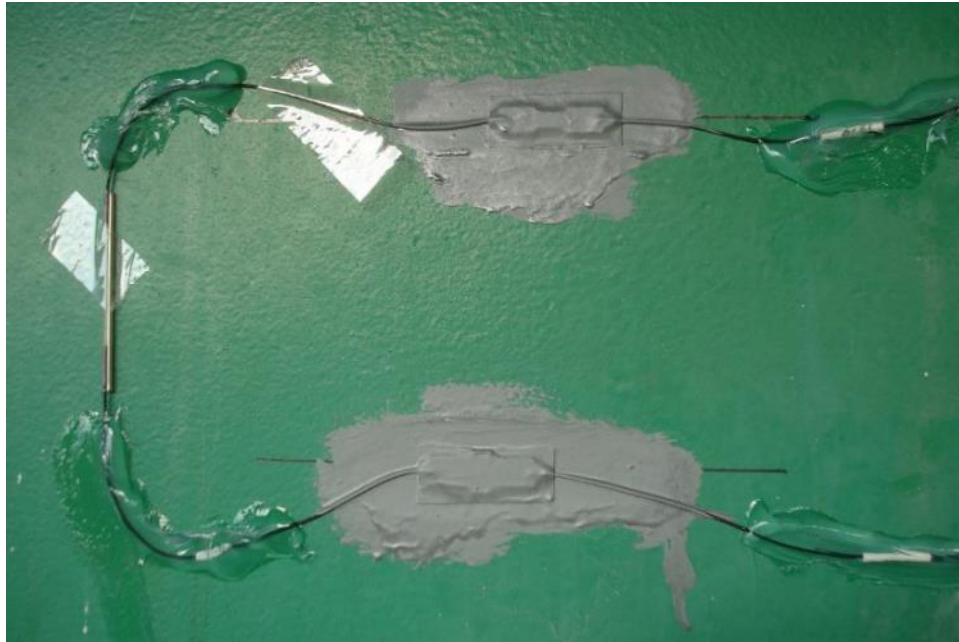


Figure 11: Installed Strain Gauge and Temperature Sensor



Figure 12: Optical Sensing Interrogator sm130  
(Micron Optics, Inc., 2014)

### 3.4 Traffic Sensors

Traffic sensors were installed at the bridge site to count the vehicles that cross the bridge. Four (4) Sensys VSN240 traffic sensors were installed in the pavement east of the bridge with two (2) sensors in each lane. Each sensor transmits data wirelessly in real-time to a nearby Sensys AP240 access point. Two-way communication with the access point allows firmware for the sensor to be updated as well as transmitting traffic data. The sensors require very little power which is provided by internal, non-replaceable Li-SOCl<sub>2</sub> 3.6V battery packs with an average life of approximately 10 years. The access point is powered via the solar power system located in the concrete vault through a 48V PoE connection. The operating temperature range of the sensors and access point is -40°F to 176°F. The wireless nature of the sensors provided a simple installation by core-drilling into the pavement, placing the sensor inside, and then filling the core with epoxy. Traffic sensor installation is shown in Figure 13 and Figure 14. The specifications of the sensors are included in Appendix E. The per-lane data processing capabilities of the access point include: counts (volume), occupancy, average and median speeds, binned speeds and vehicle lengths over selectable time intervals. The per-vehicle data processing capabilities include: initial vehicle detection time, gap, speed, and length. The data from the access point is then transmitted through the series of antennas and finally made

available from any computer with an internet access. The access point is shown in Figure 15 with specifications included in Appendix F.



Figure 13: Traffic Sensor



Figure 14: Installed Traffic Sensor



Figure 15: Traffic Sensor Access Point



### 3.5 Environmental Sensor Station

An Environmental Sensor Station (ESS) was installed at the bridge site to provide data regarding the ambient weather conditions at the bridge. Equipment installed on the ESS tower is able to measure air temperature, relative humidity, wind speed and direction, precipitation accumulation, and two (2) surface temperatures. All devices at the ESS are powered via a self-contained solar power system for all sensors attached to the ESS. The equipment was provided by Campbell Scientific and includes:

- Vaisala HMP45C Temperature and Relative Humidity Probe with 41003-5 Solar Radiation Shield, shown in Figure 17. Specifications are included in Appendix G.
- RM Young 05103 Wind Monitor, shown in Figure 18. Specifications are included in Appendix H.
- Texas Electronics TE525WS Rain Gauge, shown in Figure 19. Specifications are included in Appendix I.

Two (2) IRS21 Lufft Intelligent Road Sensors were installed in the bridge deck approximately 15 feet from the east abutment with one sensor in each lane as shown in Figure 16 above. The sensor power and data leads were trenched in the roadway and connected to a data logger on the ESS tower. The sensors measure road surface temperature, up to two (2) sub-surface temperatures, salt concentration, water film height, and road condition (dry, damp, wet, ice, snow, residual salt, freezing). The salt concentration measurements are used to determine the freeze temperature. A pavement sensor during installation is shown in Figure 20. Specifications are included in Appendix J.

The data logger is the CR1000 by Campbell Scientific. The operating temperature range for the data logger is -13°F to 122°F. The data logger is shown in Figure 21. Specifications of the data logger are included in Appendix K. Data from the ESS is transmitted to the data logger on the tower and then through series of antennas and finally made available from any computer with an internet access. The ESS tower is shown in Figure 22.

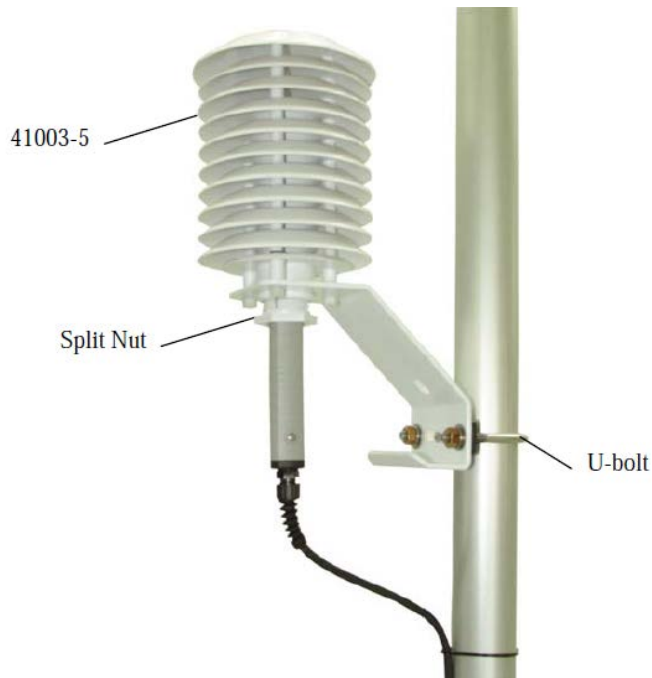


Figure 17: Temperature and Relative Humidity Probe  
(Campbell Scientific, Inc., 2015)

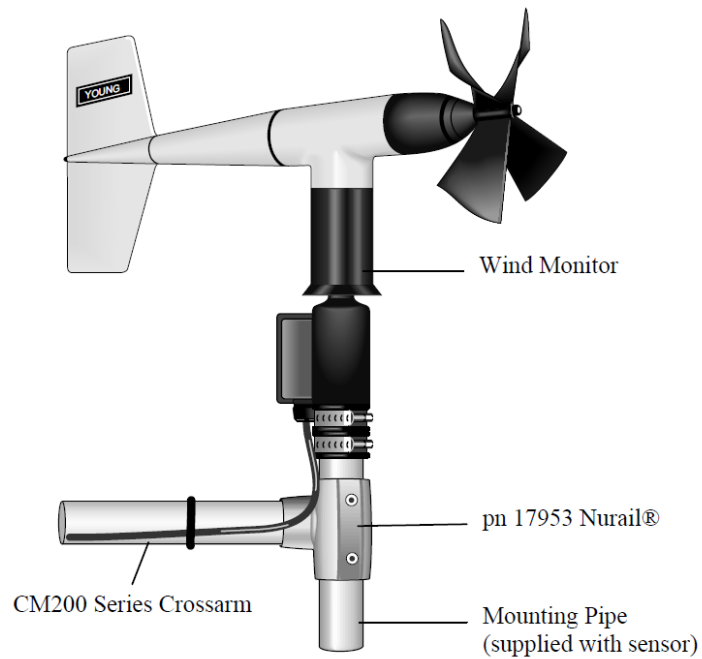


Figure 18: Wind Monitor  
(Campbell Scientific, Inc., 2015)

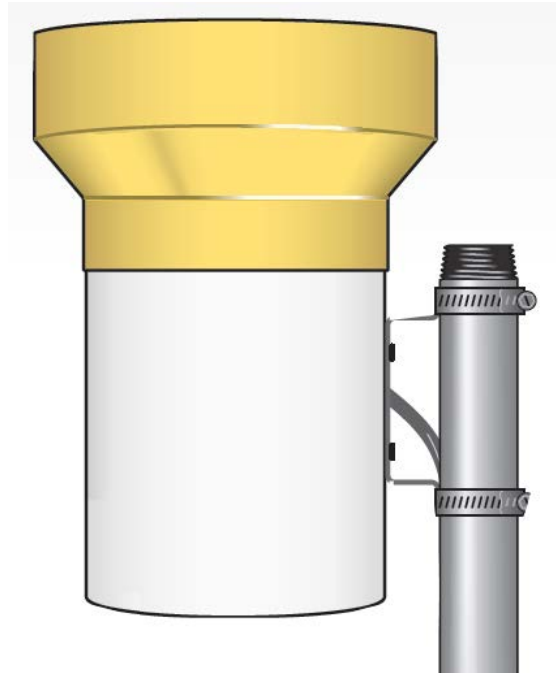


Figure 19: Rain Gauge  
(Campbell Scientific, Inc., 2015)



Figure 20: Lufft Intelligent Road Sensor

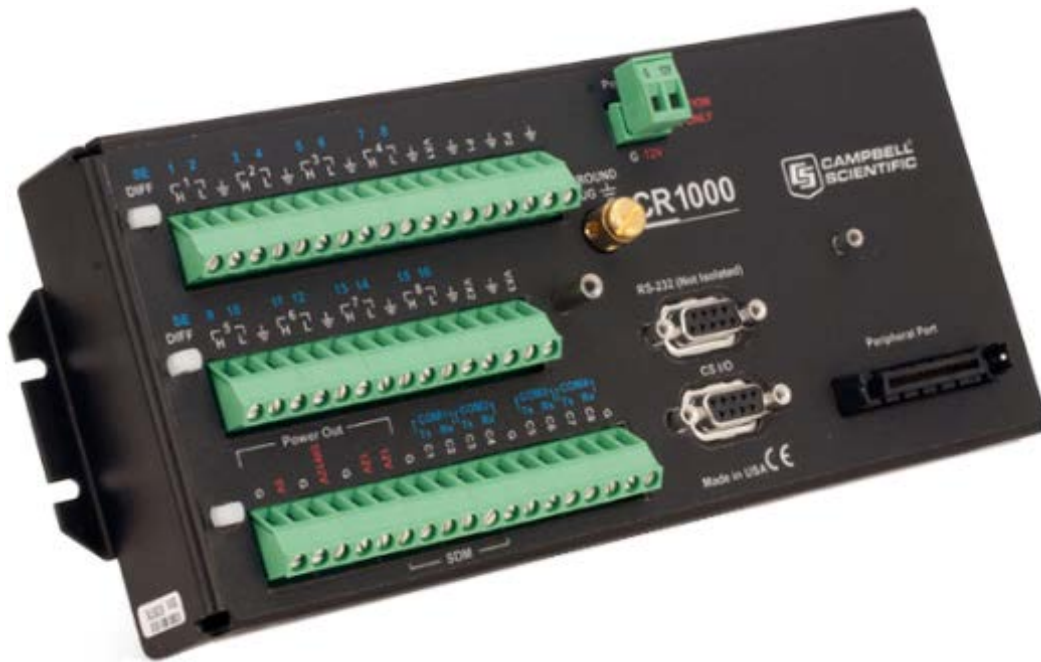


Figure 21: ESS Data Logger  
(Campbell Scientific, Inc., 2015)

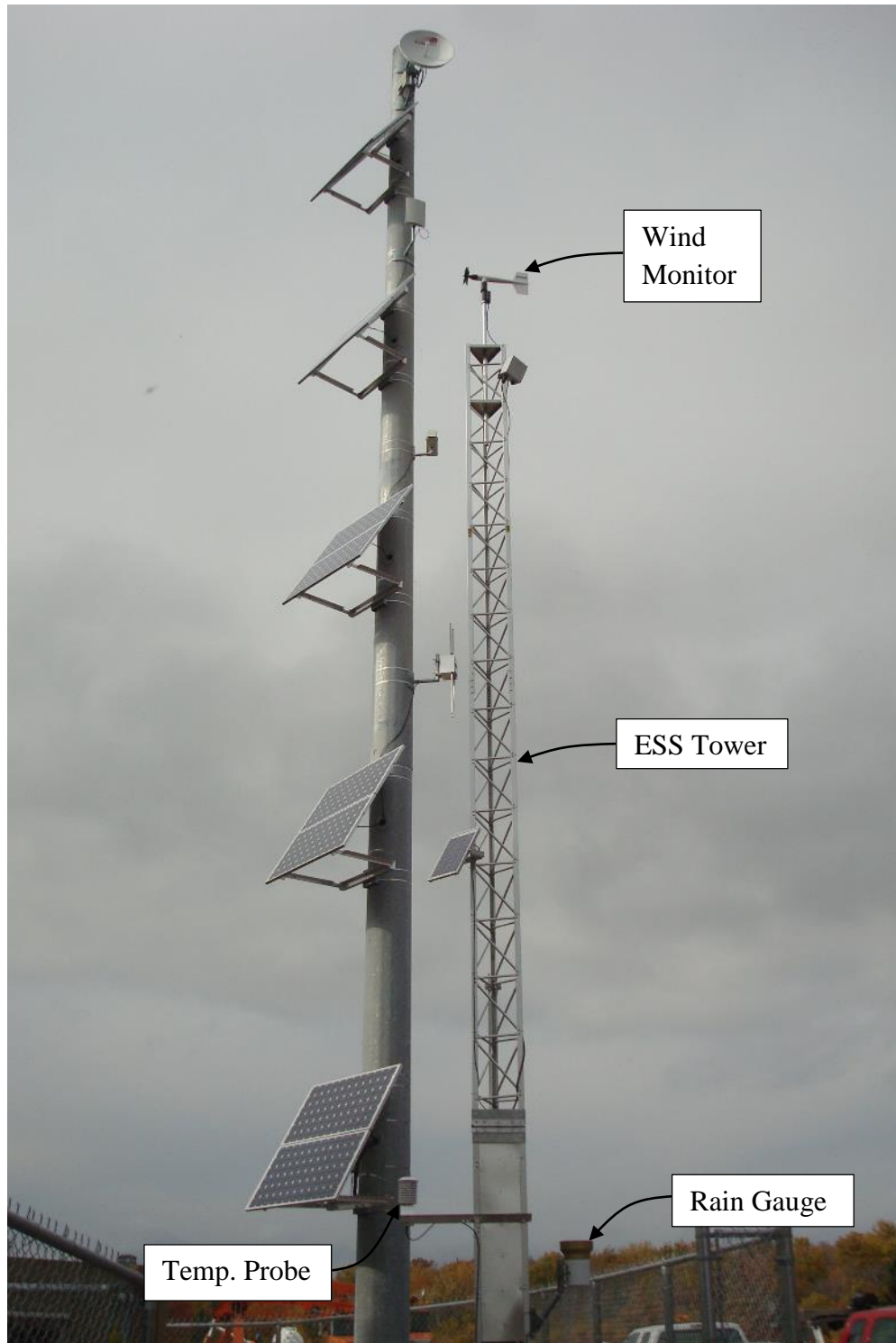


Figure 22: Towers at Bridge Site

### 3.6 Traffic Cameras

Traffic cameras were installed to provide a real-time visual of the site and provide verification of conditions observed by the equipment. The cameras were installed at two (2) locations: the bridge site and the WIM station. The camera at the bridge site is the NetCamSC ip camera shown in Figure 23 with a screenshot shown in Figure 24. This camera has a resolution of 5 megapixels and an operating temperature range of -40°F to 122°F. Specifications are included in Appendix L. The camera is powered by a 48V PoE connection to the solar power system in the concrete vault. The camera at the WIM station is the Axis 211M as shown in Figure 25 with a screenshot shown in Figure 26. This camera has a resolution of 1.3 megapixels and an operating temperature range of 32°F to 113°F. Specifications of the camera are included in Appendix M . The live video feeds are then transmitted through the series of antennas and finally made available from any computer with an internet access.



Figure 23: Traffic Camera at Bridge Site  
(StarDot Technologies, 2015)



Figure 24: Bridge Camera Screenshot



Figure 25: Traffic Camera at WIM Station  
(Axis Communications, 2015)

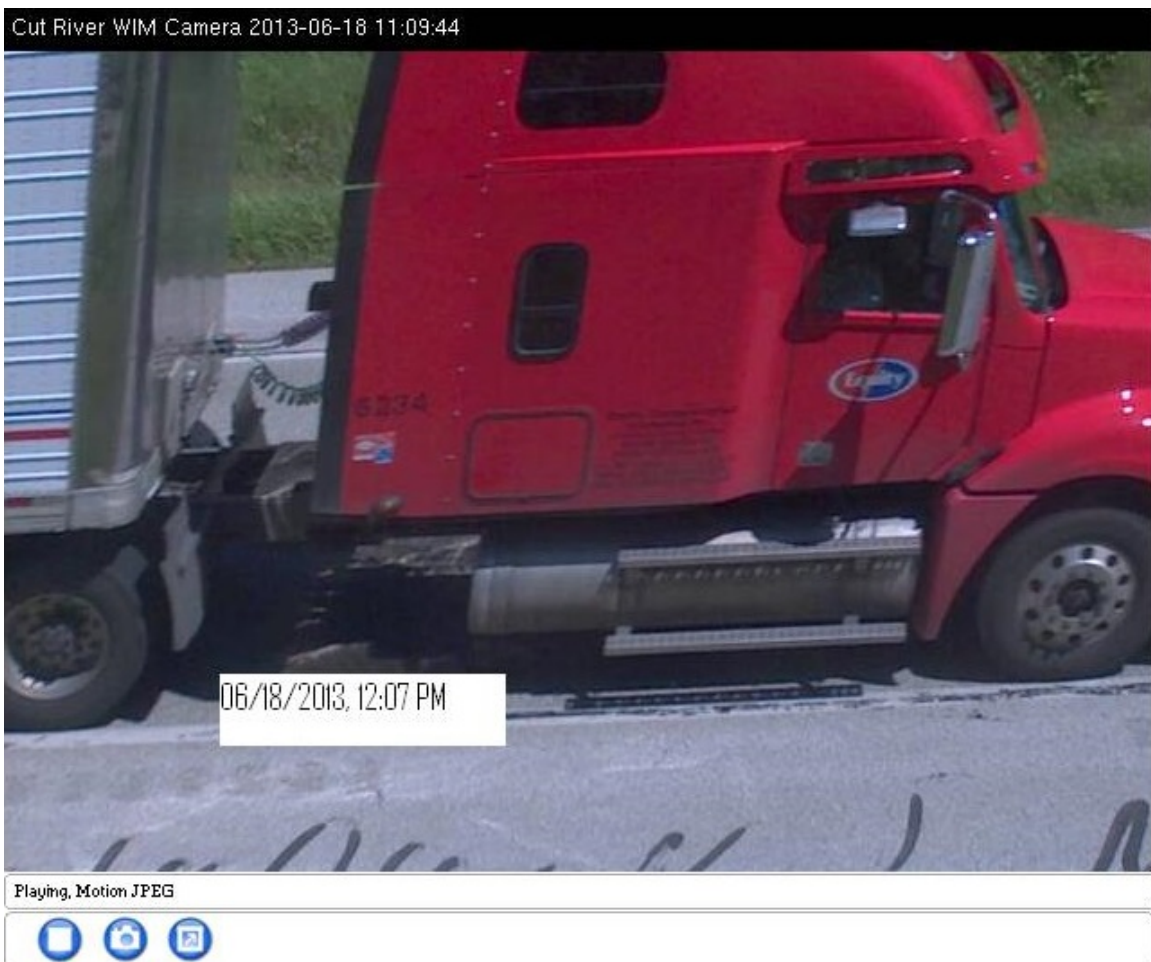


Figure 26: WIM Station Camera Screenshot

## **4 Data Collection and Processing**

### **4.1 Data Collection Overview**

All data from the Cut River Bridge was able to be collected from any computer with internet access. The data was collected from a computer located at the Engineer's office. This computer was equipped with the necessary software to collect data from the site. It was also equipped with a Control DeviceMaster, shown in Figure 28, in order to obtain the data from the WIM station. Specifications for this device are included in Appendix N. This device acts as an adapter between the incoming Ethernet connection and the serial port connection which is used by the WIM station software. The objective of the data collection process was to be able to obtain data regarding weights and axle configurations of the trucks that cross the bridge as well as the strain in the bridge members caused by these trucks. After the data collected, it was then processed to correlate the truck information with the strain information. This information is useful to make comparisons between actual loads experienced by the bridge to the design loads according to current AASHTO and MDOT standards. Data regarding traffic, pavement, and weather conditions was also collected throughout this process. Details of each component are described in further sections.

### **4.2 Truck Data**

#### **4.2.1 Introduction**

The truck information from the WIM station was collected throughout the data collection phase of this project. The information collected included lane, time truck crossed the WIM, axle weights, gross weight, number of axles, axle spacing, total length, and truck class. This data is used to gather information with regard to trucks that currently cross the bridge.

#### **4.2.2 Methodology: Data Collection and Processing**

Truck information was acquired using WPC software by International Road Dynamics (IRD). This software collects data from the WIM station and also provides a message if a truck weight exceeds a threshold value. The WPC software is not able to save collected data and therefore, another software, Advanced Serial Data Logger by AGG Software, is used to save the collected data. A screenshot showing WPC and Advanced Serial Data Logger is shown in

Figure 27. The data was saved in a spreadsheet with each daily recorded data saved in a separate file. This data was then compiled into one spreadsheet which contained all data collected from the WIM station.

The speed of the truck crossing the WIM station was used to calculate the time the same truck crosses the bridge. The WIM station is located approximately 2 miles east of the bridge and based on the recorded truck speed, the travel time to the bridge was determined. To determine the time a truck crossed the bridge, the travel time was added to the time it crossed the WIM station if it was travelling westbound. Similarly, the travel time was subtracted from the time it crossed the WIM station if the truck was travelling eastbound. This time is used when correlating the WIM station data with the strain gauge data.

### 4.2.3 Collected Data

Throughout the course of data collection, data from approximately 16,000 trucks was collected from the WIM station. The data collected for each truck included:

- Travel lane
- Time
- Number of axles
- FHWA vehicle classification
- Gross weight
- Overall length
- Speed
- Spacing between each axle
- Weight of each axle

The data collected shows a wide variety of trucks that crossed the bridge. The following figures show the data collected from May 2013 until September 2014.

Figure 29 shows the number of trucks per lane. As shown, the volume of truck traffic was equally distributed between the two lanes of the bridge.

The average truck weight in the eastbound and westbound lanes were 45.1 kips and 52.1 kips, respectively. The westbound lane was subjected to trucks with an average weight 7.0 kips higher than those in the eastbound lane.

Figure 30 shows the hourly truck traffic volume. As shown, a large percentage of truck volume traffic occurs during the day and tapered down throughout the night. The peak truck volume occurs between 10:00 AM and 3:00 PM.

Figure 31 shows the truck volume per number of truck axles. As shown, most of the trucks that cross the bridge are 5-axle trucks. There are also a significant volume of 2-axle trucks.

Figure 32 shows the number of trucks per FHWA classification. See Appendix A for FHWA vehicle classification definitions. As shown, most of the trucks that cross the bridge are Class 9 which corresponds to 5-axle trucks shown in Figure 28. There is also a significant volume of Class 5 trucks which corresponds to 2-axle trucks shown in Figure 28. A classification of 15 indicated that the WPC software was unable to detect the classification.

Figure 33 shows the number of truck volume per gross weight. Majority of trucks crossed the bridge were under 80 kips.

Figure 34 shows the variation of truck gross weight per the number of axles. Data of the Michigan legal trucks, AASHTO H-15 truck, and AASHTO HS-20 truck are also plotted. For a given number of axles, the majority of trucks that cross the bridge have gross weights that are less than the average Federal or Michigan truck. Approximately 96% of the 2-axle trucks have a gross weight that is less than the H-15 truck weight. Also, 100% of the 3-axle trucks have a gross weight that is less than the HS-20 truck weight. For 9- and 10-axle trucks, 69% and 79% of the trucks have a gross weight that is less than the average Michigan legal truck weight, respectively.

Figure 35 shows the truck gross weight per overall truck length. Also, Michigan legal trucks in addition to Federal trucks are included for comparison. As shown, the Michigan legal trucks provide an upper bound compared to the trucks that crossed the bridge. Truck data of approximately 16,000 trucks were collected from the WIM station. Approximately 30 trucks that crossed the bridge have gross weights more than the heaviest Michigan legal truck #25 (164 kips gross weight).

Figure 36 shows truck volume per overall length. As shown, most trucks cross the bridge are less than 80 feet long.

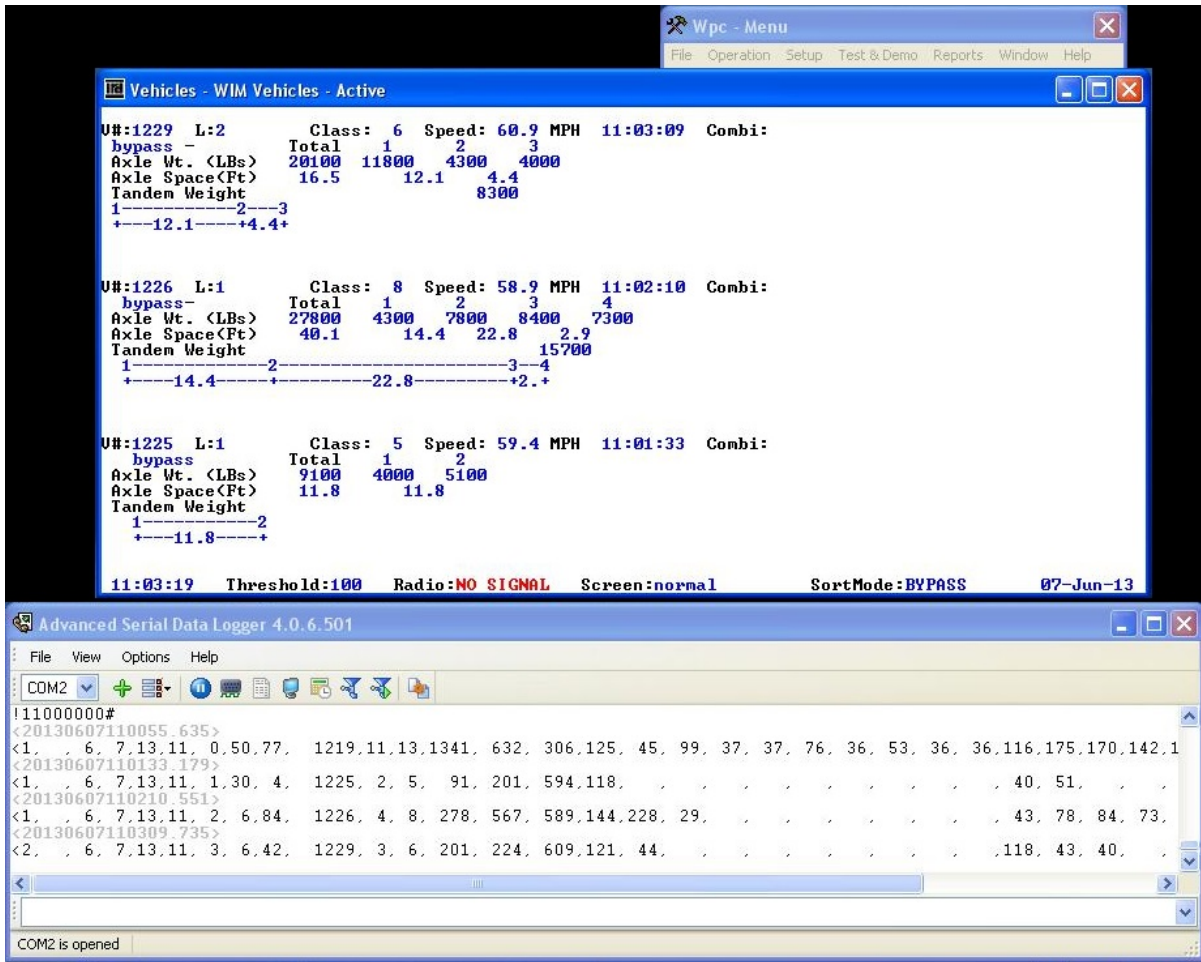


Figure 27: WPC and Advanced Serial Data Logger Screenshot



Figure 28: Control DeviceMaster  
(Comtrol, 2015)

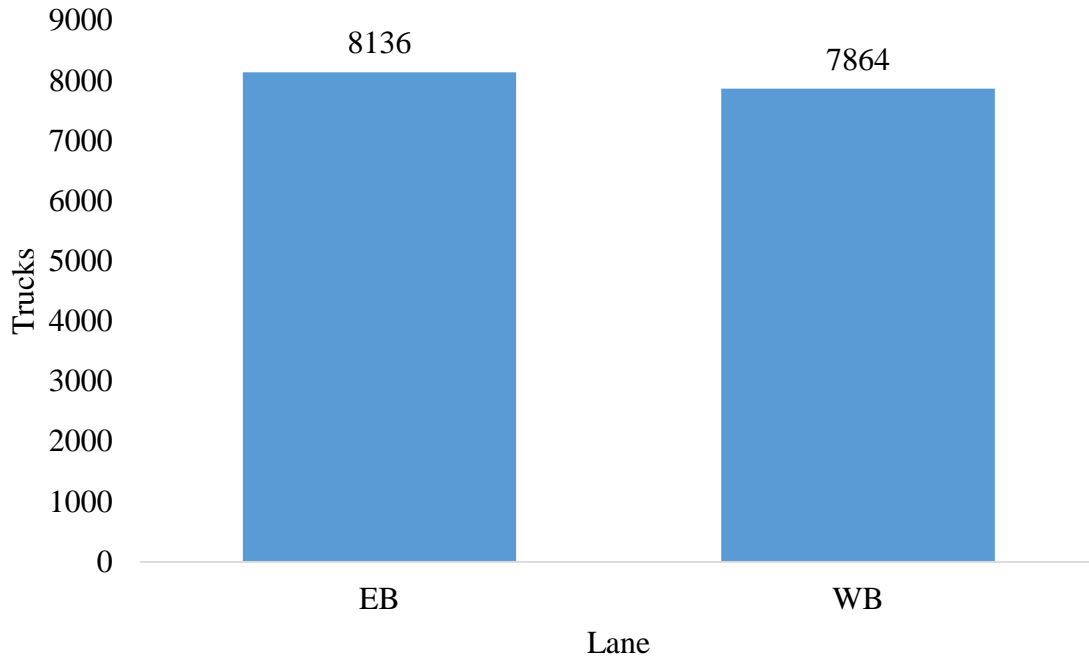


Figure 29: Number of Trucks per Lane

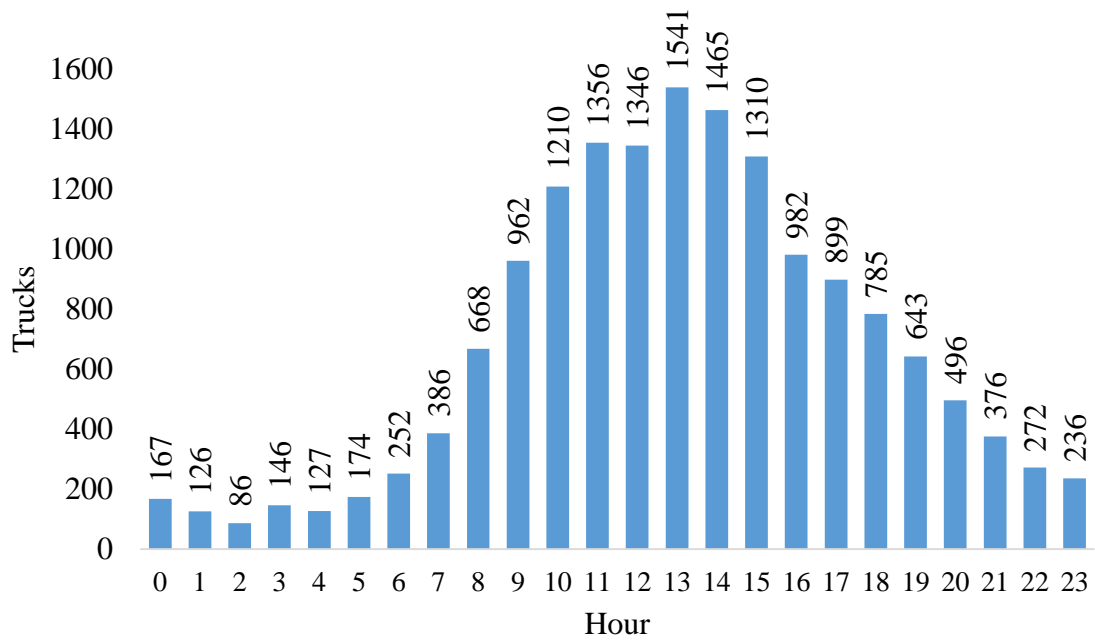


Figure 30: Hourly Truck Traffic Volume

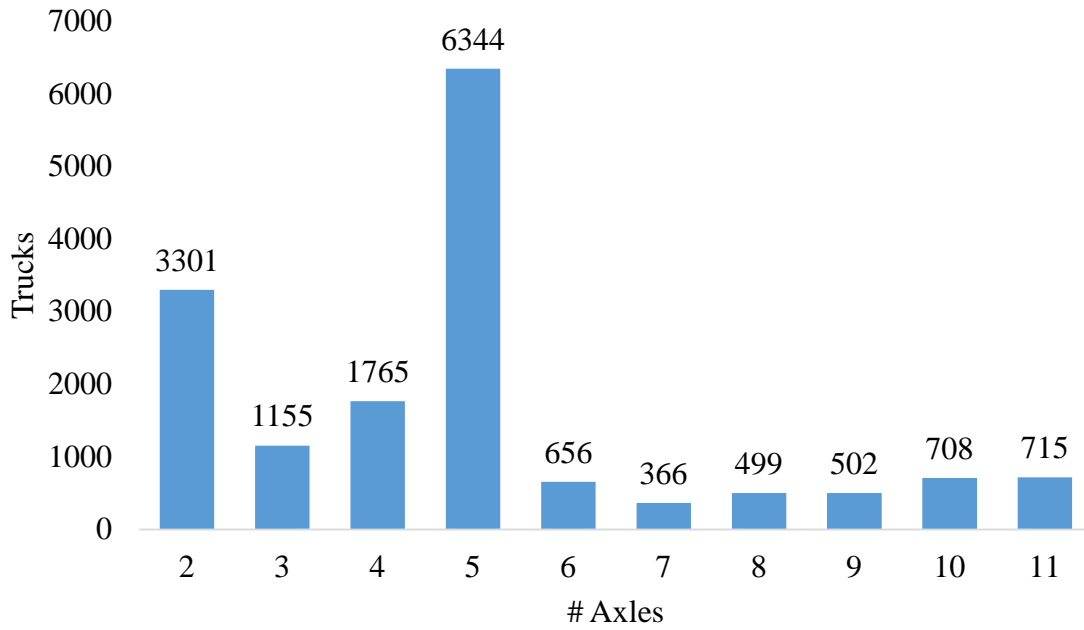


Figure 31: Truck Volume per Number of Truck Axles

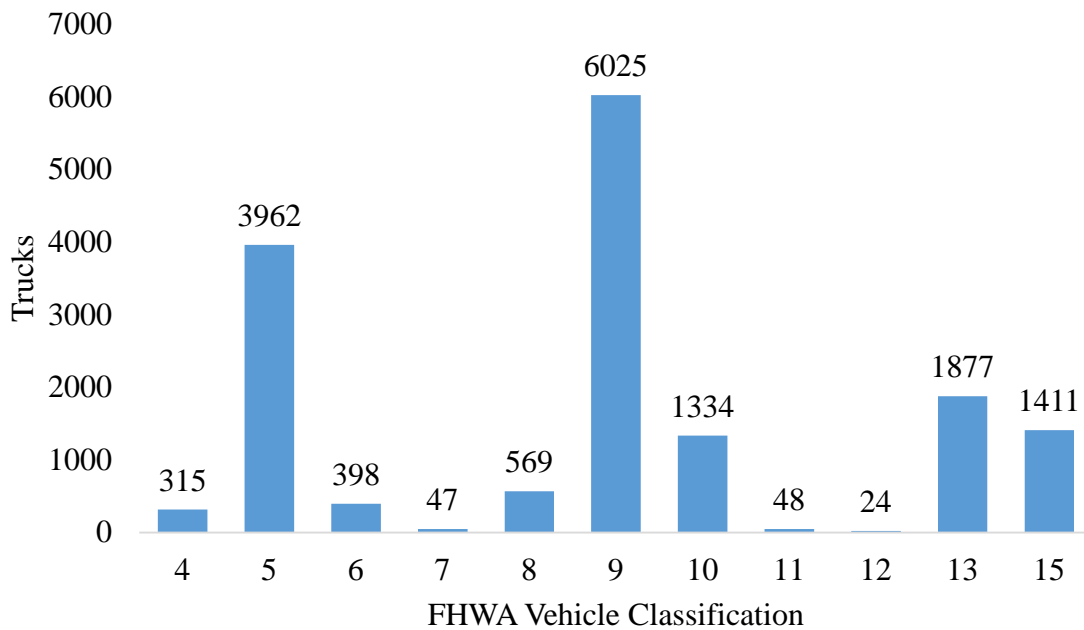


Figure 32: Volume of Trucks per FHWA Vehicle Classification

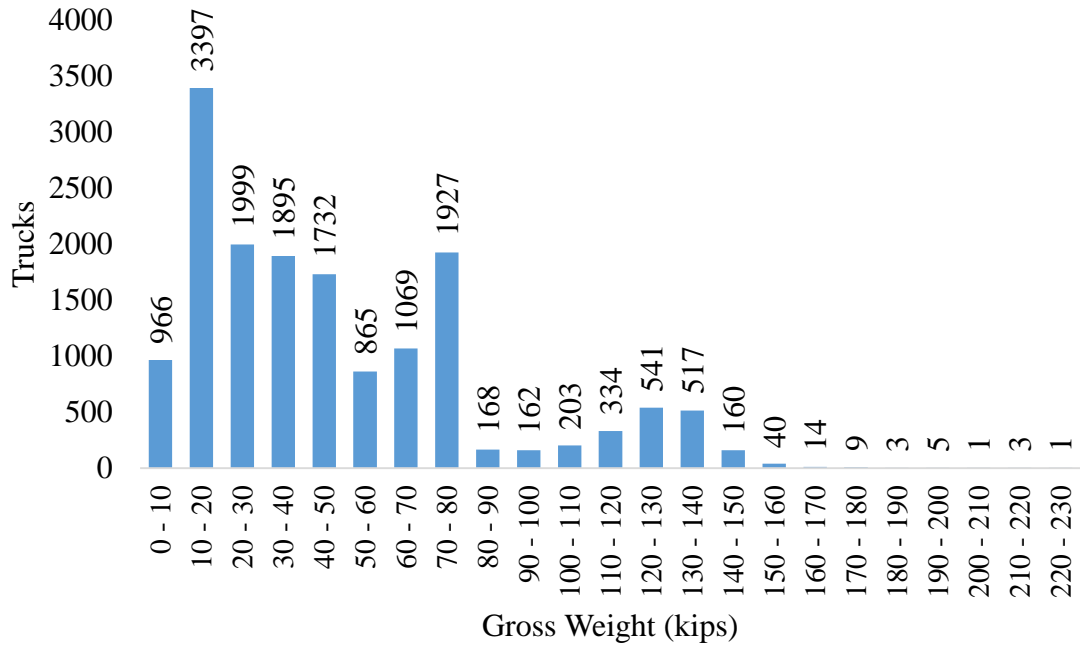


Figure 33: Truck Volume per Truck Gross Weight

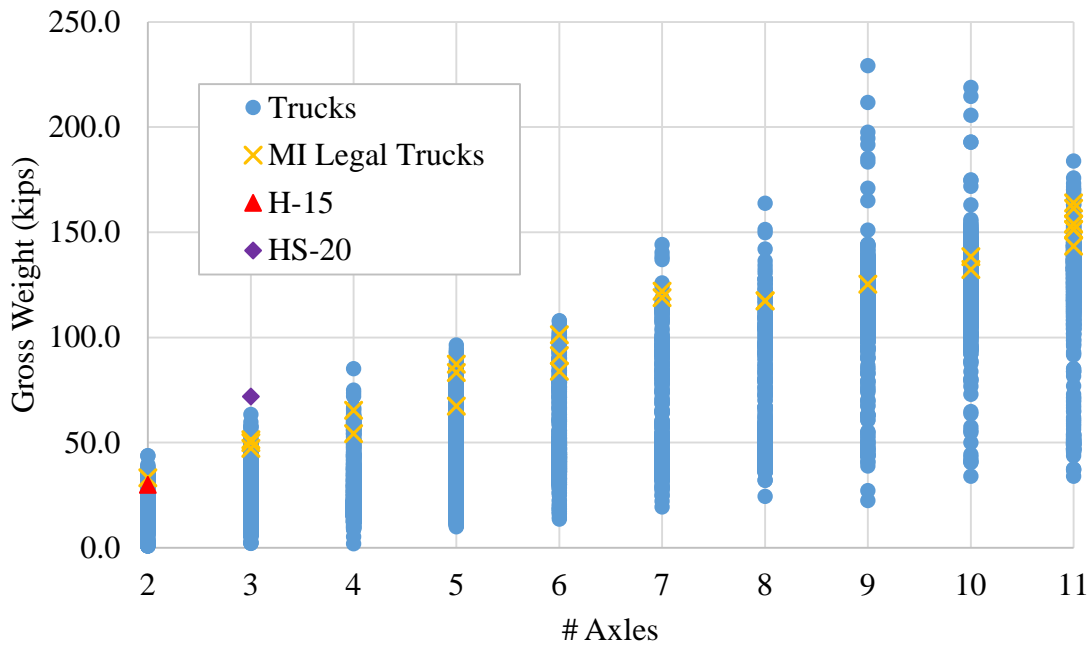


Figure 34: Gross Weight per Number of Axles

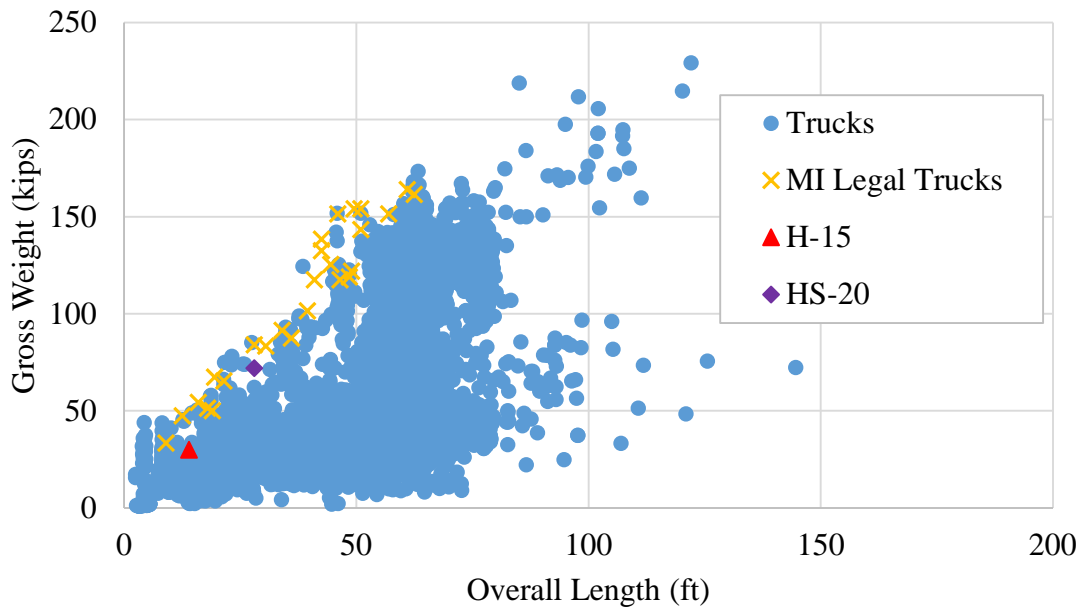


Figure 35: Gross Truck Weight per Overall Truck Length

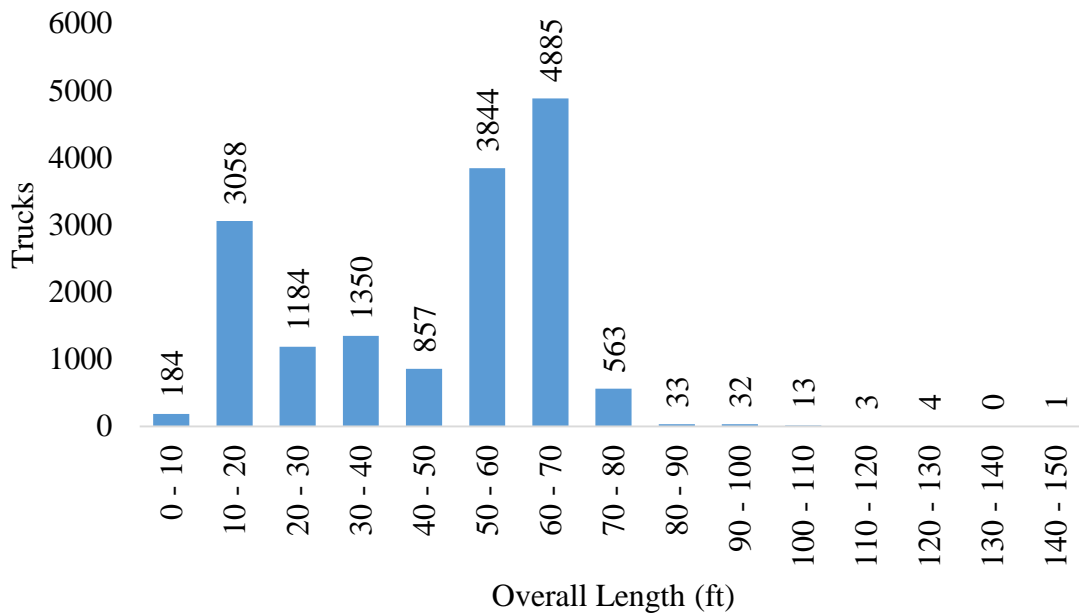


Figure 36: Truck Volume per Overall Truck Length

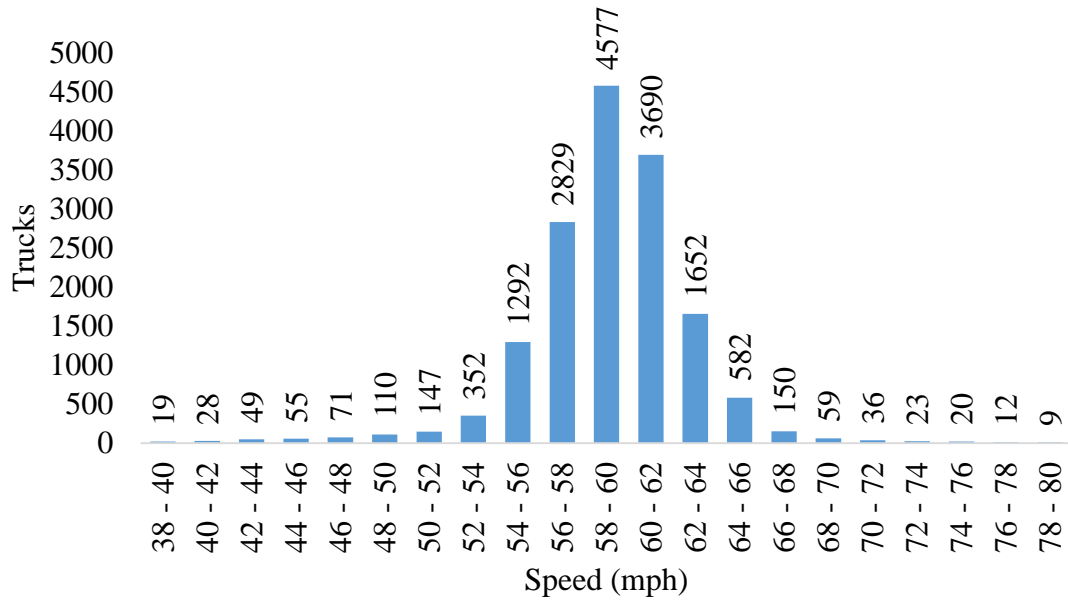


Figure 37: Truck Volume per Speed

Figure 37 shows truck volume per speed. Majority of trucks crossed the bridge between 52-68 mph. The average speed was 59.0 mph with a standard deviation of 6.8 mph. The figure is only showing data in the range of the mean within three standard deviations.

#### **4.2.4 Summary and Discussion**

The truck information collected from the WIM station show that there is a wide variety of trucks cross the bridge. This information was used to determine the characteristics of these trucks. Comparisons were made with the AASHTO Federal trucks and the Michigan legal trucks. It was determined that an equal volume of trucks travel in each direction. The peak hour was determined to be from 10:00 AM to 3:00 PM. Most of the trucks are 5-axle or 2-axle trucks corresponding to an FHWA classification of 9 and 5. Most of the trucks have a gross weight of under 80 kips and an overall length of under 80 feet. Majority of trucks were traveling between 52 and 68 mph. Axle spacing varied significantly from AASHTO or Michigan legal trucks. Most of the axle weights were less than those of AASHTO or Michigan legal trucks.

This information can be useful to determine if the design trucks are a good representation of the actual trucks that cross the bridge. As shown in Figure 35, the Michigan legal trucks seem to provide a good representation of the maximum gross weight of trucks that cross the bridge.

### **4.3 Strain Gauge Readings**

#### **4.3.1 Introduction**

The strain information from the bridge was also collected throughout the data collection phase of the project. This information was used to determine the live load strain in the bridge members caused by a passing truck. These values were then compared to the maximum allowable strain to determine if the bridge members were overstressed.

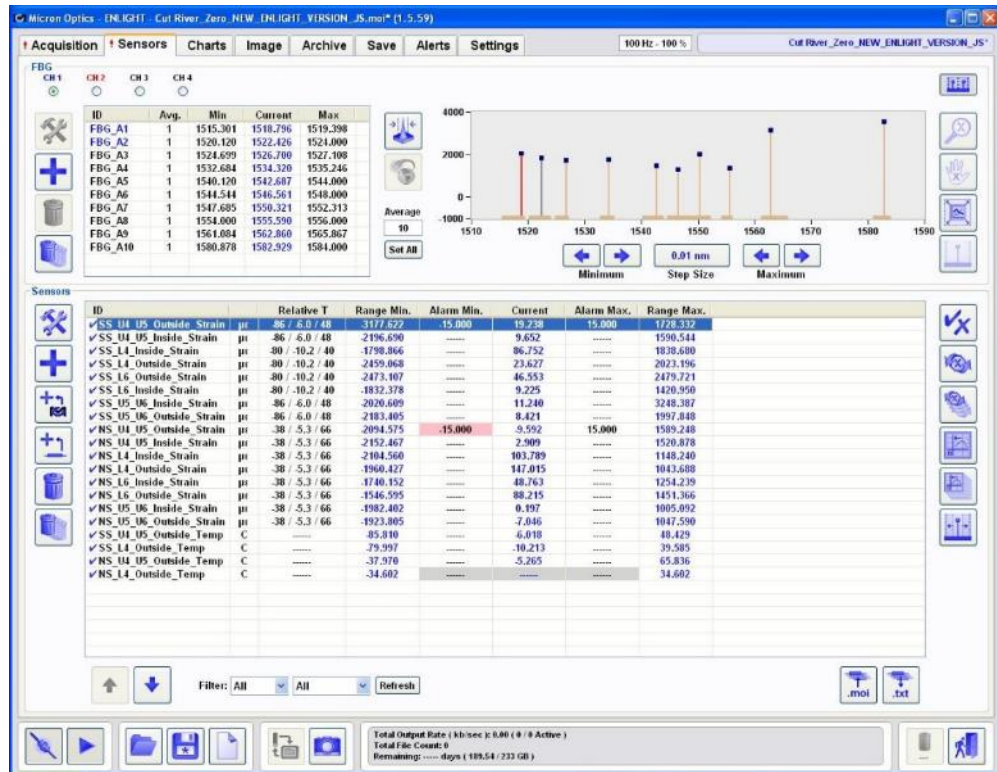


Figure 38: ENLIGHT Screenshot (Strain Values)



Figure 39: ENLIGHT Screenshot (Plot of Strain Values)

### 4.3.2 Methodology: Data Collection and Processing

Strain information from the bridge was collected using ENLIGHT software from Micron Optics. A screenshot showing the real-time strain values is shown in Figure 38 and a real-time plot of the strain values in Figure 39. ENLIGHT was continuously monitoring the strain in the bridge members, however the strain information was saved only when a truck crossed the bridge. A trigger event in ENLIGHT was created that began saving strain data once it exceeded a predetermined threshold. The threshold used for this project was  $15 \mu\epsilon$  on the NS\_ or SS\_U4\_U5\_Outside\_Strain sensor. This threshold was found to be sufficient to save data for a truck. The strain was recorded for a period of time to ensure strain data history is captured while the truck is crossing the bridge. The strain data for each trigger event was saved in a separate text file. ENLIGHT has the capability to send a data file via email if the strain reaches above a specified threshold strain value, which can alert the Engineer that the bridge member was nearly overstressed.

The absence of a temperature sensor at each strain gauge caused the strain readings to increase slowly over time. Eventually, the strain readings would exceed the limit set for the trigger event in ENLIGHT causing data to be continuously saved. To overcome this issue, a correction factor was used in the program to ensure strain readings maintained values close to zero until a truck crossed the bridge. The correction factor applied to the data helped in recording data, with reasonable accuracy, from trucks crossing the bridge. However, long term effect was not able to be captured as strain data was continuously normalized.

### 4.3.3 Collected Data

Each text file for the strain data was processed to determine the maximum strain caused by each truck. The values for each strain gauge were normalized by subtracting the initial value. Then, the values from the gauges on the same member were averaged. From these values, the maximum strain at each member was determined and saved in a spreadsheet along with the corresponding time that data was recorded. The maximum allowable live load strain was determined to be  $300 \mu\epsilon$  for the top chord members and  $231 \mu\epsilon$  for the diagonal members.

Figure 40 shows time vs strain history for each strain gauge for one truck crossing the bridge. This was a 5-axle truck with a gross weight of 52.1 kips and an overall length of 64.3 feet.

Maximum strains for all trucks that crossed the bridge between May 2013 and September 2014 for the top chord members and diagonals are shown in Figure 41 and Figure 42, respectively. As shown, the maximum strains are  $52.5 \mu\epsilon$  for the top chord members and  $117$

$\mu\epsilon$  for the diagonal members. The recorded strain values are well below the maximum allowable live load strain for each member. These measured strains correspond to a maximum live load stress for the SS\_U5\_U6 and NS\_L4\_U5 members of 1.5 ksi and 3.4 ksi, respectively. The design live load stresses for these members, as shown in the existing plans, are 3.9 ksi and 4.6 ksi, respectively. Dead load stresses for the SS\_U5\_U6 and NS\_L4\_U5 members are 11.1 ksi and 13.1 ksi, respectively. The steel used in the bridge has a yield strength of 33 ksi with an allowable stress of 18 ksi. This indicates that the bridge was operating at a safe level throughout the data collection period.

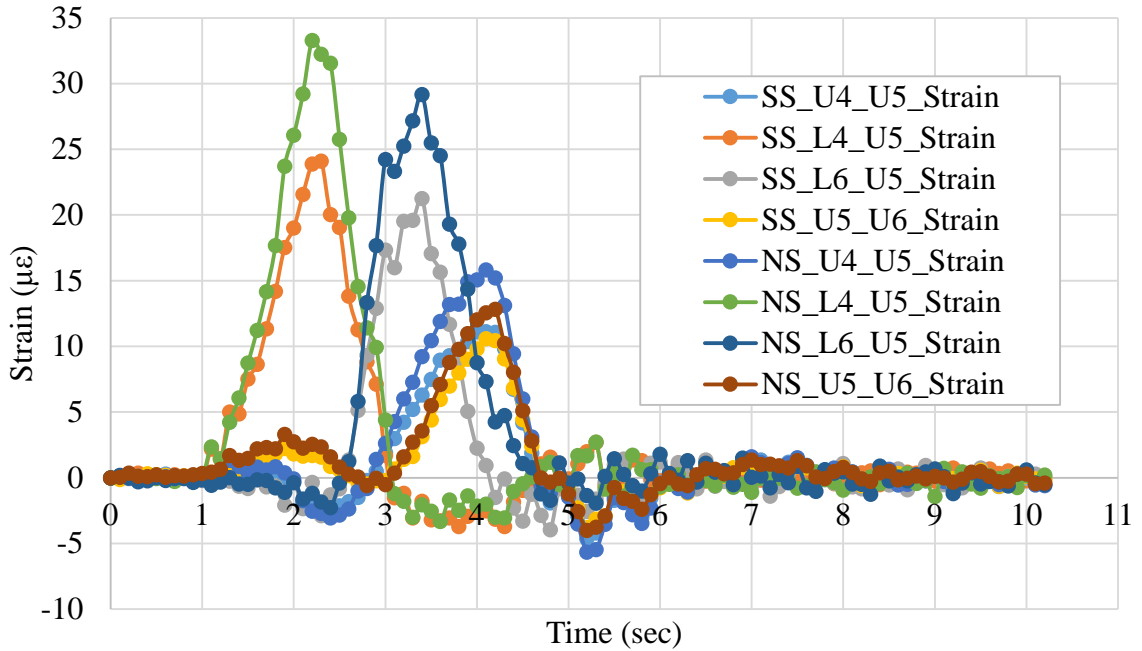


Figure 40: Example Graph of Strain vs Time

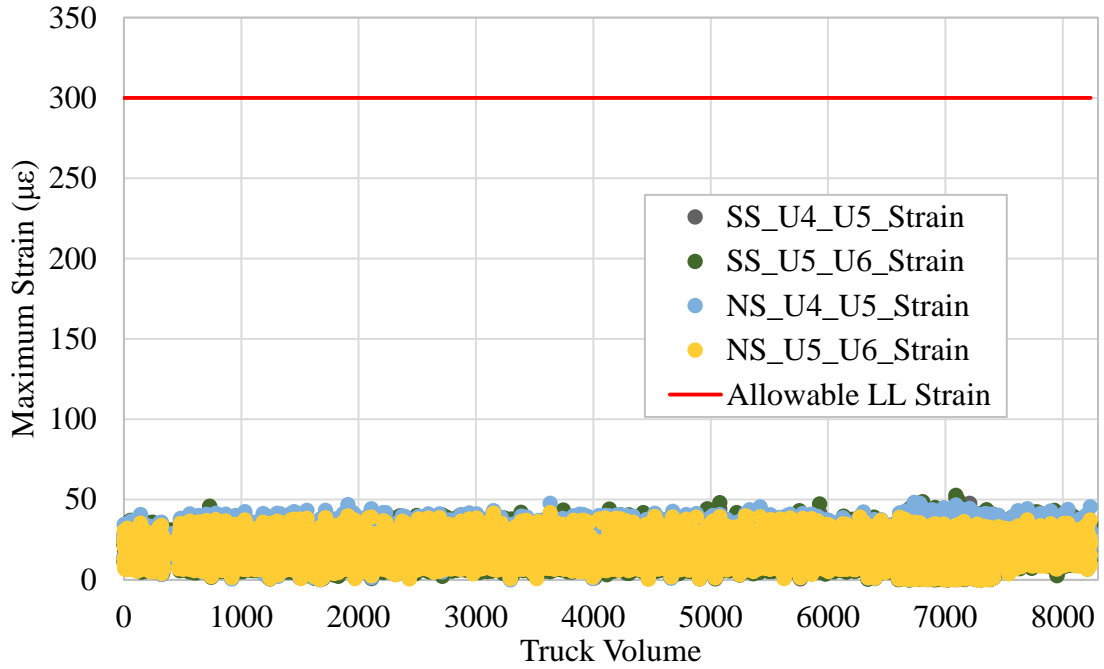


Figure 41: Maximum Strains in Top Chord Members

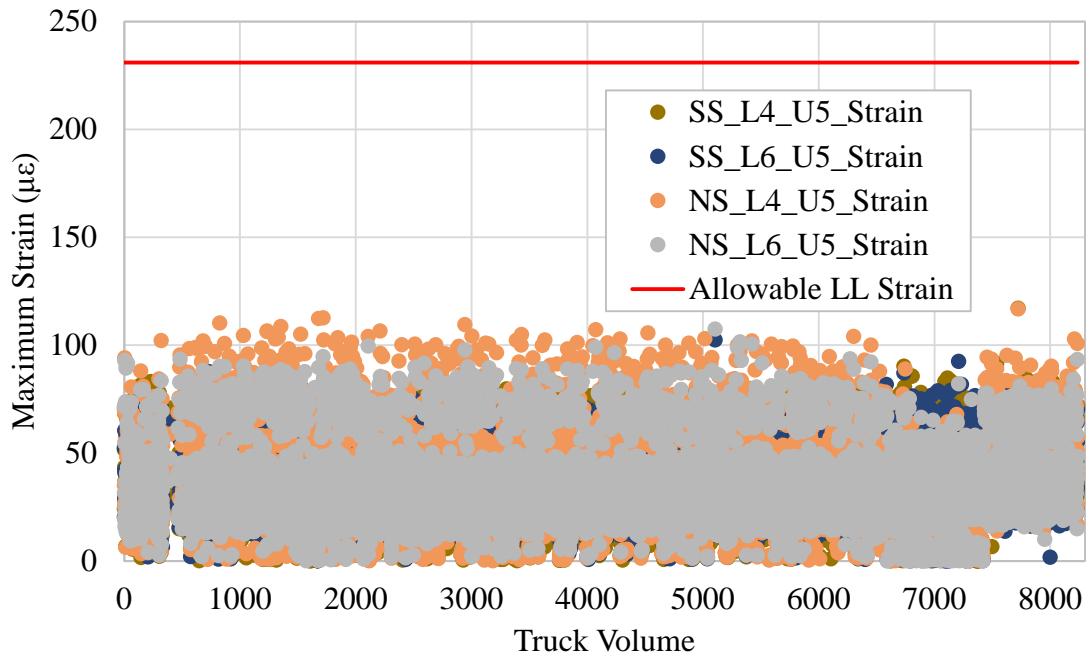


Figure 42: Maximum Strains in Diagonal Members

## **4.4 Traffic Count**

### **4.4.1 Introduction**

The traffic count data from the bridge was also collected throughout the data collection phase of this project. This included the count of all types of vehicles. This information was used to determine the ADT and ADTT of the bridge.

### **4.4.2 Methodology: Data Collection and Processing**

Traffic information from the traffic sensors was collected using TrafficDOT 2 from Sensys. A screenshot from of this software is shown in Figure 43. Data from four (4) traffic sensors were recorded. There are two (2) sensors in the eastbound lane and two (2) sensors in the westbound lane. The traffic sensors in the same lane should have given the same results, however it was found that the data from the sensors in the same lane varied by as much as 15% in some cases. Therefore, the maximum traffic count between sensors in the same lane was used to determine the traffic count in the lane for the day. Further, frequent communication errors occurred which limited the amount of complete days a traffic count was obtained.

### **4.4.3 Collected Data**

Throughout the course of data collection, 186 complete days of traffic count data was collected due to communication errors with the access point. Figure 44 shows the Average Daily Traffic (ADT) averaged for each month. As shown, the traffic count peaked during the summer months and declined during the winter months. The ADT was determined to be 2040 for the eastbound lane and 2020 for the westbound lane, considering all complete days collected. The number of trucks that crossed the bridge was determined using the data collected from the WIM station. Due to the numerous communication and software errors with the data collection from WIM station, there were only eleven (11) complete 24-hour periods of data collected from the WIM station. From those eleven (11) days, the Average Daily Truck Traffic (ADTT) was determined to be 240 for the eastbound lane and 230 for the westbound lane.

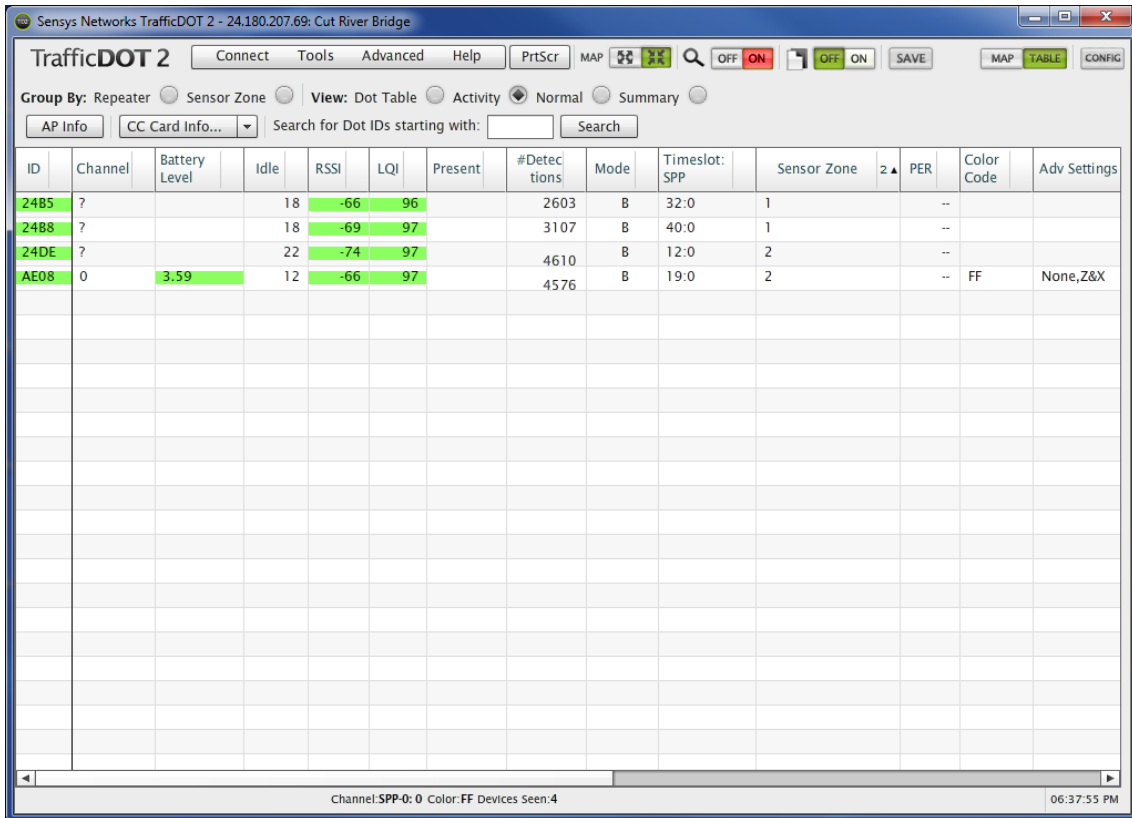


Figure 43: TrafficDOT 2 Screenshot

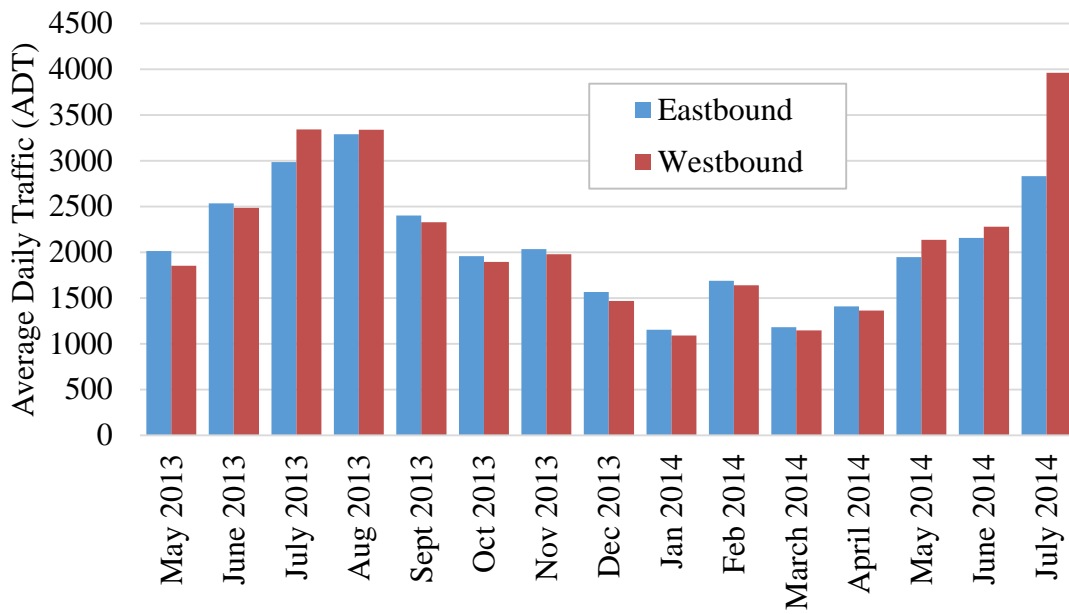


Figure 44: Average Daily Traffic (ADT) per Month

## 4.5 Pavement and Weather

Pavement and weather information from the bridge site was also collected throughout the data collection phase of this project. This data included air temperature, dew point, relative humidity, wind speed, wind direction, precipitation accumulation, surface condition, road temperature, freezing temperature, and surface temperature. This data was collected using software called LoggerNet from Campbell Scientific into a spreadsheet format. A screenshot of this software is shown in Figure 45. The data was able to be downloaded in 24-hour, 12-hour, 6-hour, 3-hour, 1-hour, 10-minute, or 2-minute intervals over a specified time period. The data was also available from the MxVision WeatherSentry Online website (<http://weather.dtn.com/dtnweather>). A screenshot of this website is shown in Figure 46. Using this data in real-time could be used to inform motorists of the current weather conditions at the site. The surface condition data could be used to determine when to deploy maintenance vehicles to apply salt to the pavement or to clear the snow.

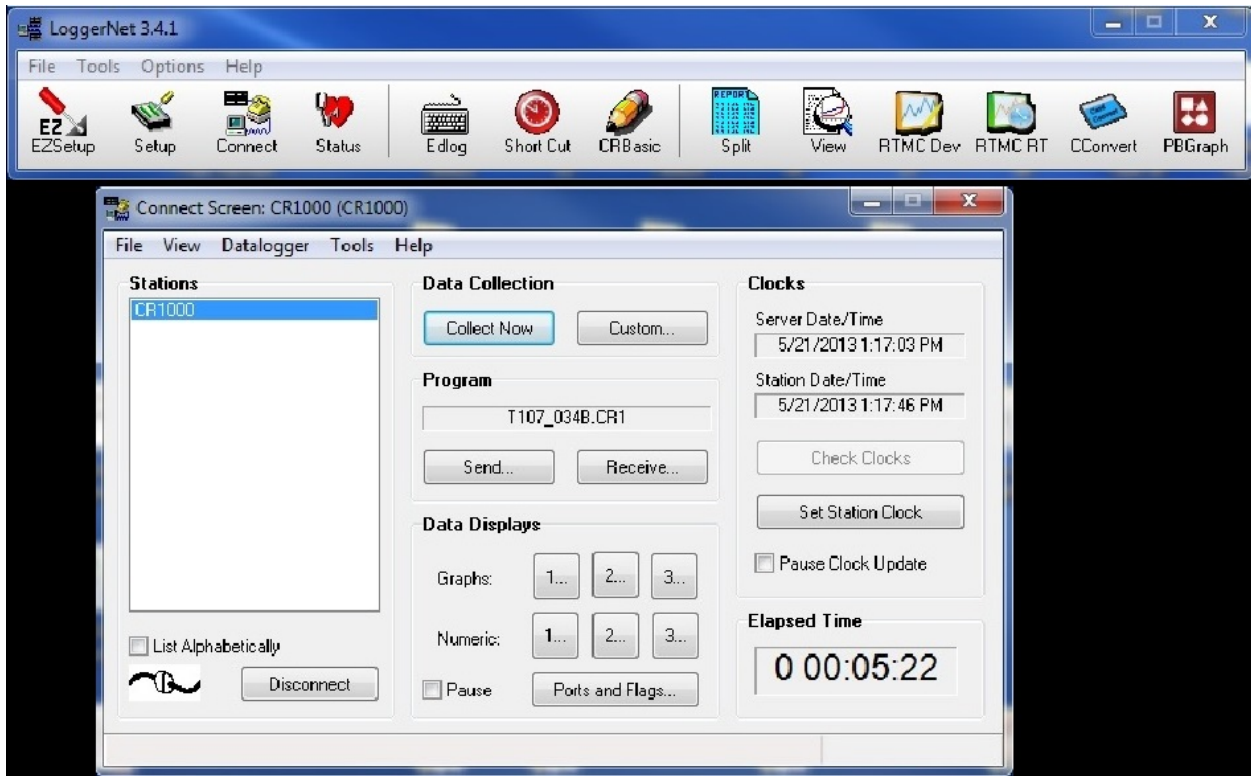


Figure 45: LoggerNet Screenshot

Schneider Electric | MxVision WeatherSentry® Online | Michigan IPO | Sign Out | Help | Customer Service

View Alerts | Monitored Locations

### RWIS Historical Weather for MI-01 Cut River Bridge

Calendar: 8/15/14 | MI-01 Cut River Bridge

MI-01 Cut River Bridge for 8/15/14

Time	Air Temp (°F)	Dew Point (°F)	Rel Hum (%)	Wind (mph)	Precip Detection	Precip Accumulation (in.)				Last Precipitation (EDT)		Surface Condition		Road Temp (°F)		Freeze Temp (°F)		Surface Temperature (°F)	
						1hr	3hr	6hr	12hr/24hr	Start	End	0	1	0	1	0	1	Min	Max
12:00 AM EDT	52.2	38.7	60	SE 5	No	0	0	0	0	-	-	0	1	0	1	0	1	57.7	57.7
12:05 AM EDT	52.3	38.8	60	ESE LV	No	0	0	0	0	-	-	0	1	0	1	0	1	57.6	57.6
12:10 AM EDT	52.2	38.7	60	SE 4	No	0	0	0	0	-	-	0	1	0	1	0	1	57.6	57.6
12:15 AM EDT	52.2	38.7	60	ESE 4	No	0	0	0	0	-	-	0	1	0	1	0	1	57.6	57.6
12:20 AM EDT	52.2	38.7	60	ESE 4	No	0	0	0	0	-	-	0	1	0	1	0	1	57.2	57.2
12:25 AM EDT	52.3	38.5	59	E 6	No	0	0	0	0	-	-	0	1	0	1	0	1	57.2	57.2
12:30 AM EDT	52.5	38.7	59	E 7	No	0	0	0	0	-	-	0	1	0	1	0	1	57.2	57.2
12:35 AM EDT	52.7	38.8	59	ESE 4	No	0	0	0	0	-	-	0	1	0	1	0	1	57.0	57.0
12:40 AM EDT	52.7	38.8	59	SE LV	No	0	0	0	0	-	-	0	1	0	1	0	1	56.8	56.8
12:45 AM EDT	52.3	38.5	59	ESE 4	No	0	0	0	0	-	-	0	1	0	1	0	1	56.8	56.8
12:50 AM EDT	52.3	38.8	60	SE LV	No	0	0	0	0	-	-	0	1	0	1	0	1	56.7	56.7
12:55 AM EDT	52.0	39.0	61	SSE 3	No	0	0	0	0	-	-	0	1	0	1	0	1	56.7	56.7
1:00 AM EDT	51.6	39.0	62	SSE 3	No	0	0	0	0	-	-	0	1	0	1	0	1	56.5	56.5
1:05 AM EDT	51.4	39.2	63	SE 3	No	0	0	0	0	-	-	0	1	0	1	0	1	56.3	56.3
1:10 AM EDT	51.3	39.6	64	SE 4	No	0	0	0	0	-	-	0	1	0	1	0	1	56.1	56.1
1:15 AM EDT	51.4	39.7	64	ESE 4	No	0	0	0	0	-	-	0	1	0	1	0	1	56.1	56.1
1:20 AM EDT	51.4	39.7	64	SE 3	No	0	0	0	0	-	-	0	1	0	1	0	1	55.9	55.9
1:25 AM EDT	51.6	39.9	64	SE 5	No	0	0	0	0	-	-	0	1	0	1	0	1	55.8	55.8
1:30 AM EDT	51.4	39.7	64	ESE 6	No	0	0	0	0	-	-	0	1	0	1	0	1	55.8	55.8
1:35 AM EDT	51.3	39.9	65	ESE 6	No	0	0	0	0	-	-	0	1	0	1	0	1	55.8	55.8

Figure 46: MxVision WeatherSentry Online Website Screenshot

## **5 Finite Element Analysis**

A three-dimensional finite element model (FEM) was created for the Cut River Bridge using LUSAS software. The FEM was initially used to analyze the bridge and determine the truss members that will be instrumented with strain gauges. The collected strain gauge data were then used to calibrate and validate the analytical model.

Finite element models can be a great asset in evaluating the structure performance of a bridge with the aid of the structure health monitoring sensors installed on the bridge. Both SHM and FEM can be used to examine trends or changes in the behavior of the bridge, and therefore maintain safety and ensure the proper planning for any future maintenance. Finite element models, calibrated with measured data, can also be used to validate the design and the load rating of the bridge.

### **5.1 FE Model Description**

Different element types were used to model the bridge. The bridge deck was modelled using shell elements with six degrees of freedom. These elements are generally used for analyzing flat and curved 3D structural elements where it is necessary to account for transverse shear. Floor beams and stringers were modelled using beam element with six degrees of freedom. Truss members were modelled using bar elements with one degree of freedom. The connection between the cantilever span and the suspended span was modelled using joint elements. Joint elements are used to release degrees of freedom between elements. The element is capable of connecting two nodes by six springs in the local x, y and z-directions. Shear connection of stringers to floor beams were modeled using rotational end releases at the end of the stringer beam elements. Material and geometric properties were modeled using the existing and rehabilitation bridge plans.

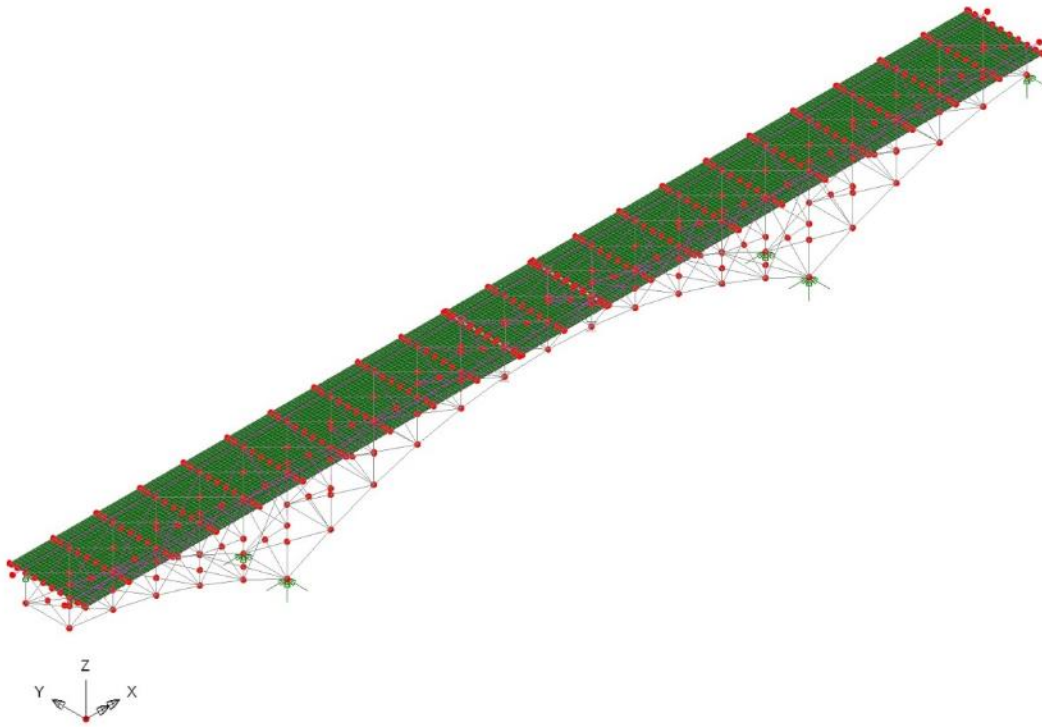


Figure 47: Three-Dimensional Finite Element Model of the Bridge

## 5.2 Validation and Verification of the Finite Element Model

Data recorded from six trucks crossing the bridge was used to calibrate the finite element model. Configuration of each truck, including axle weight, axle spacing, speed, FHWA classification, gross weight, total length, and direction of travel were recorded at the WIM station. Table 5.1 shows the configuration of the trucks used to calibrate the finite element model.

**Table 5.1: Truck Configuration used for the Calibration of The Finite Element Model**

<b>Truck No</b>	<b>1</b>	<b>2</b>	<b>3</b>	<b>4</b>	<b>5</b>	<b>6</b>
<b>Lane</b>	WB	WB	EB	WB	EB	WB
<b>Number of Axles</b>	10	7	8	9	9	6
<b>FHWA Class</b>	13	13	13	13	13	15
<b>Gross Weight (kip)</b>	135.6	96.6	106.2	121.4	136	74.2
<b>Overall Length (ft)</b>	66.2	56.2	72.5	84	81.7	32.6
<b>Speed (mph)</b>	62.2	57.5	59.9	63.5	62.7	57
<b>Spacing 1-2 (ft)</b>	14	12.2	20.1	20.1	17.7	9
<b>Spacing 2-3 (ft)</b>	4.4	4.4	4.3	4.2	4.6	3.8
<b>Spacing 3-4 (ft)</b>	8.8	9	9.4	12.7	11.9	4.3
<b>Spacing 4-5 (ft)</b>	9.1	9.1	9	9.1	9.2	4.4
<b>Spacing 5-6 (ft)</b>	9.2	9.1	9	9.1	9.2	4.1
<b>Spacing 6-7 (ft)</b>	3.8	4.2	4.1	9.6	9.5	-
<b>Spacing 7-8 (ft)</b>	3.6	-	4.1	9.2	9.3	-
<b>Spacing 8-9 (ft)</b>	3.6	-	-	3.9	4.1	-
<b>Spacing 9-10 (ft)</b>	3.7	-	-	-	-	-
<b>Weight Axle 1 (kip)</b>	10	11.6	11.5	10.3	11.4	16.2
<b>Weight Axle 2 (kip)</b>	14.6	13.3	14.5	13.8	15.5	9.2
<b>Weight Axle 3 (kip)</b>	17.1	14.6	13.9	14	14.3	9.7
<b>Weight Axle 4 (kip)</b>	14.4	13.7	12.3	15.1	21.8	14.5
<b>Weight Axle 5 (kip)</b>	16	15	13.1	15.9	17.9	14.5
<b>Weight Axle 6 (kip)</b>	12.7	13.4	14	16.1	17.3	10.1
<b>Weight Axle 7 (kip)</b>	11.6	15.1	13.5	15.2	15	-
<b>Weight Axle 8 (kip)</b>	13.5	-	13.5	10.8	12.6	-
<b>Weight Axle 9 (kip)</b>	13.3	-	-	10.4	10.2	-
<b>Weight Axle 10 (kip)</b>	12.4	-	-	-	-	-

The strain gauge data of each of the six trucks were also collected using the ENLIGHT software. Using the geometric and material properties of the truss members, the maximum live load force in each of the instrumented truss member due to the passing truck on the bridge were then calculated. Table 5.2 shows the maximum truck force in each instrumented truss member. The recorded strain data at the outside and inside face of each truss member were averaged to calculate the axial force.

**Table 5.2: Maximum Truck Force in Instrumented Truss Members**

Truck No.	Maximum Measured Truss Member Force (Kips)							
	SS_U4_U5	SS_L4_U5	SS_L6_U5	SS_U5_U6	NS_U4_U5	NS_L4_U5	NS_L6_U5	NS_U5_U6
1	55.01	32.28	28.21	54.80	74.93	47.15	39.98	62.15
2	40.56	23.41	20.48	37.89	57.88	37.88	32.90	47.70
3	49.43	31.09	30.20	48.44	46.19	23.26	21.32	34.88
4	44.18	24.40	20.77	41.83	64.28	38.39	33.70	50.51
5	68.91	41.36	35.15	71.47	65.78	31.65	23.76	48.81
6	30.17	17.78	16.79	28.84	41.04	26.70	25.52	35.37

In order to calibrate the finite element model created for the bridge, each of the trucks shown in Table 5.1 was modeled in LUSAS and the maximum truss member forces corresponding to the instrumented truss member are then determined. The following assumptions were made when determining the truss member forces:

1. The truck is located within the striped lane limits only.
2. The truck is travelling in the same direction as recorded at the WIM station.
3. No other live loads are on the bridge except the modelled truck.

Collected strain gauge data for each truck include vehicular dynamic impact, which could not be separately measured. In order to compare the finite element model results to the collected data, it was important to reasonably estimate the dynamic impact factor to be applied to the computed forces from the finite element model of the bridge. Dynamic impact is a function of many variables

including vehicle speed, vehicle type, vehicle gross weight, axle configuration, axle weight, bridge span length, actual bridge condition, road roughness and transverse position of truck on the bridge.

In general, dynamic load factor is considered as an equivalent static live load expressed in terms of DLF. A method described by A.S. Nowak (Nowak, Kim, & Szerszen, 1999) is used to calculate the dynamic impact factor. This method is based on field measurements that were performed to determine the actual truck load effects. For each truck passage, the dynamic response is monitored by recording strain data. In this research, DLF is taken as the ratio of dynamic increment and static response,

$$DLF = \epsilon_{dyn}/\epsilon_{stat}$$

where,

DLF = dynamic load factor,

$\epsilon_{dyn}$  = dynamic component of strain (measured from test data,  $\epsilon_{dyn} = \epsilon_{total} - \epsilon_{stat}$ )

$\epsilon_{stat}$  = static component of strain, (maximum total strain obtained from the filtered dynamic response).

For each strain gauge data, the equivalent measured static response of each truck passing the bridge was obtained by filtering the dynamic response using a moving average of five points. The above procedure was performed at each strain gauge location for the six trucks selected to determine DLFs at each instrumented truss member.

Figure 48 shows the measured data from strain gauge SS\_U4\_U5\_Outside\_Strain due to Truck 1.

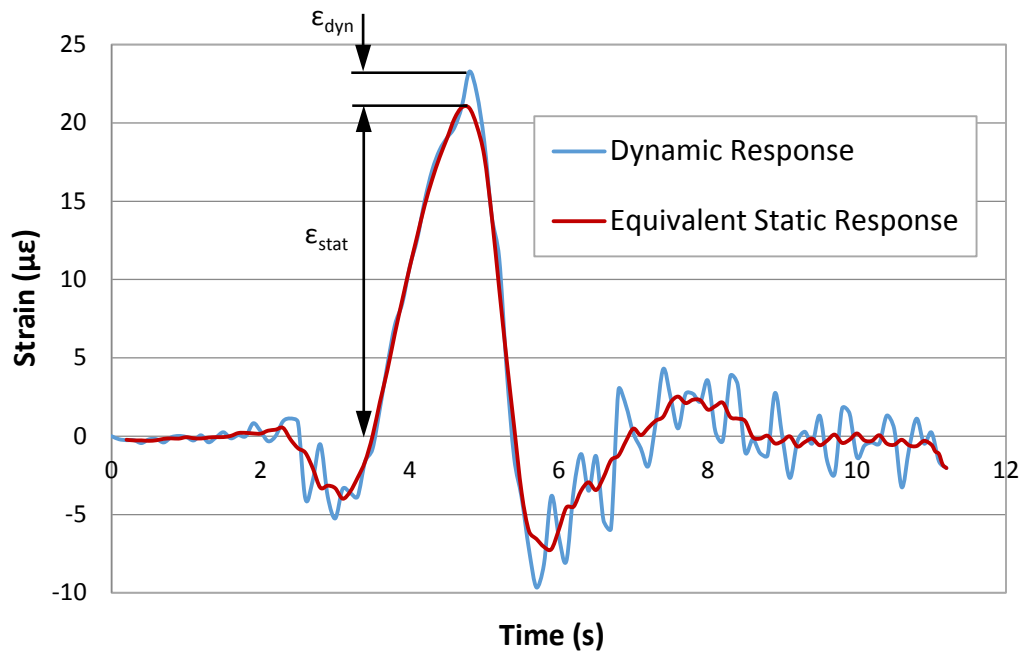


Figure 48: Measured Dynamic Strain and Equivalent Static Strain

In order to calibrate the FEM, sensitivity analyses were carried in order to determine the parameters that affect truss forces. In the analyses, one parameter was changed at a time and the changes in the truss member forces were recorded. The following parameters were found to have an effect on the truss member forces:

1. Stiffness of the connection between floor beams and the supporting truss
2. Stiffness of the connection between the suspended span and the cantilever spans
3. Composite action between floor beams and deck
4. Deck stiffness
5. Soil-structure interaction, which includes the flexibility of the supporting foundation
6. Stiffness of the lateral bracing

Calibration of the finite element model was carried out by adjusting stiffness coefficients of the parameters listed above until the measured and computed truss forces are within a reasonable limit. Table 5.3 through Table 5.8 show comparisons between the measured member forces (utilizing measured strain data) and forced computed by the finite element model for the six trucks. DLFs calculated using the above described method are also included in the Tables.

In general, the FEM forces for the top chord members are in agreement with the measured forces. However, computed forces in diagonal members vary by up to 49% from the measured forces. The variation between the computed and measured forces can be attributed to the accuracy of the FEM, variation between specified and actual material and geometrical properties of structural members, actual location of truck within the lane compared to assumed truck location in the FEM, actual vs. computed dynamic load factors, and arching or compressive membrane action in the reinforced concrete slab which can affect the live load distribution from the deck to the supporting beams.

**Table 5.3: Measured Vs. Computed Member Forces for Truck 1**

Member	FEM Force (kip)	(1+DLF)	FEM Force x (1+DLF) (kip)	Measured Force (kip)	% Difference
<b>SS_U4_U5</b>	47	1.10	51	55	-7%
<b>SS_L4_U5</b>	35	1.11	39	32	20%
<b>SS_L6_U5</b>	34	1.10	37	28	33%
<b>SS_U5_U6</b>	45	1.11	50	55	-10%
<b>NS_U4_U5</b>	60	1.09	65	75	-13%
<b>NS_L4_U5</b>	50	1.12	56	47	19%
<b>NS_L6_U5</b>	51	1.10	56	40	40%
<b>NS_U5_U6</b>	63	1.11	70	62	12%

**Table 5.4: Measured Vs. Computed Member Forces for Truck 2**

Member	FEM Force (kip)	(1+DLF)	FEM Force x (1+DLF) (kip)	Measured Force (kip)	% Difference
<b>SS_U4_U5</b>	34	1.10	37	41	-8%
<b>SS_L4_U5</b>	27	1.12	30	23	28%
<b>SS_L6_U5</b>	25	1.13	28	20	38%
<b>SS_U5_U6</b>	33	1.11	37	38	-4%
<b>NS_U4_U5</b>	44	1.12	49	58	-15%
<b>NS_L4_U5</b>	38	1.12	42	38	11%
<b>NS_L6_U5</b>	38	1.13	43	33	30%
<b>NS_U5_U6</b>	47	1.12	53	48	10%

**Table 5.5: Measured Vs. Computed Member Forces for Truck 3**

Member	FEM Force (kip)	(1+DLF)	FEM Force x (1+DLF) (kip)	Measured Force (kip)	% Difference
<b>SS_U4_U5</b>	48	1.04	50	49	1%
<b>SS_L4_U5</b>	40	1.11	44	31	43%
<b>SS_L6_U5</b>	38	1.08	41	30	36%
<b>SS_U5_U6</b>	50	1.06	53	48	10%
<b>NS_U4_U5</b>	37	1.07	40	46	-14%
<b>NS_L4_U5</b>	29	1.08	31	23	33%
<b>NS_L6_U5</b>	26	1.10	28	21	33%
<b>NS_U5_U6</b>	35	1.10	39	35	12%

**Table 5.6: Measured Vs. Computed Member Forces for Truck 4**

Member	FEM Force (kip)	(1+DLF)	FEM Force x (1+DLF) (kip)	Measured Force (kip)	% Difference
<b>SS_U4_U5</b>	40	1.10	44	44	0%
<b>SS_L4_U5</b>	30	1.11	33	24	36%
<b>SS_L6_U5</b>	28	1.11	31	21	49%
<b>SS_U5_U6</b>	37	1.08	40	42	-5%
<b>NS_U4_U5</b>	52	1.06	55	64	-15%
<b>NS_L4_U5</b>	42	1.10	46	38	20%
<b>NS_L6_U5</b>	43	1.09	46	34	37%
<b>NS_U5_U6</b>	53	1.09	58	51	14%

**Table 5.7: Measured Vs. Computed Member Forces for Truck 5**

Member	FEM Force (kip)	(1+DLF)	FEM Force x (1+DLF) (kip)	Measured Force (kip)	% Difference
<b>SS_U4_U5</b>	59	1.11	65	69	-6%
<b>SS_L4_U5</b>	48	1.12	54	41	30%
<b>SS_L6_U5</b>	47	1.04	49	35	40%
<b>SS_U5_U6</b>	61	1.10	67	71	-6%
<b>NS_U4_U5</b>	46	1.12	51	66	-22%
<b>NS_L4_U5</b>	34	1.10	38	32	20%
<b>NS_L6_U5</b>	31	1.06	33	24	39%
<b>NS_U5_U6</b>	43	1.10	47	49	-3%

**Table 5.8: Measured Vs. Computed Member Forces for Truck 6**

Member	FEM Force (kip)	(1+DLF)	FEM Force x (1+DLF) (kip)	Measured Force (kip)	% Difference
<b>SS_U4_U5</b>	27	1.10	30	30	-1%
<b>SS_L4_U5</b>	22	1.09	24	18	36%
<b>SS_L6_U5</b>	21	1.10	23	17	38%
<b>SS_U5_U6</b>	27	1.11	30	29	4%
<b>NS_U4_U5</b>	35	1.10	39	41	-6%
<b>NS_L4_U5</b>	32	1.10	35	27	29%
<b>NS_L6_U5</b>	32	1.11	35	26	37%
<b>NS_U5_U6</b>	38	1.07	41	35	16%

## **6 Future Implementation and Improvements**

One of the primary objectives of this pilot project at the Cut River Bridge is to develop a SHMS that could be employed at the Mackinac Bridge and other locations throughout the state of Michigan. SHM is a way to further develop MDOT's core goals and CV initiatives and a useful tool for structure management. The experience from this project can be utilized to advance this new technology to any future project. A significant amount of knowledge has been gained from this project which can be directly implemented on future SHM projects.

Many of the issues on the Cut River Bridge SHM project have stemmed from the equipment installed at the structure and the communication with that equipment. In some instances, the issue was specific to one device or coordinating multiple instruments to work together. However other issues can be attributed to the harsh weather condition at the bridge site. Additionally, the remote location has created difficulties such as accessing the equipment to perform maintenance. The frequent interruption of the SHMS resulted in collecting data for a short period of time during the duration of the project. There are specific equipment improvements as well as overall system improvements that any future SHMS can incorporate.

One of these improvements is to implement redundancy in the SHMS. On many occasions during the project, communication with the bridge was lost due to power supply failure, sensors malfunction, or other equipment issues. This has limited the ability to continuously collect data from the bridge. A future system should investigate ways to provide redundancy in SHMS including power supply, sensors, data storage, and communication equipment. Factors that may impact the need for redundancy implementation include availability of maintenance staff to address potential issues, weather conditions at the bridge site, the importance of the bridge, the structural condition of the bridge, available funding, bridge location, and long distance communication challenges between the bridge and monitoring location. Future projects should perform a cost-benefit analysis to determine if adding redundancy is a viable option.

### **6.1 Equipment and Communication Improvements**

Communication with the SHMS at the Cut River Bridge has been intermittent throughout the course of the project. The SHMS relies on radio waves sent between the WIM station, the Cut River Bridge, the Mackinac Bridge, and the Mackinac Bridge Authority office in St. Ignace. If a link in the communication path malfunctioned, then all or part of the data collection and monitoring was disrupted. Weather also played a very significant role with the radio communications. Severe weather conditions and harsh winters experienced at the bridge have greatly impacted the operation of the SHMS. Redundancy in the communication equipment can minimize disruption in collecting data. Cellular modems and other forms of wireless

communication can be incorporated into a future system to serve as a backup method of communication.

The SHMS at the Cut River Bridge only uses solar panels as a power source. These solar panels charge a bank of batteries stored in a concrete vault near the east abutment. During colder months of the year, sunlight for the solar panels is limited and the charge on the battery bank can run low. Cold weather can damage low charged batteries, which was experienced multiple times at the Cut River Bridge. The batteries in the concrete vault have had a short lifespan during the course of the project. Redundancy can be added to the SHMS power generation with new technology and existing methods. An example of new technology is utilizing power supplies that implement wireless energy transfer in lieu of using solid wires or conductors. In this system, a transmitter device connected to a power source such as main power lines, transmits power by electromagnetic fields to one or more receiver devices at the bridge site, where it is then converted back to electric power. An example of an existing method is to install a generator fueled by propane or natural gas (if available) to charge the batteries when the solar panels cannot provide enough energy. The generator can be set only to run when the charge on the batteries falls below a set level. Similar systems are common throughout the Upper Peninsula at off-grid cabin locations.

The fiber optic strain gauges are one of the primary components of the SHMS at the Cut River Bridge. The strain gauges have been performing satisfactory during the project. However lost communication with the bridge resulted in disruption in data collection from strain gauges. Of the sixteen fiber optic strain gauges installed on the deck truss of the Cut River Bridge, only four of them were paired with temperature sensors. The remaining twelve fiber optic strain gauges on the structure have no correction for thermal effect. Future improvements to the system includes the installation of a temperature sensor at each fiber optic strain gauge location. The values from the fiber optic strain gauges tend to “drift” due to a lack of correction for thermal effect. A temperature sensor paired with a fiber optic strain gauge minimizes the drift experienced in strain gauge readings.

Two of the four temperature sensors were not working properly from the beginning of data collection. Due to the high sensitivity of these sensors, several possible factors could contribute to the malfunctioning. For instance, any small amount of epoxy that was inadvertently placed between the sensor and steel during installation or improper welding to mount the sensor would cause it to work improperly. A potential improvement to future systems would be to implement or improve quality control and assurance procedures during installation. Also, additional gauges could be ordered at the start of the project to replace gauges that are no longer working. Additionally, a future system could request extended warranties on the gauges in the event that a gauge stops working after installation. Additional strain gauges and extended warranties would be options to add redundancy to the system.

Different sensors and equipment utilized in the SHMS are manufactured by several companies. This has resulted in using different computer programs that can communicate with the sensors for data collection, which has required several human resources to process, store, and analyze the data. Certain sensors and equipment have unique software, while other equipment required software from outside developers. For instance, the WIM station software utilizes a separate software to operate concurrently with the manufacturer software in order to store data. The software interacting with each other frequently causes the computer running the software to freeze and halt data collection. For future implementation of similar SHMS, it is recommended to centralize data collection and minimize the number of different software required to store and process data. It is also recommended that redundancy is added by storing data on a server or multiple computers in case the primary computer malfunctions.

The WIM station is located approximately two miles east of the Cut River Bridge. The long distance required additional equipment and 120 feet tall tower to communicate with the tower installed at the bridge. Additionally, the long distance required coordination in data processing in order to match each truck with a corresponding strain value at the structure. It is recommended that future SHMS includes WIM stations that are installed at the bridge site, which will improve data processing and increase reliability of the collected data.

Other potential improvements to be incorporated into future models would be in data collection and verification. Testing the system during the installation with known truck configurations would help ensure that the readings from the strain gauges and the WIM station are accurate. These known readings would also aid in calibrating the finite element model (if performed) with static and dynamic truck loads. These known truck loads would be more reliable than the real-time data collected from normal traffic. Accelerometers could also be added to the system to aid in capturing the dynamic response of the bridge.

Any SHMS will require future maintenance and troubleshooting in case of equipment or sensor malfunctions. Adequate training, schedule, and budget for a maintenance team is required in order to maintain the system. Also, maintenance of the system can be contracted out if an in-house resources are not available. It is recommended that similar SHMS are used across the State, if possible, in order to minimize training efforts and streamline maintenance efforts.

## **6.2 New Technologies**

Several studies are currently in progress to further develop future SHMS. At the Laboratory for Intelligent Systems and Technologies at the University of Michigan, extensive research is being performed using wireless technologies to monitor structures. The research team has recently worked on a bridge on Telegraph Road in Monroe, MI, that is equipped with wireless

sensors. The sensors are using a method known as Compressed Sensing (CS) to save wireless sensor energy. The method will simultaneously reduce data sampling rates, on-board storage requirements, and communication data payloads (O'Conner, Lynch, & Gilbert, 2014). Research is also being performed at Michigan State University in the Civil and Environmental Engineering Department with self-powering sensors. The research is focused on harnessing the energy from vibrations of the structure to power wireless sensors. (Elvin, Lajnef, & Elvin, 2006). These research efforts may address some of the power supply issues encountered during this Cut River Bridge pilot project.

### **6.3 Future Implementation/DUAP**

The final step for the pilot research project at the Cut River Bridge is to integrate this research with MDOT's Data Use Analysis Processing (DUAP) project to create an automated and functioning SHM system. To accomplish this, the SHMS needs to be able to monitor the strain values from the fiber optic strain gauges and alert MDOT and / or other emergency personnel when an established threshold strain value in any of the instrumented truss members is reached, if any. This will require coordination with the strain gauge manufacturer and the DUAP project.

The strain gauge manufacturer's software should be capable of sending warnings through the DUAP system when the threshold strain values are exceeded. This will assist in the automated data processing and obtaining real-time results.

In addition to the fiber optic strain gauges at the Cut River Bridge, the WIM station can be utilized to provide alerts to MDOT if overweight trucks, exceeding a pre-established threshold, are travelling on U.S. Route 2. The information collected at the WIM station in conjunction with the strain gauge data collected can be used to determine the truck configuration that causing any abnormal strain in the instrumented bridge elements.

The weather station and pavement sensors can also provide alerts to hazardous driving conditions. The collected traffic count data can show traffic volumes and peak traffic volume hours along Route 2 which will assist future planning and maintenance of the bridge. Coordination with all of the equipment, corresponding software, and the DUAP project will be required in order to obtain real-time and useful data from the SHMS.

## 7 Recommendations and Conclusions

### 7.1 Recommendations

The pilot project at the Cut River Bridge has provided useful lessons learned in deploying a SHMS. The experiences obtained at the Cut River Bridge will aid in developing future SHMS across the state of Michigan. The lessons learned are summarized in the list below. Many recommendations have previously been described in this report. The recommendations are applicable to the Cut River Bridge SHM project and future projects.

- Improve the Contract Administration process. Administrator a single contract with a single vendor. This single primary vendor for the SHMS should be required to instrument the bridge, provide all data communication backhaul, data storage, data management, and all data applications to the DOT. Therefore, the single primary vendor (within related sub-vendors) would be responsible for all systems operations and maintenance for the entire project duration. This would eliminate the complex problem of dealing with multiple vendors to accomplish data collection and usage for a bridge SHMS.
- Build redundancy into the SHMS in as many aspects as feasibly possible. This will increase the reliability of the system. Perform a cost-benefit analysis to verify that any additional costs are indeed worthwhile.
- Provide backup forms of communication for any off-grid system. For the Cut River Bridge location, cellular modems or other forms of wireless communication can supplement the current radio transmission system. This will reduce the communication outages that have been experienced.
- Provide multiple sources of power to the SHMS for any off-grid system. Wireless energy transfer technology or generators powered by propane or natural gas can complement the solar panels and keep the battery system adequately charged to operate the SHMS.
- Use temperature sensors at every fiber optic strain gauge location to compensate for any drift in strain gauge reading due to thermal effect. This will give the SHMS the ability to monitor changes of strain over a long period of time.
- Take additional precautions to ensure proper installation of all strain gauges and other equipment. Strict quality control and assurance measures will reduce the risk of equipment malfunctioning due to improper installation.
- Obtain extended equipment warranties or replacement parts for the equipment at the beginning of the project if feasible. This added redundancy will be beneficial if any of the equipment breaks down by reducing delays and keep the system functioning as intended.

- Use equipment and corresponding software from fewer manufacturers to reduce coordination time and the possibility of incompatibilities within the system.
- Coordinate location of the SHM equipment to streamline the system, reduce overall cost, and reduce areas for potential maintenance.
- Store data obtained from the SHMS in multiple locations.
- Perform load tests in calibrating the system to ensure accurate readings are being obtained from the equipment.
- Develop a maintenance team with adequate training, schedule, and budget to maintain the SHMS. The same maintenance team could be utilized across the State at multiple SHMS locations to minimize training and streamline maintenance efforts.
- At the Cut River Bridge, a predetermined threshold strain values should be established for each instrumented truss member to alert MDOT if the threshold is exceeded when a truck crossed the bridge.
- For integration with the DUAP project, coordinate with the strain gauge manufacturer so that the strain gauge software will not trigger alarms for inaccurate strain readings. Similar precautions should be taken for the WIM station and other equipment.
- The use of FEM to examine trends or changes in the behavior of the bridge, in addition to the SHM should be evaluated based on the complexity of the bridge and whether it is feasible to calibrate the FEM with the measured data.

## 7.2 Conclusions

The pilot project at the Cut River Bridge has provided MDOT with a valuable means of meeting its core goals and a learning experience for future projects involving SHM. It is an effective tool to meet MDOT's core goals at the Cut River Bridge and other locations throughout Michigan. Any future SHM project in Michigan will be able to benefit from the lessons learned at the Cut River Bridge. There are improvements that would benefit the current system before full implementation with the DUAP project. Communication, power supply, and other improvements will increase the reliability of the SHMS. These same improvements can be incorporated into future SHM applications as well.

Once the SHMS at the Cut River Bridge is implemented with the DUAP project, the SHMS will be able to meet MDOT's core goals of safety, mobility, asset management, and planning. Safety will be achieved with a known safety factor of the loads acting on the bridge and a constant monitoring system in place. Mobility will be enhanced with real time weather and traffic conditions available to motorists. Asset management benefits from a better

understanding the safety factor of the bridge and evaluating risks associated with the structure. Planning is improved with the real-time information stream from the bridge which can be used to observe maintenance or structure issues prior to or shortly after they occur.

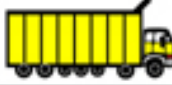
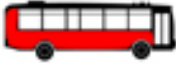
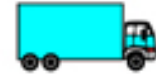
Both SHM and FEM can be used to examine trends or changes in the behavior of the bridge, and therefore maintain safety and ensure the proper planning for any future maintenance. Finite element models, calibrated with measured data, can also be used to validate the design and the load rating of the bridge. However, depending on the complexity of the structure, calibration of FEM with measured data can be a time consuming process and a reasonable agreement between the measured data and data computed by the FEM may not be achieved.

## 8 References

- Ahlborn, T. M., Shuchman, R., Sutter, L. L., Brooks, C. N., Harris, D. K., Burns, J. W., . . . Oats, R. C. (2010). *The State-of-the-Practice of Modern Structural Health Monitoring for Bridges: A Comprehensive Review*.
- Axis Communications. (2015). Retrieved from <http://www.axis.com/>
- Campbell Scientific, Inc. (2015). Retrieved from <https://www.campbellsci.com/>
- Chan, T., Yu, L., Tam, H., Ni, Y., Liu, S., Chung, W., & Cheng, L. (2006). Fiber Bragg grating sensors for structural health monitoring of Tsing Ma bridge: Background and experimental observation. *Engineering Structures*, 648-659.
- Comtrol. (2015). Retrieved from <http://www.comtrol.com/>
- Cook, S. J. (n.d.). *MDOT Cut River and Mackinac Bridge Wireless Infrastructure Monitoring: An Integration of Communication, Sensor, and Data Collection Technology*.
- Elvin, N. G., Lajnef, N., & Elvin, A. A. (2006). Feasibility of structural monitoring with vibration powered sensors. *Smart Materials and Structures*, 15(4).
- Kilic, G. (November 2012). *Application of Advanced Non-destructive Testing Methods on Bridge Health Assessment and Analysis*. University of Greenwich.
- Koh, B. H., & Dyke, S. J. (2007). Structural health monitoring for flexible bridge structures using correlation and sensitivity of modal data. *Computers and Structures*, 117-130.
- Lwin, M. M. (2012, June 20). Memo: Clarification of Requirements for Fracture Critical Members. Federal Highway Administration.
- Magalhaes, F., Cunha, A., & Caetano, E. (2008). Dynamic monitoring of a long span arch bridge. *Engineering Structures*, 3034-3044.
- Magalhaes, F., Cunha, A., & Caetano, E. (2011). Vibration based structural health monitoring of an arch bridge: From automated OMA to damage detection. *Mechanical Systems and Signal Processing*.
- MDOT. (2015). Retrieved from [http://www.michigan.gov/mdot/0,4616,7-151-9620\\_11154\\_11188-29665--,00.html](http://www.michigan.gov/mdot/0,4616,7-151-9620_11154_11188-29665--,00.html)
- Micron Optics, Inc. (2012). *Sensing Instrumentation & Software | ENLIGHT User Guide Revision 1.138*. Retrieved from <http://www.micronoptics.com/uploads/documents/Manual.pdf>

- Micron Optics, Inc. (2014). Retrieved from <http://www.micronoptics.com/>
- Micron Optics, Inc. (2015). *Optical Fiber Sensors Guide: Fundamentals & Applications*. Retrieved from [http://www.micronoptics.com/uploads/documents/Updated\\_Optical\\_Fiber\\_Sensors\\_Guide\\_130529.pdf](http://www.micronoptics.com/uploads/documents/Updated_Optical_Fiber_Sensors_Guide_130529.pdf)
- Necati Catbas, F., Grimmelsman, K. A., & Aktan, A. E. (2000). Structural Identification of the Commodore Barry Bridge. *Nondestructive Evaluation of Highways, Utilities, and Pipelines IV* (pp. 84-95). Proceedings of SPIE.
- Necati Catbas, F., Gul, M., & Burkett, J. L. (2008). Conceptual damage-sensitive features for structural health monitoring: Laboratory and field demonstrations. *Mechanical Systems and Signal Processing*, 1650-1669.
- Necati Catbas, F., Susoy, M., & Frangopol, D. M. (2008). Structural health monitoring and reliability estimation: Long span truss bridge application with environmental monitoring data. *Engineering Structures*, 2347-2359.
- Nowak, A. S., Kim, S., & Szerszen, M. M. (1999). Dynamic Loads for Steel Girder Bridges. *Proceedings of the International Modal Analysis Conference & Exhibit*, (pp. 731-737).
- O'Conner, S. M., Lynch, J. P., & Gilbert, A. C. (2014). Compressed sensing embedded in an operational wireless sensor network to achieve energy efficiency in long-term monitoring applications. *Smart Materials and Structures*, 23(8).
- Sohn, H., Czarnecki, J. A., & Farrar, C. R. (November 2000). Structural Health Monitoring Using Statistical Process Control. *Journal of Structural Engineering*, 1356-1363.
- Sohn, H., Farrar, C. R., Hemez, F., & Czarnecki, J. (2002.). A Review of Structural Health Monitoring Literature 1996-2001. *Eng. Science and Applications Div., Los Alamos National Laboratory*.
- StarDot Technologies. (2015). Retrieved from <http://www.stardot.com/>
- Tedesco, J. W., Stallings, M. J., & El-Mihilmy, M. (1999). Finite element method analysis of a concrete bridge repaired with reinforced plastic laminates. *Computers and Structures*, 379-407.
- Underwood, S. E., Cook, S. J., & Tansil, W. H. (2008). *Line of Business Strategy for Vehicle Infrastructure Integration, Part IV: History and Background*.

## Appendix A: FHWA Vehicle Classifications

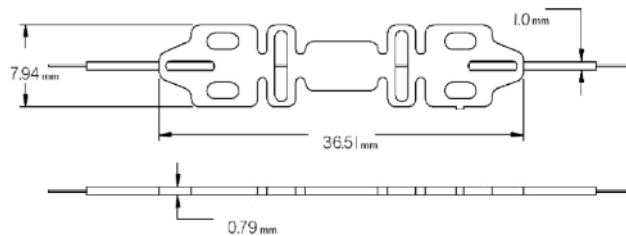
<b>Class 1</b> Motorcycles		<b>Class 7</b> Four or more axle, single unit		
<b>Class 2</b> Passenger cars		<b>Class 8</b> Four or less axle, single trailer		
				
				
				
<b>Class 3</b> Four tire, single unit		<b>Class 9</b> 5-Axle tractor semitrailer		
				
				
<b>Class 4</b> Buses		<b>Class 10</b> Six or more axle, single trailer		
				
		<b>Class 11</b> Five or less axle, multi trailer		
<b>Class 5</b> Two axle, six tire, single unit			<b>Class 12</b> Six axle, multi-trailer	
				
		<b>Class 13</b> Seven or more axle, multi-trailer		
<b>Class 6</b> Three axle, single unit				
				
				

## Appendix B: Strain Gauge Specifications

### Optical Strain Gage | os3100

#### Specifications <sup>ⓑ</sup> 1

	os3110 SpotWeld	os3120 Epoxy Mount
<b>Performance Properties</b>		
Strain Sensitivity <sup>2</sup>	~ 1.4 pm/με	
Gage Length	22 mm	
Operating Temperature Range	-40 to 120° C (150° C short-term)	
Strain Limits	± 2,500 με	
Fatigue Life	100 x 10 <sup>4</sup> cycles, ± 2,000 με	
<b>Physical Properties</b>		
Dimensions	See Diagram Below	
Weight	2.6 g	
Carrier Material	302 Stainless Steel	
Cable Length	1 m (± 10 cm), each end	
Fiber Type	SMI 28-Compatible	
Cable Type	1 mm Fiberglass Braid	
Connectors	FC/APC optional	
Cable Bend Radius	≥ 17 mm	
Fastening Methods <sup>3</sup>	SpotWeld	Epoxy Mount
<b>Optical Properties</b>		
Peak Reflectivity (R <sub>max</sub> )	> 70%	
FWHM (-3 dB point)	0.25 nm (± .05 nm; apodized grating)	
Isolation	> 15 dB (@ ± 0.4 nm around center wavelength)	
Notes:		
1. Denotes Beta product. For more details see <a href="http://www.micronoptics.com/product_designation.php">www.micronoptics.com/product_designation.php</a> .		
2. Actual gage factor provided with gage. Note: F <sub>G</sub> is different for os3110 and os3120.		
3. See <a href="http://www.micronoptics.com/support_downloads/Sensors/">http://www.micronoptics.com/support_downloads/Sensors/</a> for installation details.		



#### Ordering Information

os31aa-*www*-1xx-1yy

(Example: os3110-1564-1FC-1FC)

aa: Model	www: Wavelength (± 1nm)	1xx: Cable 1, Length & Connector	1yy: Cable 2, Length & Connector
10 SpotWeldable	Standard: 1516 to 1588nm in 4nm intervals.	1 1 m Standard, Cable Length	1 1 m Standard, Cable Length
20 Epoxy Mount	Extended: 1460 to 1620nm	UT Underminated FC FC/APC Connector	UT Underminated FC FC/APC Connector



Micron Optics, Inc.  
1852 Century Place NE  
Atlanta, GA 30345 USA

phone 404 325 0005  
fax 404 325 4082  
[www.micronoptics.com](http://www.micronoptics.com)

Copyright ©2010, Micron Optics, Inc. os3100\_0905 b\_0905.1

2

# Appendix C: Temperature Sensor Specifications

## Temperature Compensation Sensor | os4100

### Specifications <sup>B</sup>

os4100

#### Thermal Properties

Operating Temperature Range	-40 to 120°C (150°C short-term)
Temperature Sensitivity	~ 28.9 pm/°C (+/-0.5pm/°C)
Cable Temperature Range	-40 to 150°C (Connectors: -40 to 80°C)
Short-Term Repeatability <sup>2</sup>	± 0.75°C (±21 pm)
Drift <sup>3</sup>	± 1.0°C (±29 pm)

#### Physical Properties

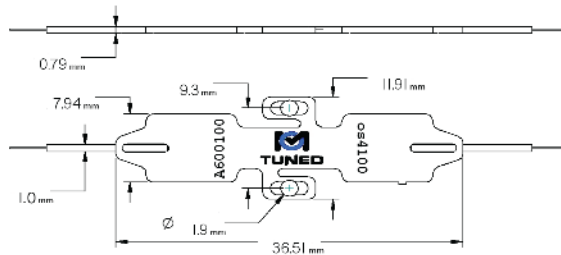
Dimensions	See Diagram Below
Weight	3.0 g
Frame Material	302 Stainless Steel
Cable Length	1 m (± 10 cm), each end
Fiber Type	SMF28-Compatible
Cable Type	1 mm Fiberglass Braid
Connectors	FC/APC optional
Cable Bend Radius	≥ 17 mm
Fastening Methods <sup>4</sup>	Screws [1-72 (M1.6)], Spot Weld or Epoxy

#### Optical Properties

Peak Reflectivity (R <sub>max</sub> )	> 70%
FWHM (-3 dB point)	0.25 nm (± .05 nm)
Isolation	> 15 dB (@ ± 0.4 nm around center wavelength)

#### Notes:

1. Denotes Beta product. For more details see [www.micronoptics.com/product\\_designation.php](http://www.micronoptics.com/product_designation.php).
2. Three thermal cycles from min to max temperature.
3. Typical: 50°C and 85% Relative Humidity. Extreme conditions: ±1.3°C (±36pm); 1,000 hour soak 75°C and 75% Relative Humidity.
4. See [http://www.micronoptics.com/support\\_downloads/Sensors/](http://www.micronoptics.com/support_downloads/Sensors/) for installation details.



### Ordering Information

os4100-**www**-**1xx**-**1yy**

(Example: os4100 -1563-1FC-1UT)

**www**: Wavelength (±1nm)

Standard: 1515 to 1587nm in 4nm intervals.  
Extended: 1460 to 1620nm

**1xx**: Cable 1, Length & Connector

1 1m Standard, Cable Length  
UT Underminated  
FC FC/APC Connector

**1yy**: Cable 2, Length & Connector

1 1m Standard, Cable Length  
UT Underminated  
FC FC/APC Connector



Micron Optics, Inc.  
1852 Century Place NE  
Atlanta, GA 30345 USA

phone 404 325 0005  
fax 404 325 4082  
[www.micronoptics.com](http://www.micronoptics.com)

Copyright ©2009, Micron Optics, Inc. os4100 0905.a 0905.1

2

## Appendix D: Interrogator Specifications

### Optical Sensing Interrogator | sm130

Specifications	sm130-200	sm130-500	sm130-700
<b>Optical Properties</b>			
Number of Optical Channels <sup>1</sup>	1	4	4
Scan Frequency	100 Hz	500 Hz	1 KHz
Wavelength Range	1520-1580 nm	1510-1590 nm	1510-1590 nm
Wavelength Stability <sup>2</sup>	2 pm typ, 5 pm max		
Wavelength Repeatability <sup>3</sup>	1 pm, 0.05 pm with 1,000 averages		
Dynamic Range <sup>4</sup>	25 dB with user-selectable gain		
Typical FBG Sensor Capacity <sup>7</sup>	15	80	80
Internal Peak Detection	Included		
Spectral Diagnostic View	Included		
sm041 Switch Compatible	No	No	Yes
Optical Connectors	FC/APC (E2000 available)		
FBG Requirements <sup>8</sup>	0.25 +/- 0.05nm, FWHM (-3dB point), >15dB Isolation		
<b>Data Processing Capabilities</b>			
Interfaces	Ethernet - other interfaces available via an sp130 Sensing Processor		
Protocols	Custom Micron Optics protocol via Ethernet		
Remote Software	Peak detection, data logger, peak tracking, and instrument control		
LabVIEW™ Source Code	Allows for customization of remote software		
Enhanced Data Management	ENLIGHT Sensing Analysis Software		
<b>Mechanical, Environmental, Electrical Properties</b>			
Dimensions/Weight	122 mm x 267 mm x 135 mm, 2.5 kg (5.5 lbs)		
Operating Temperature, Humidity	0° to 50° C, 0 to 80%, non-condensing		
Storage Temperature, Humidity	-40° to 70° C, 0 to 95%, non-condensing		
Input Voltage	7-36 VDC; (100~240 VAC, 47~63 Hz), AC/DC converter included		
Power Consumption at 12V	25 W typ, 50 Max		
<b>Options</b>			
8 or 16 Channel Expansion	Please see our 8 or 16 channel sm041 multiplexers		
2 kHz Scan Rate <sup>8</sup>	Available with 40nm wavelength range, (1525-1585nm)		
Expanded FBG Sensor Capacity <sup>6,8</sup>	Wavelength range of 1460 - 1620nm doubles maximum FBG sensors per channel		
Notes:			
1. Expansion requires 4 integrated optical channels and 1kHz scan rate to operate an sm041-408 or sm041-416 switch-type multiplexer (500Hz scan rate is sufficient with 160 nm wavelength range)			
2. Captures effects of long-term use over full operating temperature range of the instrument. (Assumes an FBG bandwidth of 0.25nm).			
3. Per NIST Technical Note 1297, 1994 Edition, Section D.1.1.2, definition of "repeatability [of results of measurements]" (Assumes an FBG bandwidth of 0.25nm)			
4. Defined as laser launch power minus detection noise floor. Adjustable 13 dB window within total range.			
5. Used for performance qualification. Bandwidths of 0.1 to 1.0 nm are compatible but may reduce some performance.			
6. Beta product or feature. For details, see <a href="http://www.micronoptics.com/product_designation.php">www.micronoptics.com/product_designation.php</a>			
7. Assuming nominal wavelength range of +/- 2nm per FBG sensor			
8. Maximum scan frequency of 500Hz			



Micron Optics, Inc. phone 404 325 0005  
 1852 Century Place NE fax 404 325 4082  
 Atlanta, GA 30345 USA www.micronoptics.com

Copyright ©2010, Micron Optics, Inc. sm130\_1207d\_12074

2

# Appendix E: Traffic Sensor Specifications

## VSN240 Wireless Flush-Mount Sensor



### Functional Specifications

<b>detection technique</b>	3-axis magnetic field sensing
<b>sampling rate</b>	128 Hz
<b>programmable vehicle detection parameters (mode B only)</b>	<ul style="list-style-type: none"> <li>• Z-axis detect threshold (mG)</li> <li>• Z-axis undetect threshold (mG)</li> <li>• X-axis undetect threshold (mG)</li> <li>• onset filter (ms)</li> <li>• holdover (ms)</li> <li>• auto-recalibration timeout (secs)</li> </ul>
<b>over-the-air protocol</b>	Sensys Networks NanoPower (SNP) protocol (TDMA)
<b>physical layer protocol</b>	EEE 802.15.4 PHY
<b>modulation</b>	Direct Sequence Spread Spectrum Offset Quadrature Phase-Shift Keying (DSSS O-QPSK)
<b>transmit/receive bit rate</b>	250 kbps
<b>frequency band</b>	2400 to 2483.5 MHz (ISM unlicensed band)
<b>frequency channels</b>	16
<b>channel bandwidth</b>	2 MHz
<b>antenna type</b>	microstrip patch antenna (mounted below top surface of sensor)
<b>antenna field of view</b>	±60° (azimuth & elevation)
<b>nominal output power</b>	0 dBm
<b>spurious emissions</b>	<ul style="list-style-type: none"> <li>• 30 - 1000 MHz: &lt; -56 dBm</li> <li>• 1 - 12.75 GHz: &lt; -44 dBm</li> <li>• 1.8 - 1.9 GHz: &lt; -56 dBm</li> <li>• 5.15 - 5.3 GHz: &lt; -51 dBm</li> </ul>
<b>typical receive sensitivity</b>	-95 dBm (PER = 1%)
<b>saturation (max input level)</b>	≥ 10 dBm

### Compliance

<b>safety</b>	2006/95/EC
<b>EMC</b>	<ul style="list-style-type: none"> <li>• FCC: This device complies with Part 15 of the FCC rules. Operation is subject to the following two conditions: (1) This device may not cause harmful interference, and (2) this device must accept any interference received, including interference that may cause undesired operation.</li> <li>• 2004/108/EC</li> </ul>

### Sensor Modes

mode	application	description
<b>B (event)</b>	count stations; advance detection	<ul style="list-style-type: none"> <li>• sends timestamped ON and OFF detection events using configurable detection parameters</li> <li>• not supported by VSN240-T</li> </ul>
<b>E (idle)</b>	status reporting	disables magnetometer and sends sensor hardware and software version information
<b>STOPBAR-# (presence detection)</b>	stop bar detection; ramp management	sends timestamped <i>ON</i> and <i>OFF</i> detection events using pre-configured detection parameters
<ul style="list-style-type: none"> <li>• 16 different stop bar detection modes can be selected</li> <li>• recommended stop bar detection modes for specific applications:</li> </ul>		
	STOPBAR-0	bicycles/scooters
	STOPBAR-2	motorcycles
	STOPBAR-5	passenger vehicles (normal recalibration)
	STOPBAR-7	passenger vehicles (fast recalibration)
	STOPBAR-14	light rail

### Power, Physical, & Environment

<b>power supply</b>	<ul style="list-style-type: none"> <li>• non-replaceable primary Li-SOCl<sub>2</sub> 3.6V battery pack</li> <li>• 7.2 Ah (nominal capacity)</li> </ul>
<b>dimensions</b>	2.9" x 2.9" x 1.9" (7.4 cm x 7.4 cm x 4.9 cm)
<b>weight</b>	0.6 pounds/0.3 kg
<b>environmental</b>	<ul style="list-style-type: none"> <li>• designed for in-pavement mounting</li> <li>• NEMA Type 6P enclosure</li> <li>• IP68 ingress protection</li> </ul>
<b>operating temp</b>	-40°F to 176°F/-40°C to +85°C

Local Distributor

Sensys Networks and the Sensys Networks logo are trademarks of Sensys Networks, Inc. All other trademarks are the property of their respective owners. Information contained herein is believed to be reliable, but Sensys Networks makes no warranties as to its accuracy or completeness.

Copyright © 2012 Sensys Networks, Inc. • ALL RIGHTS RESERVED • P/N 153-240-100-001 Rev D

# Appendix F: Traffic Sensor Access Point Specifications

## AP240 Access Point



### Functional Specifications

<b>interfaces</b>	<ul style="list-style-type: none"> <li>to/from sensors via 802.15.4 PHY radio</li> <li>to/from repeaters via 802.15.4 PHY radio</li> <li>to/from configuration device (PC) via TCP/IP over 10Base-T Ethernet</li> <li>to roadside traffic controller via CC card</li> <li>to/from central network management/data collection facilities via TCP/IP                     <ul style="list-style-type: none"> <li>10Base-T Ethernet</li> <li>cellular data modem</li> </ul> </li> </ul>
<b>IP connectivity</b>	<ul style="list-style-type: none"> <li>Telnet, FTP, HTTP, PPP, PPTP, optional encryption over tunnel</li> <li>10/100Base-T via RJ45 connector</li> <li>GSM GPRS connectivity (optional)                     <ul style="list-style-type: none"> <li>dual-band 850/1900 MHz GSM (N. American version)</li> <li>dual-band 900/1800 MHz GSM (int'l version)</li> <li>up to 85.6 kbps</li> </ul> </li> <li>CDMA2000 1xRTT connectivity (optional)                     <ul style="list-style-type: none"> <li>dual-band 800/1900 MHz CDMA (per specific cellular service provider)</li> <li>up to 153.6 kbps</li> </ul> </li> </ul>
<b>per-lane data processing</b>	<ul style="list-style-type: none"> <li>counts (volume)</li> <li>occupancy</li> <li>average and median speeds</li> <li>binned speeds and vehicle lengths over selectable time intervals</li> </ul>
<b>per-vehicle data processing</b>	<ul style="list-style-type: none"> <li>initial vehicle detect time</li> <li>gap</li> <li>speed</li> <li>length</li> </ul>
<b>memory resources</b>	<ul style="list-style-type: none"> <li>~130 kB for event caching</li> <li>~500 kB for processed data storage</li> </ul>
<b>over-the-air protocol</b>	Sensys Networks NanoPower (SNP) protocol (TDMA)
<b>physical layer protocol</b>	IEEE 802.15.4 PHY
<b>modulation</b>	Direct Sequence Spread Spectrum Offset Quadrature Phase-Shift Keying (DSSS O-QPSK)
<b>transmit/receive bit rate</b>	250 kbps
<b>frequency band</b>	2400 to 2483.5 MHz (ISM unlicensed band)
<b>frequency channels</b>	16
<b>channel bandwidth</b>	2 MHz
<b>antenna type</b>	microstrip patch antenna (behind front face panel)
<b>antenna field of view</b>	±60° (azimuth & elevation)
<b>nominal output power</b>	0 dBm
<b>spurious emissions</b>	<ul style="list-style-type: none"> <li>30 - 1000 MHz: &lt; -56 dBm</li> <li>1 - 12.75 GHz: &lt; -44 dBm</li> <li>1.8 - 1.9 GHz: &lt; -56 dBm</li> <li>5.15 - 5.3 GHz: &lt; -51 dBm</li> </ul>
<b>typical receive sensitivity</b>	-95 dBm (PER ≤ 1%)
<b>saturation (max input level)</b>	≥ 10 dBm

### Power, Physical, & Environmental

<b>input voltage</b>	<ul style="list-style-type: none"> <li>via PoE cable to RJ45 connector</li> <li>36-58 VDC (48 VDC nominal)</li> <li>10-20 VDC (12 VDC nominal)</li> </ul>
<b>power consumption</b>	<ul style="list-style-type: none"> <li>AP240-S, -E, -ES: 2 W</li> <li>AP240-EG, -EC, -ESG, -ESC: 3.5 W</li> </ul>
<b>dimensions</b>	6 1/4" x 6 1/4" x 3 1/2" / 15.9 cm x 15.9 cm x 8.9 cm
<b>weight</b>	<ul style="list-style-type: none"> <li>AP240-S, -E, -ES: 1.9 lbs/0.9 kg</li> <li>AP240-EG, -EC, -ESG, -ESC: 2.1 lbs/0.9 kg</li> <li>mounting kit: add 1.2 lbs/0.5 kg</li> </ul>
<b>environmental</b>	<ul style="list-style-type: none"> <li>designed for weatherproof, outdoor operation</li> <li>NEMA Type 4x enclosure</li> <li>IP67 ingress protection</li> </ul>
<b>operating temp</b>	-10°F to 176°F / -10°C to +80°C

### Types of Access Points

	stats processing capability	power options		detection data interfaces			
		48 VDC	12 VDC	contact closure	10 Base-T	GSM GPRS	CDMA2000 1xRTT
AP240-S		•		•			
AP240-E	•	•	•		•		
AP240-ES	•	•		•	•		
AP240-EG	•	•	•		•	•	
AP240-EC	•	•	•		•		•
AP240-ESG	•	•		•	•	•	
AP240-ESC	•	•		•	•		•

### Compliance

<b>safety</b>	2006/95/EC
<b>EMC</b>	<ul style="list-style-type: none"> <li>FCC: This device complies with Part 15 of the FCC rules. Operation is subject to the following two conditions: (1) This device may not cause harmful interference, and (2) this device must accept any interference received, including interference that may cause undesired operation.</li> <li>2004/108/EC</li> </ul>

Local Distributor

Sensys Networks and the Sensys Networks logo are trademarks of Sensys Networks, Inc. All other trademarks are the property of their respective owners. Information contained herein is believed to be reliable, but Sensys Networks makes no warranties as to its accuracy or completeness.

Copyright © 2012 Sensys Networks, Inc. • ALL RIGHTS RESERVED • P/N 153-240-015-001 Rev D

# Appendix G: Temperature & Relative Humidity Probe Specifications

## Manufacturer Specifications

<b>Supply Voltage:</b>	12 Vdc nominal
<b>Current Consumption:</b>	≤4 mA (active)
<b>Dimensions</b>	
Diameter:	1 in. (2.5 cm)
Length:	10 in. (25.4 cm)
<b>Weight:</b>	0.6 lb. (0.27 kg)
<b>Filter:</b>	0.2 μm Teflon® membrane
<b>Filter Diameter:</b>	0.75 in. (1.9 cm)
<b>Operating Temperature:</b>	-40° to +60°C

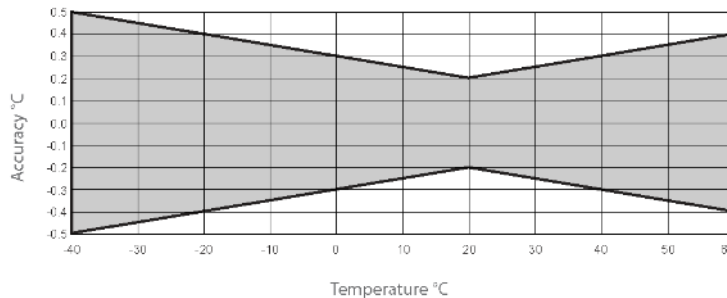
### Air Temperature

<b>Temperature Sensor:</b>	1000 ohm PRT
<b>Measurement Range:</b>	-39.2° to +60°C
<b>Output Signal Range:</b>	0.008 to 1.0 V
<b>Temperature Accuracy:</b>	see graph below

### Relative Humidity (RH)

<b>Sensor:</b>	Vaisala's HUMICAP® H-chip
<b>Measurement Range:</b>	0.8 to 100% RH, non-condensing
<b>Output Signal Range:</b>	0.008 to 1 Vdc
<b>Accuracy at 20°C</b>	
against factory reference:	±1% RH
field-calibrated	
against references:	±2% RH (0 to 90% RH) ±3% RH (90% to 100% RH)
<b>Temperature Dependence:</b>	±0.05% RH/°C
<b>Long-Term Stability:</b>	Typically, better than 1% RH per year
<b>Response Time:</b>	15 seconds with membrane filter (at 20°C, 90% response)
<b>Settling Time:</b>	500 milliseconds

Temperature Accuracy Graph



### Notes:

- (1) The black outer jacket of the cable is Santoprene® rubber. This compound was chosen for its resistance to temperature extremes, moisture, and UV degradation. However, this jacket will support combustion in air. It is rated as slow burning when tested according to U.L. 94 H.B. and will pass FMVSS302. Local fire codes may preclude its use inside buildings.
- (2) The HMP45C is manufactured by Vaisala, Inc. (Woburn, MA) but cabled and modified by Campbell Scientific for use with our dataloggers.



Campbell Scientific, Inc. | 815 W 1800 N | Logan, Utah 84321-1784 | (435) 753-2342 | www.campbellsci.com  
 USA | AUSTRALIA | BRAZIL | CANADA | COSTA RICA | ENGLAND | FRANCE | GERMANY | SOUTH AFRICA | SPAIN

Copyright © 1998-2011  
 Campbell Scientific, Inc.  
 Printed January 2011

# Appendix H: Wind Monitor Specifications

## Specifications

### Wind Speed

	05103 Wind Monitor	05103-45 Wind Monitor-Alpine	05106 Wind Monitor-MA	05305 Wind Monitor-AQ
Range	0 to 100 m s <sup>-1</sup> (0 to 224 mph)			0 to 50 m s <sup>-1</sup> (0 to 112 mph)
Accuracy	±0.3 m s <sup>-1</sup> (±0.6 mph) or 1% of reading			±0.2 m s <sup>-1</sup> (±0.4 mph) or 1% of reading
Starting Threshold	1.0 m s <sup>-1</sup> (2.2 mph)		2.4 mph (1.1 m s <sup>-1</sup> )	0.4 m s <sup>-1</sup> (0.9 mph)
Distance Constant (63% recovery)	2.7 m (8.9 ft)			2.1 m (6.9 ft)
Output	ac voltage (3 pulses per revolution); 1800 rpm (90 hz) = 8.8 m s <sup>-1</sup> (19.7 mph)			ac voltage (3 pulses per revolution); 1800 rpm (90 hz) = 9.2 m s <sup>-1</sup> (20.6 mph)
Resolution	(0.0980 m s <sup>-1</sup> )/(scan rate in seconds) or (0.2192 mph)/(scan rate in seconds)			(0.1024 m s <sup>-1</sup> )/(scan rate in sec.) or (0.2290 mph)/(scan rate in sec.)

### Wind Direction

	05103 Wind Monitor	05103-45 Wind Monitor-Alpine	05106 Wind Monitor-MA	05305 Wind Monitor-AQ
Range	0° to 360° mechanical, 355° electrical (5° open)			
Accuracy	±3°	±5°	±3°	
Starting Threshold	1.1 m s <sup>-1</sup> (2.4 mph)			0.5 m s <sup>-1</sup> (1.0 mph)
Distance Constant (50% recovery)	1.3 m (4.3 ft)			1.2 m (3.9 ft)
Damping Ratio	0.3			0.45
Damped Natural Wavelength	7.4 m (24.3 ft)			4.9 m (16.1 ft)
Undamped Natural Wavelength	7.2 m (23.6 ft)			4.4 m (14.4 ft)
Output	analog dc voltage from potentiometer—resistance 10 kΩ; linearity 0.25%; life expectancy 50 million revolutions			
Power	switched excitation voltage supplied by datalogger			

### Physical

	05103 Wind Monitor	05103-45 Wind Monitor-Alpine	05106 Wind Monitor-MA	05305 Wind Monitor-AQ
Operating Temperature Range	-50° to +50°C, assuming non-riming conditions			
Overall Height	37 cm (14.6 in)			38 cm (15 in)
Overall Length	55 cm (21.7 in)			65 cm (25.6 in)
Main Housing Diameter	5 cm (2 in)			
Propeller Diameter	18 cm (7.1 in)	14 cm (5.5 in)	18 cm (7.1 in)	20 cm (7.9 in)
Mounting Pipe Description	34 mm (1.34 in) outer diameter; standard 1.0 in IPS schedule 40			
Weight	1.5 kg (3.2 lb)	1 kg (2.2 lb)	1.5 kg (3.2 lb)	1.1 kg (2.5 lb)



Campbell Scientific, Inc. | 815 W 1800 N | Logan, UT 84321-1784 | (435) 227-9000 | www.campbellsci.com  
 USA | AUSTRALIA | BRAZIL | CANADA | CHINA | COSTA RICA | ENGLAND | FRANCE | GERMANY | SOUTH AFRICA | SPAIN

© 1991, 2014  
 Campbell Scientific, Inc.  
 February 3, 2014

# Appendix I: Rain Gauge Specifications

## Ordering Information

### Tipping Bucket Raingages

Enter the cable length, in feet, after the -L. Recommended length is 25 ft, but many customers will order a 50 ft cable to place the gage away from the tower or tripod. Must choose a cable termination option.

- TE525WS-L** Tipping bucket with 8 inch diameter orifice and 0.01 in. tips.
- TE525-L** Tipping bucket with 6 inch diameter orifice and 0.01 in. tips.
- TE525MM-L** Tipping bucket with 24.5 cm diameter orifice and 0.1 mm tips.

### Cable Termination Options (choose one)

- PT** Cable terminates in stripped and tinned leads for direct connection to a datalogger's terminals.
- PW** Cable terminates in a connector for attachment to a prewired enclosure.
- CWS** Cable terminates in a connector for attachment to a CWS900-series interface. Connection to a CWS900-series interface allows this sensor to be used in a wireless sensor network.
- C** Cable terminates in a connector for attachment to a CS110 Electric Field Meter or ET107 weather station.
- RQ** Cable terminates in a connector for attachment to a RAWS-P Permanent Remote Automated Weather Station. This option is not offered for the TE525MM.

### Mounting Poles

- CM300** 23 inch Mounting Pole with Cap
- CM305** 47 inch Mounting Pole with Cap
- CM310** 56 inch Mounting Pole with Cap

### Pedestal Options for Mounting Poles (choose one)

- NP** No Pedestal Base
- PJ** CM340 Pedestal J-Bolt Kit
- PS** CM350 Pedestal Short Legs (23 in. legs)
- PL** CM355 Pedestal Long Legs (39 in. legs)

### Common Accessories

- CS705** Snowfall adapter for the TE525WS
- 10869** Four one-gallon containers of 50:50 PG:E Antifreeze; only U. S. ground shipments
- CM270** CM270 Mounting Kit
- 260-953** Novalynx Alter-type Rain Gage Wind Screen

## Specifications

	TE525	TE525WS	TE525MM
<b>Sensor Type</b>	tipping bucket/potted magnetic momentary contact reed switch		
<b>Switch Ratings</b>	30 Vdc at 2 A; 115 Vac at 1 A; closure time: 135 ms; bounce settling time: 0.75 ms		
<b>Bucket Material</b>	white powder coated spun aluminum		
<b>Funnel Collector Material</b>	gold anodized spun aluminum		
<b>Screen Material</b>	gold anodized spun aluminum		
<b>Locking Snap Ring Material</b>	stainless steel		
<b>Operating Temperature</b>	0° to +50°C (32° to 125°F)		
<b>Resolution</b>	1 tip		
<b>Volume per Tip</b>	4.73 ml/tip (0.16 fl. oz/tip)	8.24 ml/tip (0.28 fl. oz/tip)	4.73 ml/tip (0.16 fl. oz/tip)
<b>Rainfall per Tip</b>	0.01 in. (0.254 mm)		0.1 mm (0.004 in)
<b>Accuracy</b>	1.0% up to 2 in./hour (50 mm/hr)		
<b>Knife Edge Funnel Collector Diameter</b>	15.4 cm (6.1 in)	20.3 cm (8 in)	24.5 cm (9.7 in)
<b>Height</b>	24.1 cm (9.5 in)	26.7 cm (10.5 in)	29.2 cm (11.5 in)
<b>Tipping Bucket Weight</b>	0.9 kg (2 lb)	1 kg (2.2 lb)	1.1 kg (2.4 lb)
<b>Cable</b>	2 conductor shielded cable		
<b>Cable Weight</b>	0.1 kg (0.2 lb) per 10 ft length		
<b>Warranty</b>	three year		

## Appendix J: Intelligent Road Sensor Specifications

# IRS21

## Intelligent Road Surface Sensor



Lufft's IRS21 is a passive sensor that monitors actual road conditions. This intelligent road surface sensor is a primary component of our Road Weather Information Stations (RWIS). When used in an RWIS application, the IRS21 is connected to a CR800, CR850, CR1000, or CR10X datalogger via the 18080 Lufft Interface and our SDM-SIO4 Serial Data Interface Module.

The IRS21 measures the following parameters:

- Road surface temperature
- Water film level (up to 4 mm)
- Freezing temperature for NaCl (others on request)
- Road condition (dry/damp/wet/ice or snow/residual salt/freezing)

The sensors use radar techniques to measure water film.



### Installation

Two IRS21 sensors are typically installed at the measurement site. Each sensor is placed inside a hole in the road and then the hole is filled with epoxy. To provide accurate measurements and prevent damage to the sensor, the IRS21 must be installed flush to the road surface.

### Ordering Information

Model	Description
IRS21	Intelligent Road Surface Sensor with 75 ft (25 m) cable.
18080	Interface that connects the IRS21 to an SDM-SIO4.
SDM-SIO4	4-Channel Serial Data Interface Module

### Specifications

Operating Humidity: 100% RH

Temperature Range: -40° to +70°C operating;  
-50° to +70°C storage

Power Requirements: 9 to 14 Vdc; less than 200 mA

Interface: RS-485

Road Condition Output: dry, damp, wet, snow,  
freezing wetness, ice

Road Temperature Range: -40° to +70°C  
(-40° to +158°F)

Road Temperature Accuracy:  
±0.2°C (-10° to 10°C); ±0.5°C (-40° to 70°C)

Road Temperature Resolution: -0.1°C

Freezing Point Range: -20° to 0°C (-4° to +32°F)

Freezing Point Accuracy: ±0.1°C

Freezing Point Resolution: -0.1°C

Dimensions: 5" (13 cm) diameter, 2" (5 cm) height

Weight: 2 lbs (0.9 kg)



815 W. 1800 N. | Logan, Utah | 84321-1784 | USA | (435) 753-2342 | www.campbellsci.com  
Australia | Brazil | Canada | England | France | Germany | South Africa | Spain | USA [headquarters]

Copyright © 2008, 2009  
Campbell Scientific, Inc.  
Printed January 2009

# Appendix K: Environmental Sensor Station Data Logger Specifications

## CR1000 Specifications

Electrical specifications are valid over a -25° to +50°C, non-condensing environment, unless otherwise specified. Recalibration recommended every three years. Critical specifications and system configuration should be confirmed with Campbell Scientific before purchase.

### PROGRAM EXECUTION RATE

10 ms to one day @ 10 ms increments

### ANALOG INPUTS (SE1-SE16 or DIFF1-DIFF8)

8 differential (DF) or 16 single-ended (SE) individually configured input channels. Channel expansion provided by optional analog multiplexers.

RANGES and RESOLUTION: Basic resolution (Basic Res) is the A/D resolution of a single A/D conversion. A DIFF measurement with input reversal has better (finer) resolution by twice than Basic Res.

Range (mV)	DF Res (µV) <sup>1</sup>	Basic Res (µV)
±5000	667	1333
±2500	333	667
±250	33.3	66.7
±25	3.33	6.7
±7.5	1.0	2.0
±2.5	0.33	0.67

<sup>1</sup>Range overhead of ~9% on all ranges guarantees that full-scale values will not cause overflow.  
<sup>2</sup>Resolution of DF measurements with input reversal.

### ACCURACY<sup>3</sup>:

±0.06% of reading + offset), 0° to 40°C  
 ±0.12% of reading + offset), -25° to 50°C  
 ±0.18% of reading + offset), -55° to 85°C (-XT only)

<sup>3</sup>Accuracy does not include the sensor and measurement noise. Offsets are defined as:

Offset for DF w/input reversal = 1.5·Basic Res + 1.0 µV  
 Offset for DF w/o input reversal = 3·Basic Res + 2.0 µV  
 Offset for SE = 3·Basic Res + 3.0 µV

### ANALOG MEASUREMENT SPEED:

Integration Type/Code	Integration Time	Setting Time	Total Time <sup>4</sup>	
			SE w/ No Rev	DF w/ Input Rev
250	250 µs	450 µs	~1 ms	~12 ms
60 Hz <sup>5</sup>	18.87 ms	3 ms	~20 ms	~40 ms
50 Hz <sup>5</sup>	20.00 ms	3 ms	~25 ms	~50 ms

<sup>4</sup>Includes 250 µs for conversion to engineering units.  
<sup>5</sup>AC line noise filter.

INPUT NOISE VOLTAGE: For DF measurements with input reversal on ±2.5 mV input range (digital resolution dominates for higher ranges).

250 µs Integration: 0.34 µV RMS  
 60/50 Hz Integration: 0.19 µV RMS

INPUT LIMITS: ±5 Vdc

DC COMMON MODE REJECTION: >100 dB

NORMAL MODE REJECTION: 70 dB @ 60 Hz when using 60 Hz rejection

INPUT VOLTAGE RANGE W/O MEASUREMENT CORRUPTION: ±8.6 Vdc max.

SUSTAINED INPUT VOLTAGE W/O DAMAGE: ±16 Vdc max.

INPUT CURRENT: ±1 nA typical, ±6 nA max. @ 50°C, ±90 nA @ 85°C

INPUT RESISTANCE: 20 GΩ typical

ACCURACY OF BUILT-IN REFERENCE JUNCTION THERMISTOR (for thermocouple measurements):

±0.3°C, -25° to 50°C  
 ±0.8°C, -55° to 85°C (-XT only)

### ANALOG OUTPUTS (VX1-VX3)

3 switched voltage, sequentially active only during measurement.

RANGE AND RESOLUTION:

Channel	Range	Resolution	Current Source/Sink
{VX1-3}	±2.5 Vdc	0.67 mV	±25 mA

### ANALOG OUTPUT ACCURACY (VX):

±0.06% of setting + 0.8 mV), 0° to 40°C  
 ±0.12% of setting + 0.8 mV), -25° to 50°C  
 ±0.18% of setting + 0.8 mV), -55° to 85°C (-XT only)

VX FREQUENCY SWEEP FUNCTION: Switched outputs provide a programmable sweep frequency, 0 to 2500 mV square waves for exciting vibrating wire transducers.

### PERIOD AVERAGE

Any of the 16 SE analog inputs can be used for period averaging. Accuracy is ±0.01% of reading + resolution, where resolution is 136 ns divided by the specified number of cycles to be measured.

### INPUT AMPLITUDE AND FREQUENCY:

Voltage Gain	Input Range (±mV)	Signal (peak to peak)		Min Pulse Width (µV)	Max <sup>8</sup> Freq (kHz)
		Min. (mV) <sup>6</sup>	Max (V) <sup>7</sup>		
1	250	500	10	2.5	200
10	25	10	2	10	50
33	7.5	5	2	62	8
100	2.5	2	2	100	5

<sup>6</sup>Signal centered around Threshold (see PeriodAvg() instruction).

<sup>7</sup>With signal centered at the cataloger ground.

<sup>8</sup>The maximum frequency is 1/(twice minimum pulse width) for 50% of duty cycle signals.

### RATIOMETRIC MEASUREMENTS

MEASUREMENT TYPES: Provides ratiometric resistance measurements using voltage excitation. 3 switched voltage excitation outputs are available for measurement of 4- and 6-wire full bridges, and 2-, 3-, and 4-wire half bridges. Optional excitation polarity reversal minimizes dc errors.

### RATIOMETRIC MEASUREMENT ACCURACY:<sup>9,10,11</sup>

±0.04% of Voltage Measurement + Offset<sup>11</sup>

<sup>9</sup>Accuracy specification assumes excitation reversal for excitation voltages < 1000 mV. Assumption does not include bridge resistor errors and sensor and measurement noise.

<sup>10</sup>Estimated accuracy: ΔX (where X is value returned from the measurement with Multiplier = 1, Offset = 0).

**BrFull()** instruction: ΔX = ΔV/V<sub>N</sub>, expressed as mV·V<sup>-1</sup>. ΔV<sub>N</sub> is calculated from the ratiometric measurement accuracy. See Resistance Measurements Section in the manual for more information.

<sup>11</sup>Offsets are defined as:

Offset for DIFF w/input reversal = 1.5·Basic Res + 1.0 µV  
 Offset for DIFF w/o input reversal = 3·Basic Res + 2.0 µV  
 Offset for SE = 3·Basic Res + 3.0 µV

Excitation reversal reduces offsets by a factor of two.

### PULSE COUNTERS (P1-P2)

2 inputs individually selectable for switch closure, high frequency pulse, or low-level ac. Independent 24-bit counters for each input.

MAXIMUM COUNTS PER SCAN: 18.7x10<sup>6</sup>

### SWITCH CLOSURE MODE:

Minimum Switch Closed Time: 5 ms  
 Minimum Switch Open Time: 6 ms  
 Max. Bounce Time: 1 ms open w/o being counted

### HIGH-FREQUENCY PULSE MODE:

Maximum Input Frequency: 250 kHz  
 Maximum Input Voltage: ±20 V  
 Voltage Thresholds: Count upon transition from below 0.9 V to above 2.2 V after input filter with 1.2 µs time constant.

### LOW-LEVEL AC MODE: Internal ac coupling removes ac offsets up to ±0.5 Vdc.

Input Hysteresis: 12 mV RMS @ 1 Hz  
 Maximum ac Input Voltage: ±20 V  
 Minimum ac Input Voltage:

Sine Wave (mV RMS)	Range(Hz)
20	1.0 to 20
200	0.5 to 200
2000	0.3 to 10,000
5000	0.3 to 20,000

### DIGITAL I/O PORTS (C1-C8)

8 ports software selectable, as binary inputs or control outputs. Provide on/off, pulse width modulation, edge timing, subroutine interrupts / wake up, switch closure pulse counting, high frequency pulse counting, asynchronous communications (UARTs), and SDI-12 communications. SDM communications are also supported.

LOW FREQUENCY MODE MAX: <1 kHz

HIGH-FREQUENCY MODE MAX: 400 kHz

SWITCH-CLOSURE FREQUENCY MAX: 180 Hz

EDGE TIMING RESOLUTION: 540 ns

OUTPUT VOLTAGES (no load): high 5.0 V ±0.1 V; low <0.1

OUTPUT RESISTANCE: 330 Ω

INPUT STATE: high 3.8 to 16 V; low -8.0 to 1.2 V

INPUT HYSTERESIS: 1.4 V

INPUT RESISTANCE: 100 Ω with inputs <6.2 Vdc

220 Ω with inputs >6.2 Vdc

SERIAL DEVICE/RS-232 SUPPORT: 0 to 5 Vdc UART

### SWITCHED 12 VDC (SW-12)

1 independent 12 Vdc unregulated source is switched on and off under program control. Thermal fuse hold current = 900 mA at 20°C, 650 mA at 50°C, 380 mA at 85°C.

### CE COMPLIANCE

STANDARD(S) TO WHICH CONFORMITY IS DECLARED: IEC61328:2002

### COMMUNICATIONS

RS-232 PORTS:

DCE 9-pin: (not electrically isolated) for computer connection or connection of modems not manufactured by Campbell Scientific.

COM1 to COM4: 4 independent Tx/Rx pairs on control ports (non-isolated); 0 to 5 Vdc UART

Basic Rates: selectable from 300 bps to 115.2 kbps.

Default Format: 8 data bits; 1 stop bit; no parity

Optional Formats: 7 data bits; 2 stop bits; odd, even parity

DS-10 PORT: Interface with telecommunications peripherals manufactured by Campbell Scientific.

SDI-12: Digital control ports C1, C3, C5, and C7 are individually configured and meet SD-12 Standard v. 1.3 for cataloger mode. Up to 10 SDI-12 sensors are supported per port.

PERIPHERAL PORT: 40-pin interface for attaching

ComocFlash or Ethernet peripherals

PROTOCOLS SUPPORTED: PakBus, AES-128 Encrypted PakBus, Modbus, DNP3, FTP, HTTP, XML, HTML, POP3, SMTP, Telnet, NTP, Web API, SDI-12, SDM.

### SYSTEM

PROCESSOR: Renesas H8S 2322 (16-bit CPU with 32-bit internal core running at 7.3 MHz)

MEMORY: 2 MB of flash for operating system; 4 MB of battery-backed SRAM for CPU usage and final data storage; 512 kB flash disk (CPU) for program files.

REAL-TIME CLOCK ACCURACY: ±3 min. per year.

Correction via GPS optional

REAL-TIME CLOCK RESOLUTION: 10 ms

### SYSTEM POWER REQUIREMENTS

VOLTAGE: 9.6 to 16 Vdc

INTERNAL BATTERIES: 1200 mAh lithium battery for clock and SRAM backup that typically provides three years of backup

EXTERNAL BATTERIES: Optional 12 Vdc nominal alkaline and rechargeable available. Power connection is reverse polarity protected.

TYPICAL CURRENT DRAIN at 12 Vdc:

Sleep Mode: < 1 mA  
 1 Hz Sample Rate (1 fast SE meas.): 1 mA  
 100 Hz Sample Rate (1 fast SE meas.): 6 mA  
 100 Hz Sample Rate (1 fast SE meas. w/RS-232 communication): 20 mA  
 Active external keyboard display adds 7 mA (100 mA with backlight on).

### PHYSICAL

DIMENSIONS: 23.9 x 10.2 x 6.1 cm (9.4 x 4 x 2.4 in);

additional clearance required for cables and leads.

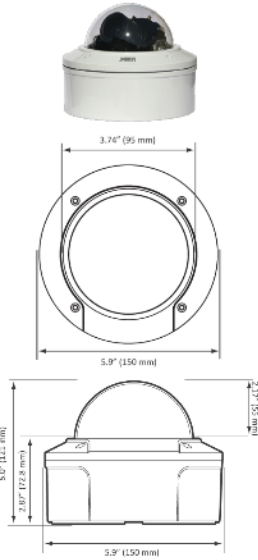
MASS/WEIGHT: 1 kg / 2.1 lb

### WARRANTY

3 years against defects in materials and workmanship.

## Appendix L: NetCam SC Specifications

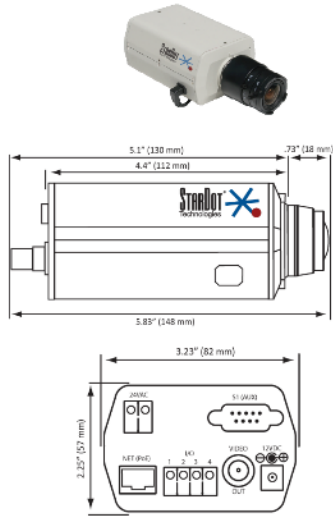
NetCam SC • SPECIFICATIONS



### VANDAL RESISTANT DOME

PHYSICAL	
Dimensions	5.9" Diameter (150mm) x 4.7" H (120mm)
Weight	44 Ounces (1247 grams)
Operating Temp	-40° - +122° F (-40° - +50° C)
<ul style="list-style-type: none"> <li>• Power Requirements: 12VDC/ 24VAC/ POE</li> <li>• EMI Approval: FCC Class A, CE (EN55024)</li> </ul>	
CONNECTIVITY	
<ul style="list-style-type: none"> <li>• 1 x 10/100-baseT, RJ-45, PoE 802.3af (Power over Ethernet)</li> <li>• 1 x BNC Video Output (NTSC/PAL)</li> <li>• 1 x DC Auto Iris Connector</li> <li>• 1 x RS-232 Serial Port, up to 115.2Kb</li> </ul>	
MODELS	
SD500VN	5MP Vandal Resistant Dome with Day/Night
SD500V	5MP Vandal Resistant Dome
SD300V	3MP Vandal Resistant Dome
SD130VN	1.3MP Vandal Resistant Dome with Day/Night
SD130V	1.3MP Vandal Resistant Dome

### OPTIONAL MOUNTS



### HYBRID IP BOX CAMERA

PHYSICAL	
Dimensions	3.23"W (82mm) 2.25" H (57mm) 4.4" L (112mm)
Weight	14 Ounces (397 grams)
Operating Temp	-40° - +122° F (-40° - +50° C)
<ul style="list-style-type: none"> <li>• Power Requirements: 12VDC/ 24VAC/ POE</li> <li>• EMI Approval: FCC Class A, CE (EN55024)</li> </ul>	
CONNECTIVITY	
<ul style="list-style-type: none"> <li>• 1 x 10/100-baseT, RJ-45, PoE 802.3af (Power over Ethernet)</li> <li>• 1 x BNC Video Output (NTSC/PAL)</li> <li>• 1 x DC Auto Iris Connector</li> <li>• 1 x RS-232 Serial Port, DB9 Male, up to 115.2Kb</li> <li>• 1 x Fully Isolated Digital Alarm Input</li> <li>• 1 x Fully Isolated Relay Rated at 28VDC 2A or 125VDC 0.5A</li> </ul>	
MODELS	
SD500BN	5MP NetCam SC with Day/Night
SD500B	5MP NetCam SC
SD300B	3MP NetCam SC
SD130BN	1.3MP NetCam SC with Day/Night
SD130B	1.3MP NetCam SC

www.stardot.com  
 Buena Park, CA USA  
 1-877-275-1616  
 714-908-2380 • 714-844-4336 fax



# Appendix M: Axis Specifications

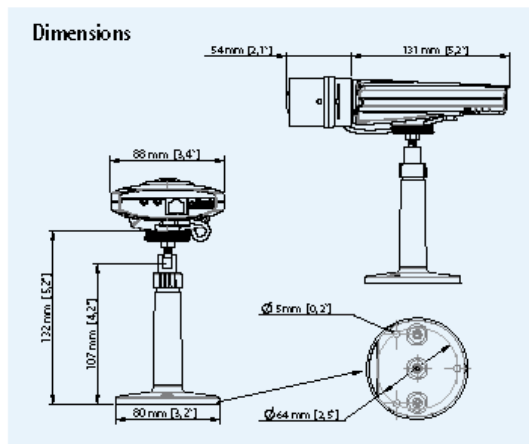
www.axis.com

37283/ENR10811

## Technical specifications – AXIS 211M Network Camera

<b>Camera</b>		<b>System integration</b>	
Image sensor	1/3" Progressive scan RGB CMOS 1.3 Megapixel	Application Programming Interface	Open API for software integration, including VAPIX® from Axis Communications available at www.axis.com
Lens	3.0 - 8.0 mm, F1.0, DC-iris, CS mount Angle of view, horizontal: 37° - 99°	Intelligent video	Video motion detection, audio detection
Minimum illumination	1 lux, F1.0	Alarm triggers	Intelligent video, external input
Shutter time	1/15000 s to 1/4 s	Alarm events	File upload via FTP, HTTP and email Notification via email, HTTP and TCP External output activation
<b>Video</b>		Video buffer	20 MB pre- and post alarm
Video compression	MPEG-4 Part 2 (ISO/IEC 14496-2) Motion JPEG	<b>General</b>	
Resolutions	160x90 - 1280x1024	Processors and memory	ARTPEC-A, 64 MB RAM, 8 MB Flash
Frame rate MPEG-4	Up to 8 fps at 1280x1024, 13 fps at 1024x768, 20 fps in 800x600 mode	Power	7 - 20 V DC, max. 5 W Power over Ethernet IEEE 802.3af Class 2
Frame rate Motion JPEG	Up to 12 fps at 1280x1024, 20 fps at 1024x768, 30 fps in 800x600 mode	Connectors	RJ-45 Ethernet 10BaseT/100BaseTX PoE, Auto-MDIX Terminal block for 1 alarm input, 1 output and alternative power connection 3.5 mm mic/line in, 3.5 mm line out
Video streaming	Simultaneous MPEG-4 and Motion JPEG Controllable frame rate and bandwidth VBR/CBR MPEG-4	Operating conditions	0 - 45 °C (32 - 113 °F) Humidity 20 - 80% RH (non-condensing)
Image settings	Compression, color, brightness, sharpness, contrast, white balance, exposure control, exposure zones, rotation, backlight compensation, mirroring, fine tuning of behavior at low light Text and image overlay Privacy mask	Approvals	EN 55022 Class B, EN 55024, EN 61000-3-2, EN 61000-3-3, FCC Part 15 Subpart B Class B, VCCI Class B, ICES-003 Class B, C-tick AS/NZS CISPR 22, EN 60950-1 Power supply: EN 60950-1, UL, cUL
<b>Audio</b>		Weight	244 g (0.5 lb.)
Audio streaming	Two-way, full, half duplex	Included accessories	Power supply, stand, connector kit, Installation Guide, CD with installation tools, recording software and User's Manual, Windows decoder 1-user license
Audio compression	AAC LC 8 kHz 32 kbit/s G.711 PCM 64 kbit/s G.726 ADPCM 3.2 or 24 kbit/s		
Audio input/output	Built-in microphone, external microphone input or line input, line level output		
<b>Network</b>			
Security	Password protection, IP address filtering, HTTPS encryption, IEEE 802.1X network access control, digest authentication, user access log		
Supported protocols	IPv4/v6, HTTP, HTTPS, QoS Layer 3 DiffServ, FTP, SMTP, Bonjour, UPnP, SNMPv1/v2c/v3 (MIB-II), DNS, DynDNS, NTP, RTSP, RTP, TCP, UDP, IGMP, RTPC, ICMP, DHCP, ARP, SOCKS		

More information is available at [www.axis.com](http://www.axis.com)



### Optional accessories

#### Various housings



#### Lenses



For information on AXIS Camera Station and video management software from Axis' Application Development Partners, see [www.axis.com/products/video/software/](http://www.axis.com/products/video/software/)

©2009 Axis Communications AB. AXIS COMMUNICATIONS, AXIS, ETRAX, ARTPEC and VAPIX are registered trademarks or trademark applications of Axis AB in various jurisdictions. All other company names and products are trademarks or registered trademarks of their respective companies. We reserve the right to introduce modifications without notice.



# Appendix N: Control DeviceMaster Specifications

## DEVICEMASTER SPECIFICATIONS::

### HARDWARE

<b>Bus Interface Specification</b>	10/100 BASE-T
<b>Memory</b>	8MB SDRAM, 4MB Flash
<b>Enclosure</b>	Stainless Steel
<b>Installation Method</b>	Panel mountable or DIN rail
<b>LED Indicators</b>	100MB Ethernet, Duplex, Ethernet Link/Activity, and Status
<b>Dimensions</b>	3.6" x 0.8" x 2.8"
	41.4 x 20.3 x 71.1 mm
<b>Product Weight</b>	7.8 oz
	0.22 kg

### ELECTRICAL SPECIFICATIONS

<b>Device Requirements</b>	200mA @ 5VDC
<b>Control Consumption</b>	2.1 Watts
<b>Control External Power Supply</b>	
Input	90 to 132VAC @ 60Hz
	90 to 264VAC @ 50-60Hz (Euro Power Supply version)
Output	420mA @ 5VDC
	5VDC @ 2A (Euro Power Supply version)
<b>Surge Protection</b>	
	Provides minimum of 15kV protection for all serial lines. All Ethernet components are rated to 1.5kV magnetic surge protection.

### ENVIRONMENTAL SPECIFICATIONS

<b>Air Temperature</b>	
System On	-37° to 74°C
System Off	-40° to 95°C
<b>Operating Humidity</b>	5% to 95%
<b>Altitude</b>	0 to 10,000 Ft
	0 to 3,048 m
<b>Heat Output</b>	7.2 BTU/Hr
<b>MTBF (Mean time between failures)</b>	48.4 Years

### SERIAL COMMUNICATIONS

<b>Connector Type</b>	D89M
<b>Number of Ports</b>	1
<b>Software Interfaces</b>	RS-232/422/485
<b>Baud Rates</b>	
50 bps to 230Kbps	
300 bps to 230.4Kbps (Euro Power Supply Version)	
Receive Buffer	1024bytes
Transmit Buffer	256bytes
<b>Device Driver Data Control</b>	
Data Bits	7 or 8
Parity	Odd, Even, None
Stop Bits	1 or 2
Flow Control	Hardware, Software or none

### ETHERNET SPECIFICATIONS

**Network Protocols**  
 ARP, BOOTP, DHCP/RARP/Ping, HTTP, ICMP, RFC 1006 (ISO over TCP), SNMP (MIB-II), TFTP & UDP socket services, Telnet, and TFTP and supports IP multicast data transmission

**Connector Type**  
 RJ45F Auto MDI/MDI-X

**Number of Ports**  
 1

### FEATURES

**SNMP Support**  
 Monitoring Only

**Other**  
 Event notification, lowest latency, NS-Link COM/TTY port redirector, PortVision DX remote management and Watchdog reset

**Manufacturer's Warranty**  
 5 Years

### EXPORT INFORMATION

<b>Package Shipping Weight</b>	1.97 lbs	0.89 kg
<b>Package Shipping Dimensions</b>	9.18" x 2.5" x 7.25"	233 x 63.5 x 184 mm
<b>UPC Code</b>	7-56727-99435-0	7-56727-99437-4
	(w/ EU power supply)	5A992
<b>ECCN</b>	8471.B0.1000	
<b>Schedule B Number</b>		

### DEVICE DRIVERS

Linux  
 Microsoft®/Windows® 7  
 Microsoft®/Windows® 2008 Server  
 Microsoft®/Windows® Vista  
 Microsoft®/Windows Server® 2003  
 Microsoft®/Windows® XP  
 Microsoft®/Windows NT® 4.0 (Legacy)  
 Microsoft®/Windows® 2000 (Legacy)

### REGULATORY STANDARDS

**Emissions**  
 Canadian EMC requirements  
 CISR-003  
 CISPR-22  
 European Standard EN55022 FCC Part 15 Subpart B Class A limit  
 AS/NZS-3548

**Immunity**  
 European Standard EN55024  
 EC 1000-4-2/EN61000-4-2 ESD  
 EC 1000-4-3/EN61000-4-3 RF  
 EC 1000-4-4/EN61000-4-4 Fast Transient  
 EC 1000-4-5/EN61000-4-5 Surge  
 EC 1000-4-6/EN61000-4-6 Conducted Disturbance  
 EC 1000-4-8/EN61000-4-8 Magnetic Field  
 EC 1000-4-11/EN61000-4-11 Dips and Voltage Variations

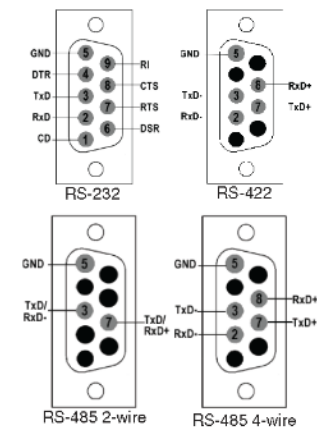
**Safety**  
 IEC 60950/EN60950 (LISTED)  
 CSA C22.2 No. 60950A1/80950 Third Edition

**Other**  
 NEMA TS2 Compliant  
 RoHS2 compliant under CE

### REGULATORY APPROVALS



### PIN ASSIGNMENTS



## RECOMMENDED PRODUCTS::

1200037 5VDC External Power Adapter



#### Warranty Information

Control offers a 30-day satisfaction guarantee and 5-year limited warranty.

#### Sales Support

+1.763.957.6000  
 sales@control.com

#### Technical Support

+1.763.957.6000  
 www.control.com/support

#### Email, FTP, and Web Support

info@control.com  
 ftp.control.com  
 www.control.com

© 2013 by Control Corporation. All Rights Reserved. Printed in the U.S.A. All trademarks used herein are the property of their respective trademark holders. Specifications are subject to change without notice. LT1551C

## Appendix O: Literature Review

### O.1 Structural Health Monitoring on Bridges

*Structural Identification of the Commodore Barry Bridge* (Necati Catbas, Grimmelmsan, & Aktan, 2000)

A 3D FE model of the Commodore Barry Bridge was developed, calibrated, and verified using experimental data. The 3D model composed of beam and shell elements. 3D beam elements were used to represent the upper chord, lower chords, verticals, diagonals, floor beams, out-of-plane truss members, bracing, and roadway stringers. In addition, the through truss piers were also modeled with 3D frame elements for computational efficiency.

The preliminary FE model utilized idealized boundary conditions (pinned supports and roller supports). The complete 3D FE model was analyzed with the nominal boundary and continuity conditions (pinned supports at intermediate piers and roller supports at exterior piers) with and without the concrete piers incorporated. Constraints were used to simulate members' connectivity between elements of the floor system. In addition to dead load analysis, temperature loads were defined in order to simulate the cambered lengths of the through truss members. Modal analysis of the model was also performed, and the frequency and mode shape information were generated. There was about a 30% difference in the lateral response of the 3D FE models, with and without piers.

Ambient vibration tests were conducted to obtain global frequencies and mode shapes (dynamic properties) of the through truss spans of the bridge. Data was collected using accelerometers, and these were placed spatially to obtain the global response of the structure. Measurements were taken under ambient conditions and daily traffic. The input that induces vibration is mainly due to traffic and wind. The collected data was analyzed for frequency of the vibration modes and corresponding mode shapes. Spectral analysis was done using Matlab software. The objective of the spectral analysis is to decompose the time histories into individual vibration components, which are represented in frequency domain.

Lateral, vertical bending and torsional modes were identified for post-processing of the data. The authors mentioned that wind and traffic might not excite some of the modes that could exist in the analytical model.

Controlled load tests were performed with a static load test at a pre-identified location with two 108 kip cranes, and a second test with trucks crossing the bridge at crawl speeds. Strain gages were used to collect strain measurements from these tests. Sample rate used was 40 data points/second for the static loading. For the first part of the test, the truck was at the location under consideration for about 30 seconds. For the crawl speed test, the sample rate used was

100 data points/second. The crawl speed was about 5-7 mph. By minimizing the dynamic effects, the crawl speed test provided a static response of the bridge to a known set of moving loads at measurements locations when the load is at any location on the bridge. The authors mentioned that when the weight of each crane-axle and the distance between them are known and the location of the crane and members' responses are measured simultaneously, it is possible to normalize and decompose the responses into normalized influence lines for the response under a unit moving load. Using this decomposed unit influence line, the magnitude of that response can be predicted under any type of load case provided the load does not cause dynamic amplification and structural linearity is satisfied.

While interpreting the results, the authors also mentioned that since the frequencies and mode shapes are a function of parameters such as mass, stiffness, damping, and boundary conditions of the structure, any differences in frequencies and mode shapes can be attributed to the misrepresentation of one of these properties. It was not mentioned if the percentage of damping ratio was an adjusted variable in the FE model.

The 3D FE model used for the calibration was the one which included the piers (boundary conditions were also modeled). Strain levels from field tests were compared to FE model. The hanger element (element connecting the suspended truss to the cantilevered truss) was modeled with released condition for rotation to simulate the rotational pin mechanism at two ends of the hanger. Strain levels were compared at this location (side South hanger) and a good agreement was observed between collected data and FE results. It was observed that the axial strain at the lower chord decreased as the crane moved closer. The authors commented that ideally, the axial response is expected to increase when the load is getting closer to the mid-span. When the finite element model response is investigated, it is seen that the axial response of the member gradually increases, reaches its maximum when the load is at the center and starts decreasing as the load is moving away from the member. These examples show that the actual behavior of a long span bridge could be much more complex than anticipated.

The authors also pointed out that DI3 engineers documented that environmental effects, structural variations and uncertainties have significant impact on the structural responses at different times of the year and even at different times of the day. The authors concluded that the stresses comparisons were considered to validate the local behavior of the FE model considering the abovementioned and the size of the bridge.

From the correlation of the 3D FE model to dead load analysis, the authors observed that the upper chord, diagonal, and vertical members show comparable member forces whereas most of the lower chords have less member forces due to the additional stiffness provided by the floor system.

The model dynamic responses were compared to the experimental values. After model improvements and calibrations, a reasonably successful correlation was achieved.

Controlled load test data proved essential for verification and local calibration of the FE models of the behavior. Test results were also correlated with the models of the bridge. Main truss model response matched quite well with the controlled load test results. When experimental results of the load test are observed, it is seen that some of the load transfer mechanisms are very complicated and further instrumentation may be required for local response characterization at these locations.

***A Review of Structural Health Monitoring Literature 1996-2001*** (Sohn, Farrar, Hemez, & Czarnecki, 2002.)

This study focused on the review of damage detection studies, which the authors summarized in the context of a statistical pattern recognition paradigm. This paradigm can be described as a four-part process: (1) operational evaluation; (2) data acquisition and cleansing; (3) feature extraction and data reduction; and (4) statistical model development. However, the authors focused on items (3) and (4).

Data can be measured under varying conditions, and the ability to normalize the collected data becomes very important to the SHM process. It is common to normalize the measured responses by the measured inputs. If environmental or operating conditions variability becomes an issue, the need of normalizing data can increase and the data normalization can be done in some temporal fashion to facilitate the comparison of data measured at similar times of an environmental or operational cycle.

Data cleansing is the process of selectively choosing data to accept for, or reject from, the feature selection process. On the other hand, feature extraction is the process of identifying damage-sensitive properties, derived from the measured system response, which allows one to distinguish between the undamaged and damaged structure.

Almost all feature extraction procedure essentially carries out some form of data compression. Data compression (into feature vectors of small dimension) is necessary if accurate estimates of the feature's statistical distribution are to be obtained. "As an example, the use of residual errors between auto-regressive model predictions and actual measured time histories represents a one-dimensional feature vector that has been used for damage detection."

***Feasibility of Structural Monitoring with Vibration Power Sensors*** (Elvin, Lajnef, & Elvin, 2006)

The research presented in this paper is centered on utilizing vibration in structures as a source of ambient energy that could be used to power wireless sensors. Sources of the vibrations can include traffic, wind, and earthquake loads. Comparisons were made between

the theoretical maximum energy levels that can be extracted from the dynamic loads and energy requirements of various wireless sensors. It was shown electrical generation increases approximately linearly as the sensor mass increases. With current technology, small sensors with a volume of approximately 5 cm<sup>3</sup> are not able to produce sufficient energy. However sensors with masses between 100 g and 1,000 g can be powered under normal bridge traffic. Further research in reducing the energy demand on the sensors would benefit smaller sensors.

***Fiber Bragg Grating Sensors for Structural Health Monitoring of Tsing Ma Bridge: Background and Experimental Observation*** (Chan, et al., 2006)

The study presented a description of the Fiber Bragg Grating (FBG) sensors used for structural health monitoring of the Tsing Ma Bridge (TMB, with a length of 1,377 meters). Forty FBG sensors divided into three arrays were installed on the hanger cable, rocker bearing and truss girders of the TMB. The objectives of the study were to investigate the feasibility of using the developed FBG sensors for structural health monitoring, via monitoring the strain of different parts of the TMB under both live loading, railway and highway loads, as well as to compare the FBG sensor's performance with the conventional structural health monitoring system – Wind and Structural Health Monitoring System (WASHMS) that has been operating at TMB since the bridge's opening in May 1997.

To investigate the feasibility the developed FBG sensors for structural health monitoring, a field test was carried out in May 2003, in which a number of such FBG sensors were installed on the Tsing Ma Bridge to conduct real time and full scale measurements. Results of the FBG sensors were also compared with existing conventional strain gages.

***Structural Health Monitoring for Flexible Bridge Structures Using Correlation and Sensitivity of Modal Data*** (Koh & Dyke, 2007)

The authors investigated the use of correlation-based damage detection methods for long-span cable-stayed bridges. The location of damage was determined using an iterative procedure in which the combination of structural parameters that maximizes the correlation coefficient through the application of genetic algorithms. Different analytical methods were used for the correlation-based damage such as damage location assurance criterions (DLAC), multiple damage localizing assurance criterion (MDLAC), genetic algorithm (GA), and modal assurance criterion (MAC).

The FE model used for this study was previously developed and details were presented in other studies. The FE model was composed of beam, cable, lumped mass and rigid elements to fully represent the bridge's dynamic characteristics. Since cable-stayed bridges present behave nonlinearly due to tensioning and sag in cables, beam-column interaction, and large

deformation resulting from the structure's self-weight. The FE analysis used the post-deformed geometry of the bridge based on the results of nonlinear static analysis.

The reduced modulus of elasticity was defined for the beam elements representing the deck to simulate a structural defect in the deck. MDLAC combined with GA was used in this study for locating damage.

The damage variable set that best represents the modal properties of the damaged bridge structure is obtained through genetic algorithms. Numerical simulations showed that the MDLAC-GA approach yielded successful localization of multiple damage locations presented in the cable-stayed bridge.

***Conceptual Damage-sensitive Features for Structural Health Monitoring: Laboratory and Field Demonstrations*** (Necati Catbas, Gul, & Burkett, 2008)

In this study, multi-input and multi-output dynamic data were used to obtain modal flexibility, which is a close approximation to the actual flexibility. It was shown that both deflection and curvature are conceptual and physically meaningful features for damage detection and localization. The aim of this investigation was the extraction of different damage condition indices (or features) from vibration data.

A damage indicator that can be used is flexibility. This parameter can be attained by using the frequencies and mass normalized mode shapes. Modal flexibility and curvature were the focus of this study. In addition, modal curvature was another feature used for damage detection. The basic premise behind using modal curvature is that the reduction in the stiffness will be reflected as an increase in the modal curvature.

Flexibility and flexibility-based displacements were observed to be conceptual and promising indices for damage detection. On the other hand, modal curvature is another very commonly used feature for damage identification.

The authors focus on extracting modal flexibility based displacement and curvature from dynamic data. First modal flexibility is obtained by using modal parameters. Then a loading vector is applied to the modal flexibility to obtain displacement patterns. After obtaining the deflection values, deflection vector is used to obtain curvature as opposed to mode shape curvature.

An important point about the real-life application of the methodology is that special care has to be taken for elimination effects from data. It may be possible to separate damage from environmentally induced conditions if the structure and the environmental effects are monitored continuously such that seasonal and yearly environmental cycles are captured. It is important to note that these features are for global condition assessment.

***Dynamic Monitoring of a Long Span Arch Bridge*** (Magalhaes, Cunha, & Caetano, 2008)

This study is focused on the installation of a monitoring system on a concrete arch bridge shortly after construction and the experimental and numerical studies to accompany it. Some of the early studies included creating an ambient vibration test with a numerical model that was calibrated with the observed values in the field. The development of numerical models is of importance after the identification of natural frequencies in order to extract the effect on natural frequencies of environmental variables (e.g. air temperature and humidity). In addition, the effect of the extra mass associated with the traffic over the bridge may need to be considered. After elimination of the influence of these factors, frequency changes can only be due to stiffness reductions associated with damage.

Finite element (FE) software, ANSYS was used to develop a 3D FE model composed of bar finite elements. Cross section properties (area, moments of inertia, torsion moment of inertia and shear deflection constants) were defined according to the geometry of the deck, arch and columns. Only one half of the bridge was instrumented with 12 accelerometers distributed along four sections, with three sensors per section. In addition, an independent static monitoring system (performing one or two acquisitions per hour) during construction, and comprises strain gages, clinometers and temperature sensors, was carried out. Temperature sensors embedded in the concrete gave important measurements for the FE models that left out the effect of temperature from identified natural frequencies. Moreover, a weather station located close to the bridge, recorded all the important environmental variables (air temperature, humidity and wind velocity and direction) whose measures can also be used to investigate their possible effect of (Chan, et al., 2006) the identified modal parameters.

At the time of this publication, the analysis of modal parameter changes with environmental conditions (e.g. temperature and humidity) had not been done and that information was documented in other communications.

Mean values associated with the ambient vibration test were consistently lower. This difference can be explained by the temperature effect, because the ambient vibration test was performed during the summer (natural frequencies decrease with temperature increase), and also by hardening of the concrete during the last 2 years (last pouring-June 2002; ambient vibration test – June 2005; monitoring – October-December 2007). On the other hand, the standard deviations of the estimates provided by the monitoring system for the natural frequencies were higher than the ones resulting from the ambient vibration test, owing to the effect of temperature, which is obviously more significant during a long observation period. Direct comparison between the mode shapes provided by the ambient vibration test and the ones estimated by the monitoring system was not possible, because the measured degrees of freedom are not exactly the same.

“The main limitations of the described procedure for the automatic identification of the modal parameters are the accuracy of the natural frequencies estimates dependency on the frequency resolution and the inadequacy to estimate modal damping ratios. It is possible to obtain estimates for these coefficients, from auto-correlation function resulting from the inverse Fast Fourier Transforms of the points selected modal domains, by the fitting exponential decays to the envelopes of those functions.”

***Structural Health Monitoring and Reliability Estimation: Long Span Truss Bridge Application with Environmental Monitoring Data*** (Necati Catbas, Susoy, & Frangopol, 2008)

The main objective of this study was to present the reliability estimation studies for all main truss components as well as the entire structural system of a long span truss bridge. This bridge was subjected to long term structural health monitoring studies where large amount of input and response data have been collected. A very detailed finite element model of the bridge was developed and calibrated using field data. The developed FE model is described in the “Structural Identification of the Commodore Barry Bridge” (Catbas, et al; 2000).

The calibrated and verified FE model from the Commodore Barry Bridge was used for reliability analysis of the bridge accounting for dead, traffic, and wind loads. A limit state function was adopted in terms of ultimate strains for the first-order reliability analysis. Long term monitoring data was also used for reliability estimations. Field test data from temperature and temperature-induced strains were collected over a one-year period, showing the behavior of the temperature and the corresponding strains. The collected data was also used to study the effects of temperature-induced stresses on the structure components and reliability. The system reliability of the structure is evaluated using the parallel/series modeling of component reliabilities where temperature-induced responses are also included. The environmental inputs and responses were monitored for a one-year period and the responses are included in the component and system reliability.

From the FEM results, nominal values of load effects and resistance values were found, and those values were used to calculate their statistical distributions. Wind load was considered to be an important factor on the reliability of the long truss bridge, and the wind load was defined as equivalent static point loads applied laterally applied at the joints. Live loading was carried out simulating the HL-93 loading. The truck was placed at several critical locations along with the distributed lane load. The authors mentioned that the effect of live load on the bridge depends on many parameters such as span length, truck weight, axle loads, axle configuration, position of the vehicle on the bridge (transverse and longitudinal), number of vehicle on the bridge (multiple presence), girder spacing, and stiffness of structural members (slab and girders).

The study observed that any temperature-induced stresses on critical truss members are difficult to conceptualize and model. For instance, bending due to temperature effects was observed in the truss members at levels approximately ten times higher than any effects of traffic. The study recommends including environmental effects in any reliability estimation due to the difficulty to model these effects in routine design. Long-term monitoring of a structure is a way to encompass these effects.

***The State-of-the-Practice of Modern Structural Health Monitoring for Bridges: A Comprehensive Review*** (Ahlborn, et al., 2010)

The research in this paper gives an overview of technologies used in bridge inspection and structural health monitoring. Standard bridge inspection procedures along with newer technologies are outlined. In-situ monitoring techniques such as accelerometers and various types of strain gauges are described in detail. NDE techniques such as eddy currents, ground-penetrating radar, and radiography are discussed as well. The paper concludes with several case studies of structural health monitoring including the Commodore Barry Bridge, Golden Gate Bridge, and the Cut River Bridge.

***Vibration Based Structural Health Monitoring of an Arch Bridge: From Automated OMA to Damage Detection*** (Magalhaes, Cunha, & Caetano, 2011)

In this study, a strategy to minimize the effects of environmental and operational factors on the bridge natural frequencies was followed. OMA represents Operation Modal Analysis. In addition, static and dynamic regression models were tested and complemented by a Principal Components Analysis (PCA). The scope of this study included:

- Study the modal parameters variations to build numerical models suitable to eliminate the effect of environmental and operational variables,
- Evaluation of the capability of the installed monitoring system to detect realistic damages.

PCA is a “multivariate statistical tool concerned with explaining the variance or covariance structure of a set of variables through a few linear combinations of these variables. It is commonly used to reduce the dimension of the problem, by substituting a group of correlated variables by a new smaller group of independent variables, which are designated principal components.”

The study also utilized control charts which are made up of data plotted with respect to time and control limits to show variation from common causes. Any data outside of the control region on the chart represents a special cause of variation. In SHM, this may be representative of damage occurring to the structure. Therefore the charts can be utilized to monitor any sample

multivariate observations that fall outside of the designated control limits which have been established by any previously collected data. In other words, to monitor collected data for values that are unsafe.

Dynamic monitoring systems in combination with a processing strategy which is based on algorithms that permit an automated and precise identification of the structural modal parameters “complemented with statistical tools for the minimization of the environmental and operational influences permit the construction of control charts that enable the detection of small stiffness reductions that might be associated with the occurrence of damages.” Damage-based detection was based on numerical simulations that had some limitations.

***Application of Advanced Non-destructive Testing Methods on Bridge Health Assessment and Analysis*** (Kilic, November 2012)

This investigation presents results of application technology using Ground Penetrating Radar (GPR), IBI-S technology/system (deflection and vibration sensor system with interferometric capability) and accelerometer sensors. Finite element models were developed for the case study using two software applications, SAP2000 and ANSYS. Analytical results were compared to those obtained from field tests using the non-destructive methods above described. With the use of the described techniques, the main goal of this study was to develop an integrated model/approach for the assessment and monitoring of the structural integrity and overall functionality of bridges.

The FEM analysis was conducted assuming no defects on the bridge for the case study. Deflections obtained from field tests data was compared to FEM results. Simulations on increasing crack lengths were carried out using the FE model created using ANSYS software. Additionally, an IBI-S interferometric radar system was utilized which measures dynamic or static displacement and vibration of structures such as bridges, towers, buildings etc., up to a hundredth of a millimeter.

Little information regarding bridge geometry and materials was available for creating the FEM. Assumptions made in the finite element model included:

- Constant temperature
- All bearings to be at the same points
- No residual stresses were applied to the model
- Damping ratio was assumed to be 5% (value found in literature, Chopra 1995)
- Stiffness was calculated using FE software
- Surface roughness was not considered in the FE models.

- For the live loading, no damping characteristics of the vehicle were taken into account. 18 metric ton vehicle with two axles and with a constant speed of 25 mph was defined for live load analysis.

For the FE model created with SAP2000, shell elements were used to model the decks. Pier and abutments and the beam elements are intended to represent the beams in the last span of the bridge. Simple connections were used. The modulus of elasticity was found for the bridge by dividing the preliminary value (value obtained using  $f'_c = 3$  ksi) by the average of the results of IBIS-S monitored deflection and the FE outputs for the same nodes. Thus, the modulus of elasticity of the concrete was found using an inverse approach. After modification of the value of the modulus of elasticity for the concrete was done, the author found acceptable similarity between field test results, displacement results, and the FE model created using SAP2000.

For the cantilever span of the bridge case study, the author did not observe good agreement between FE results using the SAP2000 model and field test results using IBI-S survey. This discrepancy was attributed to the deterioration of the bridge structure.

ANSYS software was used to create a 3D FE model to account for the cracks in the structure using material capabilities that the software has. The purpose of the FE model created using ANSYS software was to assess the health condition of the bridge case study, especially in the region where the cracked supporting beam has led to doubts regarding the structural adequacy of the structure.

***Compressed Sensing Embedded in an Operation Wireless Network to Achieve Energy Efficiency in Long-Term Monitoring Applications*** (O'Conner, Lynch, & Gilbert, 2014)

The focus of the research in this study is on compressed sensing within wireless sensors that are deployed in SHM. Compressed sensing can be used to reduce data sampling rates, on-board storage requirements, and communication data for wireless sensors. This reduces the energy demand for a wireless SHM system which can then increase reliability. In order to deploy this method, mode shapes were obtained using acceleration data from a steel, multi-girder bridge on Telegraph Road in Monroe, MI. Through the performed analysis, it is concluded that the compressed sensing procedures do succeed in reducing the amount of data transmitted at a cost of modal accuracy. The study also shows that the energy reductions through compressed sensing are significant for large sensor networks.

## O.2 Dynamic Impact Factor

### *Dynamic Axle Loads and Pavement Response* (Christison and Woodrooffe, 1986)

Field test investigations involved placing perturbations on the road surface to vertically excite axles of an instrumented vehicle and recording axle forces and pavement surface deflections as the vehicle passed over surface – set deflection transducers. "A single perturbation was used to generate relatively high frequency axle dynamics and a series of perturbations were employed to obtain a lower frequency whole body dynamic loading condition."

Maximum static deflections were obtained at the time that the wheels of an axle were directly placed over the transducers, and dynamic axle forces coinciding with the time of monitoring maximum deflections were made available for a number of test runs. Ratios of the recorded dynamic to static axle loads (DLF) were determined and used in analyses carried out to assess the effect of dynamic axle loadings on pavement deflections. It was observed that the magnitude of pavement surface deflections increased with increasing vehicle speed.

### *Dynamic Wheel Loads from Bridge Strains* (O'Connor and Hung Tin Chan, 1988).

AASHTO 1977 defined impact I as the ratio of additional stress to the equivalent static live-load stress. Collected data from the weighbridge and the data logger made possible to compute impact values as the ratio of additional mid-span bending moment to equivalent static live-load bending moment. The authors calculated impact values ranging from -0.08 to 1.32, which is much higher than the 0.3 AASHTO value. The widespread in values was attributed to possible vehicle defects, resonance between the vehicle and the bridge, and road roughness (O'Connor and Pritchard 1985).

Two type of analyses are described in this study: the predictive analysis generates the theoretical bridge response, and the interpretive analysis then uses this response in order to recover the original dynamic loads.

The following are the conclusions of the research project:

- Acceptable values have been obtained theoretically using either deflections or bending moments as input data.
- Error studies show that predictions based on deflections are more sensitive error than those using measured bending moments.
- The preferred method of using bridge measurements to estimate dynamic loads is therefore by the use of measured total bending moments at a series of transverse cross sections of the bridge.

***Simulation of Dynamic Load for Bridges*** (Hwang, and Nowak; 1991).

This paper focuses on the analysis of dynamic loads in bridges. Models are developed for trucks, road surface (roughness) and the bridge. Truck parameters include mass, suspension, and tires. Random variables include the truck type, total weight, axle distances, and speed. Dynamic load factors were found to be lower for heavier trucks and even lower for two trucks (side by side). Simulated deflections indicate that the dynamic component is not correlated with the static component.

It has been observed that the dynamic load depends on dynamic properties of the vehicle (self-weight, physical dimensions, suspension system, and tires), dynamic properties of the bridge (mass, flexural stiffness, and span length), and pavement roughness (also affected by conditions of the approach road). The authors determined the dynamic load effect in a bridge in terms of the maximum static and dynamic deflections ( $D_{sta}$ ,  $D_{dyn}$ ). In this study, the dynamic load factor (DLF) is defined as the maximum dynamic deflection divided by the maximum static deflection at mid-span.

From results, it was seen that the dynamic load factor decreases as the weight increases. This not caused by decrease of dynamic load deflection but by increase of static load deflection. In addition, dynamic load factor (DLF) varies with truck speed. The effect of axle distance varies from span to span. For longer spans, the DLF increases as the axle distance increases, because the maximum dynamic mid-span deflection increases and the maximum static mid-span deflection decreases.

The following are the conclusions of the research project:

- DLF decreases as the vehicle weight increases.
- Dynamic and static live loads were considered to be uncorrelated except for 30-m span.
- The DLF for two side-by-side trucks was found to be lower than for one truck case.

***Design of Highway Bridges: Based on AASHTO LRFD, Bridge Design Specifications***  
(Barker and Puckett, 1997)

Vehicle suspension system reacts to roadway surface conditions by compression and extension of the suspension system. This creates axle forces that exceed the static weight during the time that the acceleration is upward, and is less than the static weight when the acceleration is downward.

It is most common to compare the static and dynamic deflections as illustrated below. The dynamic effect is defined as the amplification factor applied to the static response to achieve the dynamic load effect.

$$IM = \frac{D_{dyn}}{D_{sta}}$$

$D_{sta}$  = maximum static deflection

$D_{dyn}$  = additional deflection due to dynamic effects

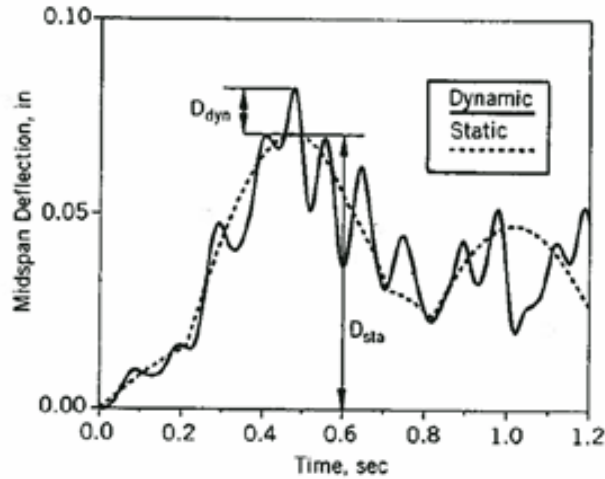


Fig. 4.12 Typical live load response. [Hwang and Nowak, 1991].

The ratio of  $D_{dyn}/D_{sta}$  varies greatly with different vehicle positions. The main variables that affect the dynamic load factor are the characteristics of the truck, the dynamic characteristics of the bridge, and the roadway roughness. “These characteristics are expected as all transient structural dynamic problems involve stiffness, mass, damping, and excitation.”

The global dynamic effects are addressed in most studies regarding impact. Global means the load effect is due to the global system response such as deflection, moment, or shear of a main girder. Local effects are the load effects that result from loads directly applied to (or in the local area of) the components being designed. These include decks and deck components. In short, if a small variation in the live load placement causes a large change in load effect then the load effect should be considered local.”

Dynamic effects on deck components are much greater and highly dependent on roadway roughness. Because the load is directly applied to these elements, also their stiffness is much greater than that of the system as a whole.

### ***Dynamic Loads for Steel Girder Bridges*** (Nowak & Kim, 1999)

According to the authors, dynamic load is time-variant, random in nature and depends on vehicle type, vehicle weight, axle configuration, bridge span length, road roughness and transverse position of truck on the bridge. Parameters considered for their experimental

program: span length, girder spacing, slab thickness, and skew. Dynamic load usually considered as an equivalent static live load expressed in terms of DLF.

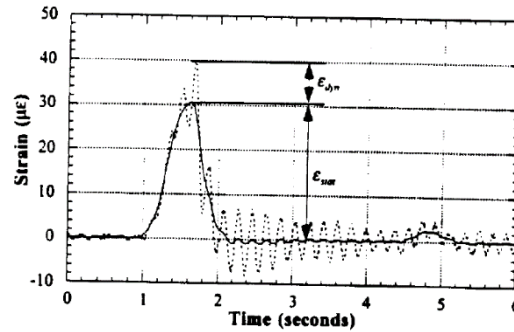


Fig. 1 Dynamic and Static Strain under a Truck Travelling with Highway Speed.

$DLF = \epsilon_{dyn}/\epsilon_{stat}$ , where

$\epsilon_{dyn}$ = dynamic component of strain (measured from test data,  $\epsilon_{dyn} = \epsilon_{total} - \epsilon_{sta}$ )

$\epsilon_{stat}$ =static component of strain, (maximum total strain obtained from the filtered dynamic response)

DLF= dynamic load factor [1 + DLA (using AASHTO Expressions)].

DLA= dynamic load amplification.

*Analytical and Experimental Evaluation of Existing Florida DOT Bridges* (Wekezer, Li, Kwasniewski, and Malachowski; 2004).

The main objective of this study was to validate dynamic responses for short and medium span high bridges. In addition, the determination of actual impact factors was of importance. Identification and evaluation of parameters having great influence on dynamic response of the structure, such as span length, vehicle speed, vehicle suspension, vehicle weight, vehicle position on bridge lanes, and road surface condition were considered. Field test data was collected by measuring strain and displacements at midspan. In addition, accelerations were also recorded at the truck axle and selected locations along the bridge.

Impact factors were calculated as follows:

$$IM = \frac{R_d - R_s}{R_s} * 100\%$$

$R_d$ = maximum dynamic response

$R_s$  = maximum static response.

From comparison of results obtained at 30 mph and 50 mph, it was observed that the vehicle speed as an important parameter in dynamic effects.

The static response was checked as part of the validation of the FE model. Some differences were observed between numerical and field tests results for static loading. The differences were attributed to the stiffness of the FE model being smaller than the actual structure. Compressive strength tests were conducted to investigate concrete material properties and those obtained were used for the validation of the FE model. In addition, natural frequencies of the model were compared to field test data. Once the FE models were validated, both models, truck and bridge were assembled together to simulate vehicle-bridge interaction for the static and dynamic tests. The road approach was incorporated to the numerical simulations. A very high impact factor was obtained from field tests for vehicle speed of 50 mph.

From field tests and numerical analyses, it can be said that there are six variables that could have a great influence in impact factors: span length, vehicle speed, suspension parameters, truck weight, truck position on bridge lanes, and road surface condition. From numerical analyses, it was observed that the impact factor increased for speeds above 50 mph obtaining values higher than those predicted by AASHTO code. In addition, FE results showed that heavier vehicles lead to smaller impact factors.

Dynamic response in bridges due to moving loads was attributed to the three major sources:

- Pure motion of constant reaction forces exerted by a vehicle along a perfectly smooth bridge surface. This has a negligible effect on the bridge response.
- Change in time of reactions due to interaction in the wheel suspension assembly. This is related to the characteristics of vehicles suspension system and its effect on the bridge dynamic response depends on bridge characteristics such as span length, number of girders and position of the loading vehicle. This factor is significant when the road surface is in good condition and the hammering effect is not present.
- Impact forces exerted by the wheels on the bridge and triggered by road surface imperfections and discontinuities (hammering effect). This last one has the most significant effect due to impact forces induced by geometric surface imperfections.

In addition, the impact factor increases when truck speed increases; the impact factor decreases with the increase in truck weight; and the impact factor gradually decreases with longer span lengths.

***Load Test of a Plain Concrete Arch Railway Bridge of 20-m Span*** (Marefat, Ghahremani-Gargary, & Ataei, 2004)

In this study, the dynamic impact factor was defined based on vertical displacement at the crown. The dynamic impact factor depends on span length, type of structure, material characteristics, support conditions, loading conditions, and response of the structure. Results

of maximum displacements computed from different speeds loadings were normalized based on the maximum displacement of 10 km/h. Thus, at a speed of 10 km/h the dynamic impact factor is 1.0 and it increases as the speed increases. In this article, the researchers calculated a maximum impact value of up to 1.2 for speed of 80 km/h. Accelerometers were used to obtain the natural frequency of the structure during moving load tests.

***Investigation of Impact Factors for Permit Vehicles*** (Wekezer, Szurgott, Kwasniewski, and Siervogel; 2008)

DLA was determined from field tests and FE analyses. An influence of the vehicle velocity on the impact factor was considered. The bridges under study were instrumented with strain gauges, LVDTs, and accelerometers. The strain gauges were oriented to measure the longitudinal component of strains.

The main objective of their experimental program was to assess an actual dynamic load impact for a selected bridge. The collected data was used to confirm the correctness of the existing FE model and performed FE analyses. Static and dynamic tests were carried out. Dynamic tests included runs of each vehicle at two different speeds, 30 and 50 mph. For the dynamic tests, strains, displacements and accelerations at chosen locations of the bridge were recorded as well as accelerations in a few points located on the vehicles. Strain readings obtained from static tests showed relatively good repeatability.

$$IM = \frac{R_{dyn} - R_{sta}}{R_{sta}} * 100\%$$

$R_{dyn}$  = maximum dynamic response (strain, displacement)

$R_{sta}$  = maximum static response (strain, displacement).

The authors mentioned that the obtained impact factors should be considered in a qualitative respect instead of the quantitative one. Longitudinal strains obtained from field test were compared to FE results. “The conducted tests and FE analyses provided significant information about determinants that influence the impact factor. The first one is undoubtedly related to the suspension parameters of the vehicle. In practice, the difference between the dynamic and static response of the bridge for a fully suspended vehicle is not so large. Heavy vehicles with very stiff suspension systems have much more effect on the bridge. Differences between static and dynamic responses are higher, consequently increasing the impact factor. The dynamic response for such vehicles can be further intensified by the “bounced” cargo located on the load deck. Vibration of the vehicle caused by road surface imperfections (e.g. thresholds, crack, potholes etc.) can generate additional oscillations of the load and intensify the dynamic influence on the bridge span.”

***Investigation of Impact Factors for FDOT Bridges*** (Wekezer, Taft, Kwasniewski, and Earle, 2010)

Dynamic impact factors were calculated as function of vehicle type and speed. Impact factors were calculated using maximum displacements and strains. Impact values calculated using strain values seemed to be more reliable and closer to the value recommended by AAHSTO. The parameters affecting dynamic impact factor are: surface imperfections (joint abutments and bridge approach depression), loosely attached cargo which causes the so-called hammering effect, and characteristics of the suspension of the vehicle. The FE software used for this investigation was LS-DYNA (explicit).

Dynamic responses of the system are influenced by span length, vehicle speed, vehicle suspension, truck weight, truck position on bridge lane, and road surface condition. Vehicle speed, surface imperfections, and vehicle mass were of major focus in this investigation. In addition, the dynamic effect due to the bouncing cargo was included in the studied through FE analysis. The trucks were actually modeled, surface interaction between the vehicle and the bridge was incorporated in the model. The deck and girders were modeled using 3D elements.

Truck suspension was also incorporated in the model with its material properties (damping and the like), and in addition the bearing pads were modeled. Strains and displacements measurements were used for validation and verification of the FE models. The three vehicles used for this investigation, were previously validated and calibrated and part of that information is presented in “Investigation of Impact Factors for Permit Vehicles” (Wekezer, et al; 2008) and “Analytical and Experimental Evaluation of Existing Florida DOT Bridges” (Wekezer, et al; 2004).

The compressive strength used for the slab part was 8 ksi. The studied bridges consisted of precast prestressed concrete type-I girders with  $f'_c = 9$  ksi. “The size of the girders has the biggest effect on the strength and structural response of a bridge subjected to dynamic loads.” The road approach was including in the FE models to study the effect on dynamic response. Maximum strains were used to compute DLA. From FE Analysis, the strains did not show a strong correlation to the vehicle speed. “The strains induced by each vehicle on the bridge, do not directly reflect the DLA, because each vehicle DLA is calculated by a comparison with its static case. Therefore a higher strain does not necessarily result in higher DLA. The FE model that allows for bouncing of the cargo resulted in higher DLA factors.”

A simplified model was created; the simplification was by using constant moving point loads instead of the vehicles models. Initial velocities were defined in the model. The rail system used for the simplified model provided a method for sliding the constant loads along a defined pathway, but the complex interaction between the vehicle and the bridge (original FE model) that includes the vehicle’s suspension system and bouncing masses is disregarded was not taken into account in the simplified model.

From the FE analyses, the maximum strains for the simplified model were considerably lower than for the original model. This difference in results was due to the fact that the complex vibrations of the vehicle's mass and the suspension system were not accounted for in the simplified model. The loads in the simplified model were applied directly to the bridge as constant moving point loads, which did not vary dynamically. In the simplified FE model neither the speed of the vehicle or the bridge approach surface had a big effect in the dynamic response of the bridge.

From the Literature Review:

$$DLA = \frac{R_{dyn}}{R_{sta}} ,$$

$R_{dyn}$  = dynamic response of any physical variable,

$R_{sta}$  = static response of any physical variable.

The physical variables most commonly used are displacements and strains measurements.

The following are the conclusions of the research project:

- No direct relationships were found between the influence of span length and the dynamic response of the bridge.
- The DLA generally increases when the speed vehicle is increased, but the relation between these two is not nearly linear.
- The bad road surface triggers vibrations in the vehicle during the interaction with the wheels which are transferred to the bridge.
- The vehicle suspension system is one factor that needs to be considered in depth when studying the interaction of vehicle and bridge. Very stiff suspensions result in worst possible case of DLA, because it is unable to dissipate vibrations through springs and dampers. Softer suspension resulted in the lowest DLAs, proving its well-designed suspension system and good load distribution.

***Assessment of a Concrete Arch Bridge Using Static and Dynamic Load Tests.*** (Caglayan, Ozakgul, & Tezer, 2011)

Accelerometers were placed on the bridge for transverse and vertical directions since mode shapes could not be obtained in the longitudinal direction. Data was recorded for the free vibration of the structure once the train passed and left the bridge. Dynamic parameters were obtained using mean values from eight tests. Significant natural frequencies of the bridge were identified and normalized based on a spectral approach in the frequency range. Natural frequencies of the structure obtained by means of accelerometers placed on the bridge were compared to frequencies obtained from finite element analysis. Comparing the first five mode

shapes of the bridges, the difference between FE models vs. Experimental studies is about 3.9% (average).

For static load analysis tests, vertical displacements were measured on the bridge by means of LVDTs. Tilt measurements were obtained prior and after loading and the difference in the measurements is caused by the external static loading. It is not clear how the calibration of the static loading was done.

For the calibration of the numerical model, parametric studies were first carried out and then sensitivity parameters were considered. The most sensitivity parameters were found to be bearing spring stiffness in the longitudinal and vertical direction, and joint lumped masses affecting dynamic characteristics. These two parameters were adjusted until a good match was obtained to those natural frequencies obtained from field data.

In this study, Impact was calculated as,  $\delta = \frac{\sigma_{dyn}}{\sigma_{stat}}$ , where,  $\delta$  is impact factor,  $\sigma_{dyn}$  is the maximum compressive stress under the test train traveling at normal speed, and  $\sigma_{stat}$  is the maximum static compressive stress due to the static loading at the same point.